INTEGRATED EXPERIMENTAL AND COMPUTER MODELING APPROACH TO UNDERSTAND PERMAFROST THAW SUBSIDENCE INDUCED OIL WELL INSTABILITY FOR ALASKA NORTH SLOPE OIL WELLS

By

Saurabh Sheshrao Suryawanshi

RECOMMENDED:

Dr. Santanu Khataniar

Dr. Matthew Bray

Dr. Abhijit Dandekar
Advisory Committee Co-chair

Dr. Shirish Patil
Advisory Committee Chair

Dr. Abhijit Dandekar
Chair, Department of Petroleum Engineering

APPROVED:

Dr. Douglas Goering
Dean, College of Engineering and Mines

Dr. John Eichelberger
Dean of the Graduate School

4/5/2016
Date

INTEGRATED EXPERIMENTAL AND COMPUTER MODELING APPROACH TO UNDERSTAND PERMAFROST THAW SUBSIDENCE INDUCED OIL WELL INSTABILITY FOR ALASKA NORTH SLOPE OIL WELLS

A

THESIS

Presented to the Faculty

of the University of Alaska Fairbanks

in Partial Fulfillment of the Requirements

for the Degree of

MASTER OF SCIENCE

By

Saurabh Sheshrao Suryawanshi, B.Tech.

Fairbanks, AK

May 2016

Abstract

Hydrocarbon reservoirs in the Arctic region of Alaska have been developed by various oil and gas producers for several years. Most of them are overlain by massive layers of permafrost soils which extend to a thickness of up to 2300 feet. Production and injection wells in such regions have experienced design and operational challenges due to heat loss from the wellbore and subsequent thawing of the permafrost soils. Thawing is a phase change of ice to water resulting in volumetric reduction of the frozen soil due to pore space contraction and segregated ice thaw, causing a major problem of thaw subsidence. Thaw subsidence affects the stability of the well, causing buckling and structural distress along the length of the wellbore within the thaw susceptible permafrost zones, thus damaging the well casing.

Two different experimental approaches, one-dimensional consolidation and three-dimensional physical scale test, were employed to study thaw subsidence mechanisms in three different types of soils; namely, clay, silt and sand. The main objective of these experiments was to understand the well-soil system and the changes occurring within it with time, which will further increase knowledge of the interaction between the wellbore and the soil in Arctic regions during progressive thaw. Due to a lack of data and information, several areas were selected for multiple experimental approaches, including lateral pressure development, soil strain and strain within well casing, to study the frictional effects along the wellbore and pore-pressure response within the soil.

Along with the experimental work, two different models were built in COMSOL Multiphysics™. The first model focused on thermal analysis of the thawing and refreezing behavior of ice-rich permafrost for drilling and production operations, while the second model focused on mechanical analysis, to study and understand the generation of the vertical and horizontal loads and stress-strain characteristics of the ice-rich permafrost. Simulations focused mainly on obtaining data for lateral pressure development, well stress-strain and temperature.

Dedication

I dedicate this thesis to my mother, Mrs. Manjusha Sheshrao Suryawanshi.

Table of Contents

List of Figures

Page

List of Tables

Page

ACKNOWLEDGMENTS

First of all, I express my sincere thanks to the chair of my advisory committee, Dr. Shirish Patil, for his constant support, encouragement, and invaluable guidance during my graduate studies. I also greatly appreciate my advisory committee members Dr. Abhijit Dandekar, Dr. Santanu Khataniar and Dr. Matthew Bray for their valuable suggestions and commitment to this thesis.

Financial support from the Petroleum Engineering Department, College of Engineering and Mines, UAF and ConocoPhillips Alaska, Inc. is gratefully acknowledged. Special thanks to COMSOL Multiphysics™ and the Department of Mechanical Engineering, College of Engineering and Mines, UAF for providing the software.

I express my deepest gratitude to my parents, Mr. Sheshrao Baburao Suryawanshi and Mrs. Manjusha Sheshrao Suryawanshi, for their unconditional love and support. Finally, I would like to thank faculty and friends at Department of Petroleum Engineering for their constant support during my time at the University of Alaska Fairbanks.

CHAPTER 1 INTRODUCTION

1.1 Permafrost

Permafrost can be defined as "Ground (soil or rock and included ice and organic material) that remains at or below 0°C for at least two consecutive years". If it is defined on the basis of temperature, then it can be said that permafrost is perennially cryotic ground, where cryotic ground means ground (soil or rock) whose temperature is either 32°F or lower. It is not necessary that permafrost should always exist in frozen state. There can be presence of some unfrozen water in the permafrost soils because the freezing point of the water in the soil can be depressed by several degrees due to the presence of some solute impurities (salt, etc.). Natural or man-made climatic changes may also affect the permafrost's temperature equilibrium and thus increase the ground temperature above 32°F which further affects the subsurface permafrost temperature. Thus it can be said that all perennially frozen ground is permafrost but not vice-versa. Figure 1.1 shows the degradation of permafrost as a result of thawing.

Figure 1.1: Permafrost after thawing.
(http://www.globalchange.gov/sites/globalchange/files/permafrost-coastal-erosion-alaska-usgs.jpg)

1.2 Methods of Permafrost Formation

Permafrost can be formed in two ways, epigenetically (or epigenesis) and syngenetically (or syngenesis). The thermal and mechanical properties of permafrost depend on the soil's

geological origin and the manner in which the permafrost was formed. In epigenesis, the permafrost is formed by freezing of the previously deposited sediments by lowering the base of the permafrost (https://nsidc.org/cryosphere/glossary/E) from the top down when the conditions at the soil surface are sufficient for deep freezing and keeping the earth material in perennially frozen state. The permafrost formed in this manner is termed epigenetic permafrost.

Permafrost that grows through the rise of the bottom of the active layer (upper most contact of the permafrost) upwards due to increasing active layer thickness as a result of sediment deposition or thinning of active layer due to organic accumulation is defined as syngenetic permafrost. Syngenesis involves two moving fronts during the formation of permafrost, namely, the sedimentation front, which is on the ground surface, and the permafrost front, which is the bottom part of the active layer. By contrast, epigenesis involves only one single front, that is, the permafrost front moving in the downward direction (Figure 1.2). The active layer is the topmost layer of ground underlain by permafrost and is subjected to a continuous cycle of annual thawing and freezing (https://nsidc.org/cryosphere/glossary/A).

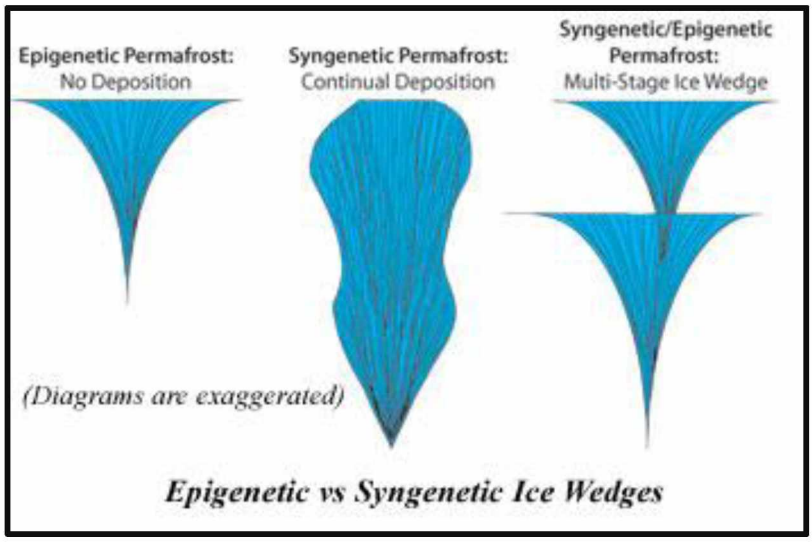

Figure 1.2: Epigenetic vs. Syngenetic permafrost. (http://permafrosttunnel.crrel.usace.army.mil/permafrost/general_facts.html)

The permafrost properties are affected by the method of formation. Epigenetic permafrost mainly occurs in consolidated soil and syngenetic permafrost in unconsolidated and/or weathered soil. Syngenetic permafrost is ice-rich due to a continuous flow of water from the active layer and has

large organic content as the formation and deposition processes take place at the same time. Epigenetic permafrost is less ice-rich and has mineral aggregates that are well consolidated. Temperature is an influential factor for the thickness of the epigenetic permafrost, whereas for syngenetic permafrost it is sedimentation (Figure 1.2). The rate of epigenetic permafrost formation decreases with time and is limited by the mean annual temperature of the permafrost base and the geothermal heat flux from the Earth's bottom. The rate of sediment accumulation is the limiting factor for the rate of syngenetic permafrost formation.

1.3 Distribution of Permafrost

On the basis of area covered, permafrost can be categorized into two types: onshore and offshore. Onshore permafrost can be categorized further into four different types or zones: continuous, discontinuous, sporadic, and isolated. The world permafrost regime is such that approximately 25% of the world's land is underlain by one of the above mentioned permafrost zones (Osterkamp and Jorgenson, 2009). As shown in Figure 1.3, more than 60% of Russia, 80% of Alaska and 60% of Canada are underlain by permafrost in the Northern Hemisphere. There is no sharp permafrost boundary between the different permafrost zones in Alaska (Shur, 2014).

Continuous permafrost can be defined as "Permafrost occurring everywhere beneath the exposed land surface throughout a geographic region with the exception of widely scattered sites, such as newly deposited unconsolidated sediments, where the climate has just begun to impose its influence on the thermal regime of the ground, causing the development of continuous permafrost." (Page no. 10, R. O. van Everdingen, 1998). The continuous permafrost zone can be defined as "the major subdivision of a permafrost region in which permafrost occurs everywhere beneath the exposed land surface with the exception of widely scattered sites" (Page no. 10, R. O. van Everdingen, 1998).

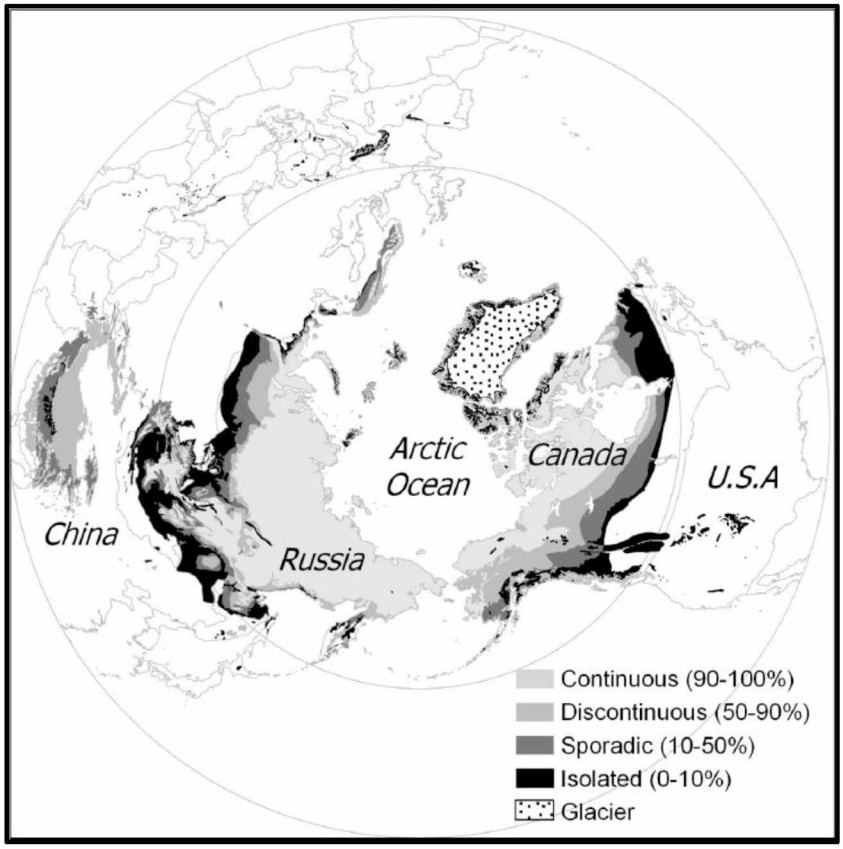

Figure 1.3: Permafrost occurrence in the northern hemisphere. (Shur, 2014)

Discontinuous permafrost can be defined as "occurring in some areas beneath the exposed land surface throughout a geographic region where other areas are free of permafrost" (Page no. 19, R. O. van Everdingen, 1998) and the discontinuous permafrost zone as "the major subdivision of a permafrost region in which permafrost occurs in some areas beneath the exposed land surface, whereas other areas are free of permafrost" (Page no. 20, R. O. van Everdingen, 1998). Sporadic permafrost can be defined as "permafrost underlying 10 to 35 percent of the exposed land surface" (Page no. 20, R. O. van Everdingen, 1998) and isolated permafrost can be defined in a similar manner, as permafrost underlying 5 to 10 percent of the exposed land surface. Figure 1.4 shows the distribution of onshore permafrost types with respect to temperature and Figure 1.5 shows the vertical distribution and thickness of permafrost.

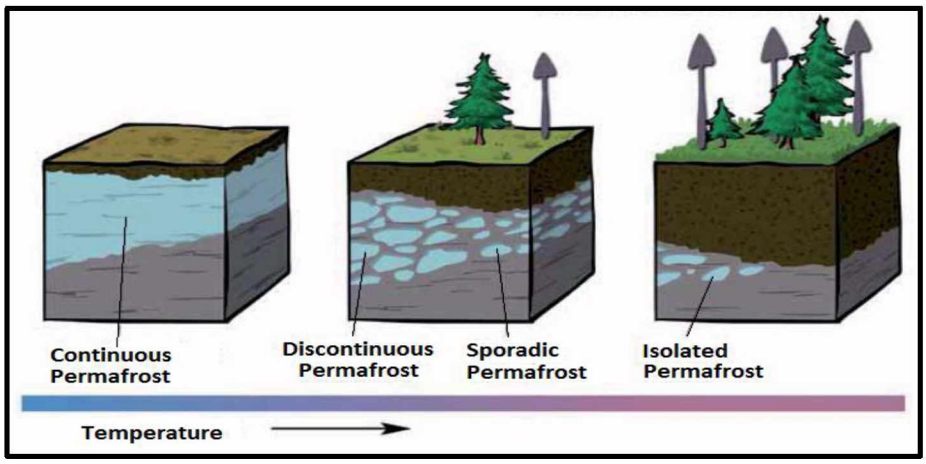

Figure 1.4: Distribution of permafrost with respect to temperature. (http://es.contenidos.climantica.org/unidades/3/a-auga-en-movemento/a-circulacio-n-da-auga-e-o-clima-das-selvas-aos-desertos/evidencias-e-impactos-do-cambio-climatico-nos-biomas)

Offshore (subsea) permafrost is believed to form when the mean annual ocean temperature in the Arctic region is below 32°F . There is not much knowledge about its distribution and occurrence but one estimate is that its areal extent should be greater than 10,000,000 km² with a thickness of several hundred meters (Shur, 2014). Based on seismic studies and laboratory analysis conducted on drilled cores from the Beaufort Sea, the existence of offshore permafrost has been proven. There is no detailed explanation about its formation, but it is also believed that it can form in several other ways:

a. It was formed onshore but later submerged due to changes in the sea level.
b. It was formed offshore under the influence of foot-bottom fast ice.
c. It exists as subsurface remnants of eroded islands.

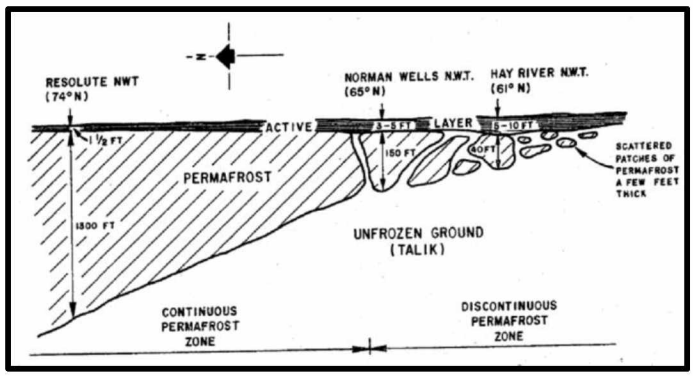

Figure 1.5: Vertical distribution and thickness of permafrost. (R. Brown, 1967)

1.4 Factors Affecting the Presence of Permafrost

According to Osterkamp and Jorgenson (2009), factors that directly or indirectly influence the current existence of permafrost are those that cause variations in the internal temperature and at the surface of the frozen body. These variations are mainly due to the energy imbalance at the surface of the permafrost body, including its sides and top and bottom surfaces. Some of the factors that contribute to this energy imbalance are: climate; geographical location; hydrology (includes surface drainage and site wetness, proximity of nearby water bodies, presence of underground flooding); vegetation; geology (soil or rock, geothermal heat flow, tectonic setting); and disturbances from humans, animals, fire etc.

Climate is one of the most important factors that impact the state of the permafrost directly. As shown in Figure 1.6, climate can be discussed in three different perspectives: air, soil and permafrost. Air climate is a result of solar radiation and air circulation (Shur, 2014). Soil climate depends on the properties of the soil and on the heat exchange processes at the soil surface. The layer of soil overlying the permafrost is called the active layer. The mean annual temperature at the bottom of the active layer is believed to change annually. These annual changes in temperature have a direct impact on permafrost formation. In the discontinuous permafrost zone or sporadic zone, such temperature changes form a temporary residual thawed layer of permafrost to the bottom of the permafrost base because of permafrost degradation, whereas the continuous permafrost zone freezes completely to the bottom of the permafrost base (Shur, 2014).

Permafrost climate does not depend on atmospheric climatic conditions directly. It is a result of the temperature of the soil surface and the active layer. It is also affected by relief, vegetation, snow, water on the soil surface, and active layer thickness. All these factors are called modifiers (Shur, 2014). The impact or effectiveness of the modifiers depends on the climatic conditions and on modifier's physical properties. These modifiers have a direct impact on the existence of the permafrost.

According to Shur and Ping (1994), the relationship between climate and permafrost can be studied in three different ways: first, climatic conditions totally favorable for permafrost formation; second, climatic conditions totally unfavorable for permafrost formation; and third,

climatic conditions neutral towards the formation of permafrost. In the first case, the existence of permafrost is a given, whereas in the second case, permafrost will only exist under special conditions, like in caves or on high mountains. In the third case, permafrost will only exist where there is thermal equilibrium between air climate and soil climate.

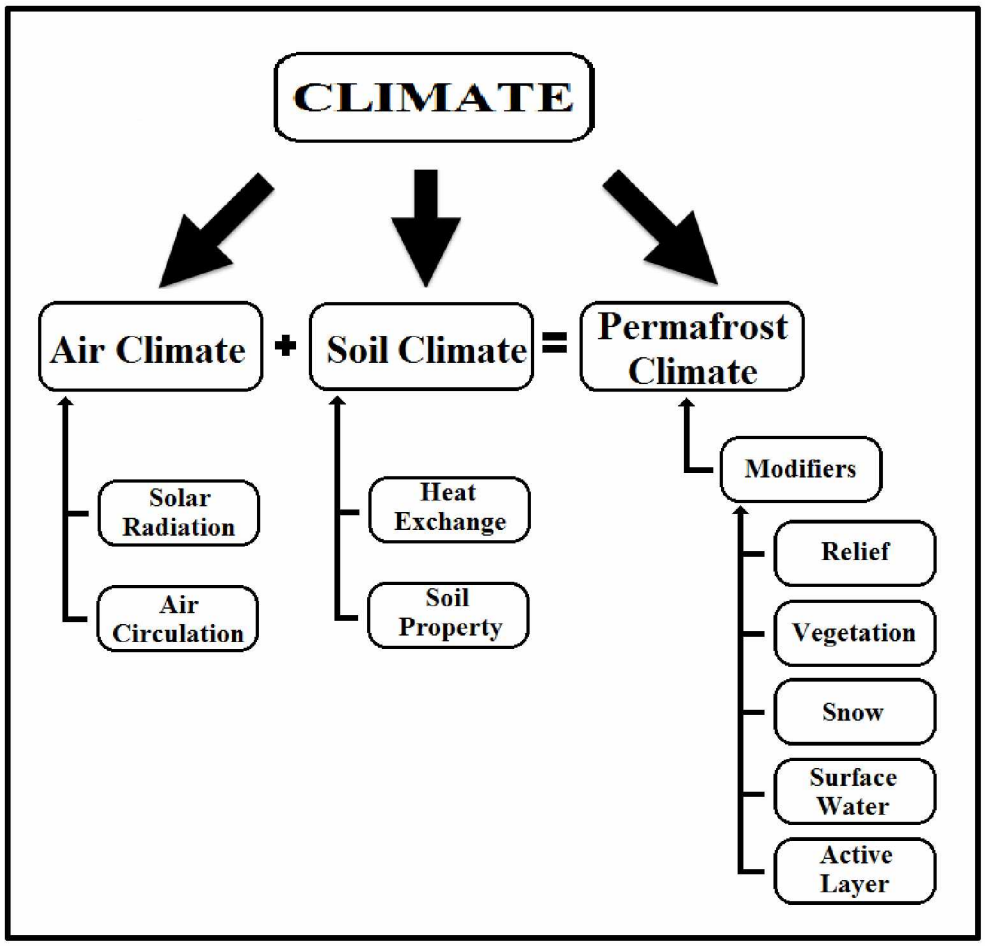

Figure 1.6: Factors contributing to climate.

In the second and third cases, modifiers play an important role, contributing to the existence of permafrost. In the second case, the local modifiers are not able to reduce the soil temperature due to the warm climate, whereas in the third case, the presence of modifiers like snow, relief, vegetation and soil is essential for permafrost to exist. These modifiers are also equally responsible for permafrost aggradation or degradation. Factors that influence annual changes in permafrost temperature include: air climate/temperature, presence of snow, soil or ground wetness and/or disturbances from humans, animals, and fire. Since the mid-1800s there has been

a global increase in the air temperature which has resulted in an increase in the permafrost temperature (Hansen and Lebedev, 1987). Figure 1.7 shows the temperature profile of permafrost with respect to different air temperatures. Though other modifiers do have an impact on the permafrost temperature, they also modify the effect of the air temperature on the permafrost temperature (Shur, 2014).

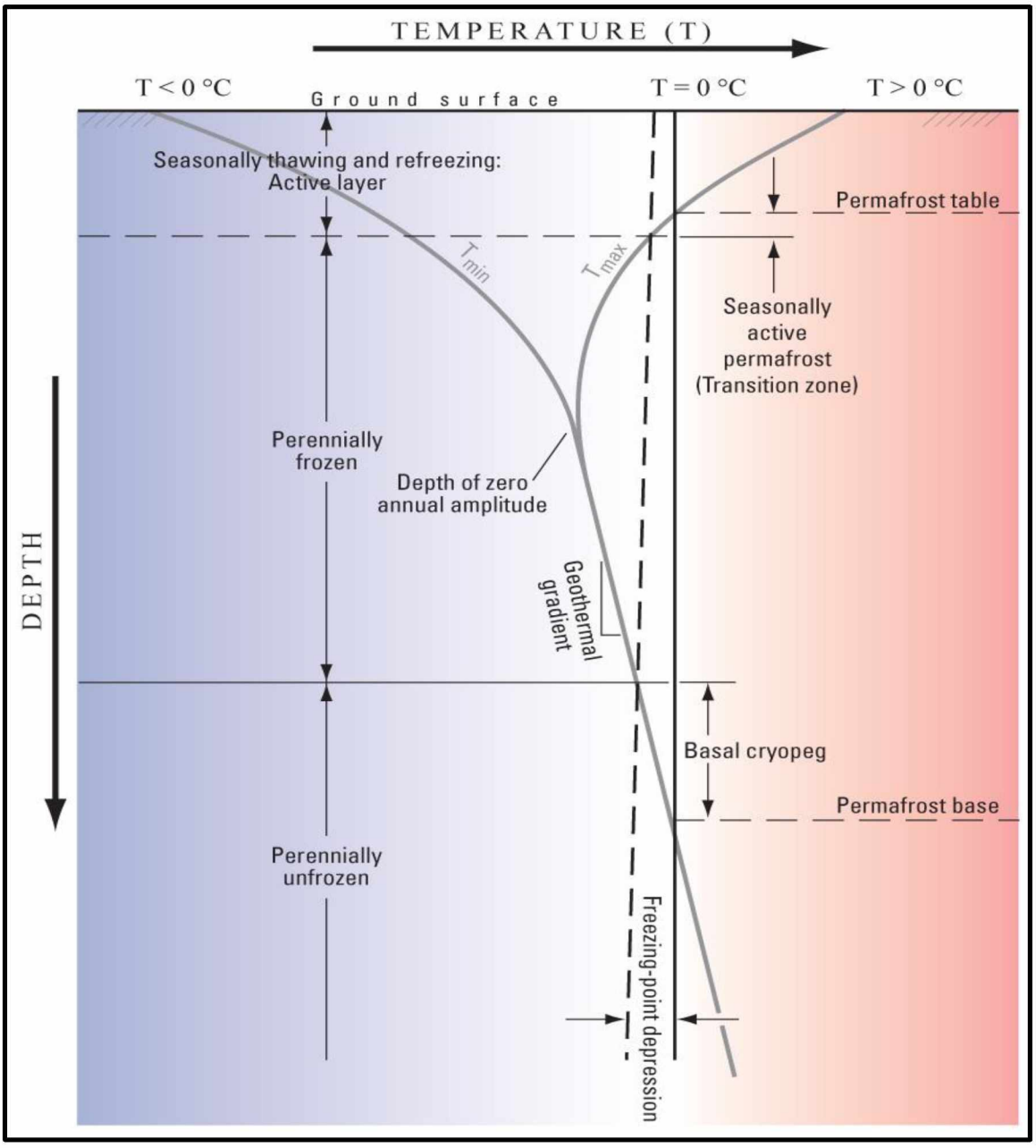

Figure 1.7: Terms used to describe ground temperature relative to 32°F in a permafrost environment. (Modified from van Everdingen et al., 1985) (http://pubs.usgs.gov/pp/p1386a/gallery5-fig01.html)

1.5 Permafrost in Alaska

Around 25% of the land on Earth is underlain by permafrost and 80% of Alaska is underlain by permafrost (Osterkamp and Jorgenson, 2009). Figure 1.8 shows the projected distribution of permafrost in Alaska. It is thickest in the northern part of Alaska, i.e., north of the Brooks Range (Figure 1.10). As shown in Figure 1.9, continuous permafrost lies mostly in northern Alaska, with discontinuous permafrost in the Interior and sporadic and isolated permafrost in southern Alaska. There is no sharp permafrost boundary between the different permafrost zones in Alaska (Shur, 2014).

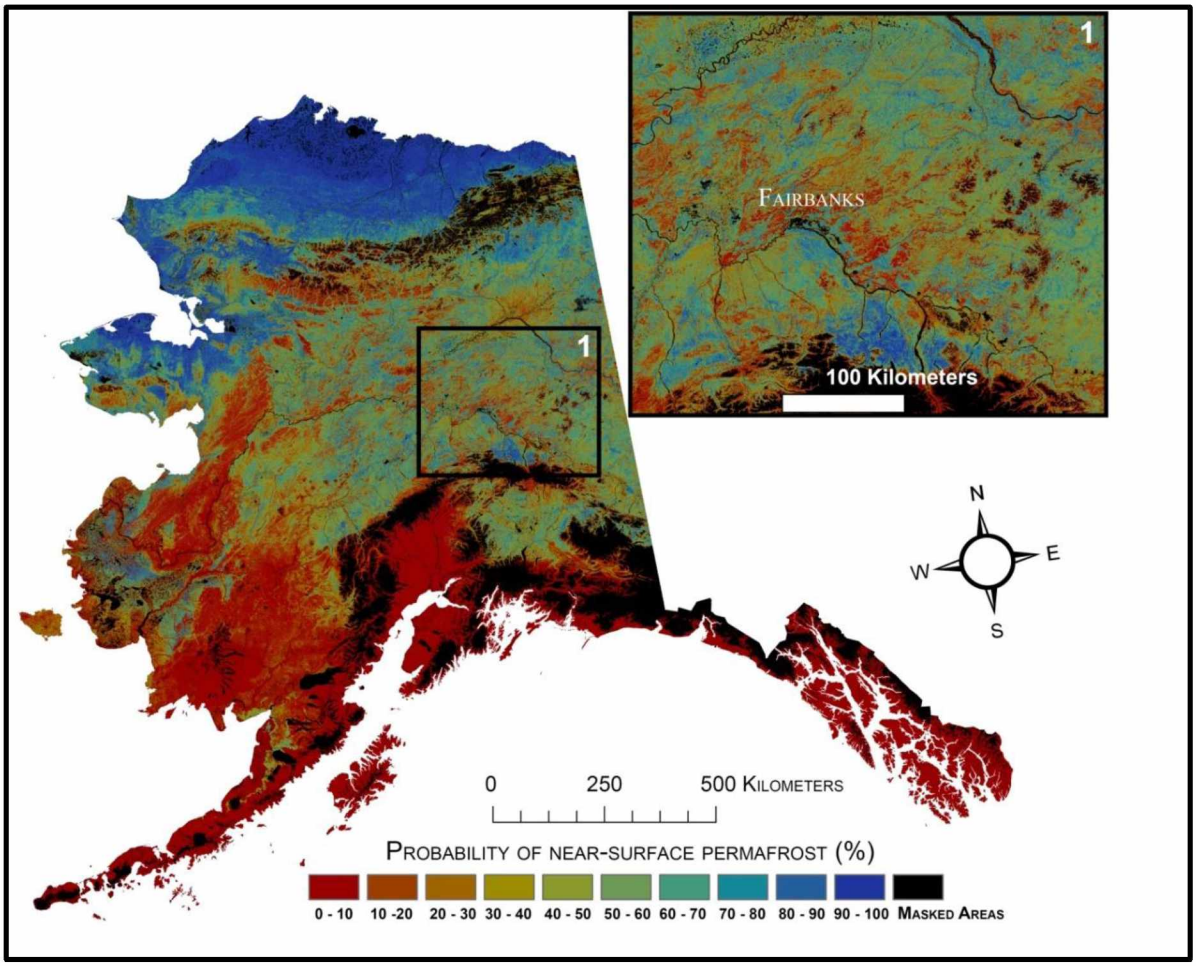

Figure 1.8: Occurrence of permafrost in Alaska.
(http://www.usgs.gov/newsroom/images/2015_11_30/ak_current.jpg)

According to Kanevskiy and others (2011), the area north of the Brooks Range has continuous permafrost and is mostly ice-rich (near surface) due to the presence of massive ground ice bodies

at various depths. The permafrost is approximately 200 to 400 m thick and reaches depths of 600 m in the Prudhoe Bay area. The most common type of massive ice found is ice wedges and most of the area is occupied by ice wedge polygons, as shown in Figure 1.11.

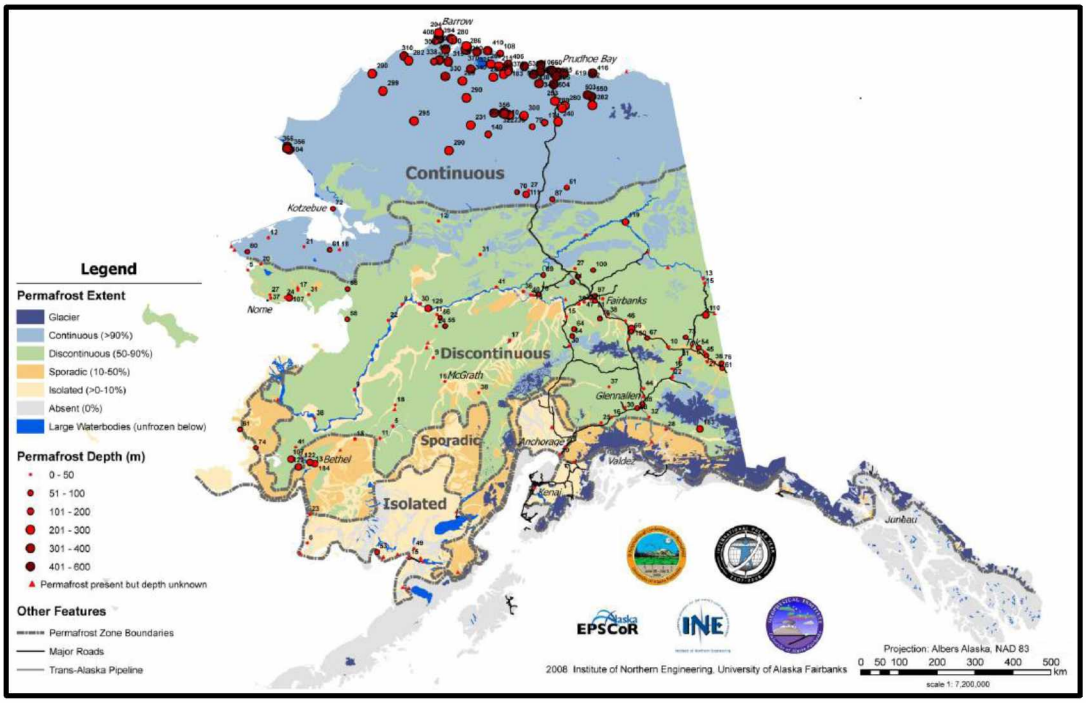

Figure 1.9: Different permafrost zones in Alaska. (http://permafrost.gi.alaska.edu/sites/default/files/AlaskaPermafrostMap_Front_Dec2008_Jorgenson_etal_2008.pdf)

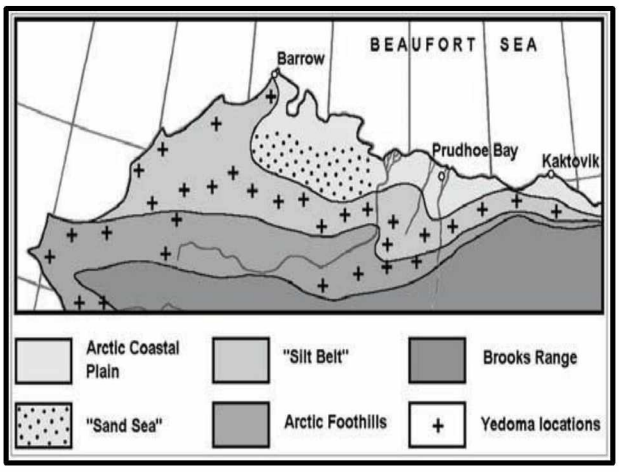

Figure 1.10: Permafrost regions of northern Alaska. (Kanevskiy et al., 2011)

Figure 1.11: Ice-wedge polygons in northern Alaska. (http://gallery.usgs.gov/images/12_17_2015/yd72WkjVVQ_12_17_2015/large/A106AK_img_9434.jpg)

Figure 1.12 shows a brief explanation of how these ice wedges were formed. The only areas that are not occupied by ice wedges are exposed bedrock or the fresh eolian, deltaic and marine deposits. Another form of ground ice found in this area is porous and segregated ice. Soil cryostructures or cryogenic structures are patterns made by ice inclusions in frozen soil (Shur, 2014). The active layer in this region is mostly thin and saturated. The average thickness of the active layer in this region is in the range of 0.5 to 1.5 m. The minimum thickness is 0.2 to 0.3 m, which is typical of organic soils.

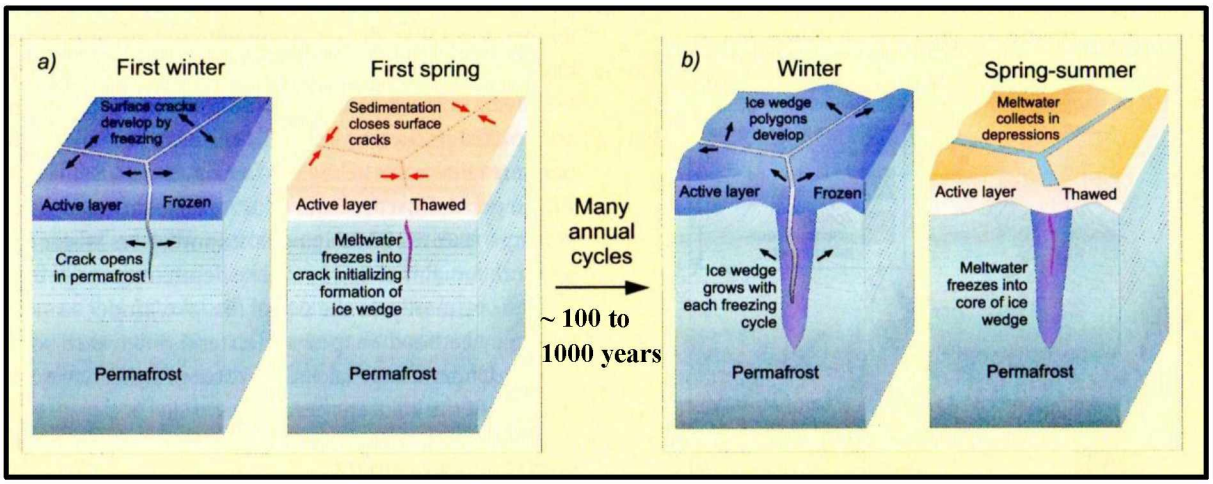

Figure 1.12: Ice wedge formation.
(https://classconnection.s3.amazonaws.com/324/flashcards/3374324/jpg/formation_of_an_ice_wedge-142EA0033D9222134ED.jpg)

Permafrost related hazards like thermokarst and thermal erosion occur in this region, mainly as a result of the increased thickness of the active layer (Kanevskiy et al., 2011). This happens due to disturbances to the tundra terrain like removal of vegetation (peat or moss) by natural activities (like tundra fire) or human activities (like construction work, vehicle movement, etc.). Thermokarst is defined as "the process by which characteristic landforms result from the thawing of ice-rich permafrost or the melting of massive ice" (Page no. 83, R. O. van Everdingen, 1998).

1.6 Permafrost Thaw Subsidence

The northern part of Alaska is rich in hydrocarbon resources. Most of these hydrocarbon reservoirs are overlain by massive layers of permafrost, which extend to a thickness of 2300 feet (~700 m). Many petroleum operators have shown interest in exploring and developing these

hydrocarbon resources. Drilling, completion and production operations in such regions may create certain design and operational issues with regard to maintaining well integrity, since all these operations will lead to thawing of the frozen permafrost soils. Drilling an oil and gas well causes an enormous amount of disturbance to the thermal regime of the permafrost body, leading to its change of state. From a well completion point of view, thawing permafrost will further cause problems for maintaining well integrity for a long period of time.

When producing hot oil from the production wells, there is a continuous heat loss from the wellbore in the radial direction into the surrounding frozen soils. This heat transfer between the wellbore and the permafrost will cause the frozen soil to thaw with time. Other than this, there are some other factors that make oil and gas operations more difficult in the Arctic region. These factors include: extreme cold surface temperatures, affecting the working crew, surface facilities and equipment; a geographic location close to the magnetic north pole, creating problems for directional drilling practices; the presence of tundra which thaws and freezes annually, causing problems for onshore operations; and the presence of thick sea ice, causing problems for offshore operations (Goodman, 1978). Other than these problems, one of the major problems for an oil and gas well in the Arctic region is that of subsidence, also known as permafrost thaw subsidence.

Due to years of production of hot oil, the radial heat transfer between the wellbore and permafrost leads to continuous thawing of the frozen soils. With time the well loses its ability to hold strongly to the surrounding soil and thus loses its support, leading to casing, buckling and/or collapse. This results in well abandonment, causing extreme economical losses and safety issues. Thawing permafrost causes a phase change from ice to water, resulting in a ~9% volumetric reduction of the frozen soil due to pore space contraction and segregated ice thaw. This further leads to compaction of the thawed soil, which induces continuous loads on the wellbore (Goodman, 1978). Permafrost thaw subsidence will be discussed and studied in more detail in the coming chapters.

CHAPTER 2 LITERATURE REVIEW

2.1 Heat Transfer

2.1.1 Basic Theory

Heat transfer is a process involving transfer of energy from one point or body to another point or body. This transfer is triggered when there is thermal disequilibrium in a system. The transfer of energy is from higher temperatures to lower temperatures and continues until the system reaches thermal equilibrium. The rate of heat transfer depends on the temperature difference between two bodies: the greater the difference, the greater the rate of transfer. It acts as a driving force in the heat transfer process. Another parameter to be taken into consideration is the thermal resistance offered by the medium of the heat transfer. The rate of heat transfer is inversely proportional to the thermal resistance of the heat flow medium.

Heat transfer can occur in three ways: conduction, convection and radiation. In this study, the main focus was on heat transfer through conduction. This is because there will always be direct contact between the wellbore and surrounding permafrost soils. In conduction, heat is transferred when there is direct contact between two bodies at different temperatures. Molecular energy is transferred from one molecule with greater energy to neighboring molecules with lesser energy (https://elearning.vtu.ac.in/P5/enotes/BT32/Unit5.pdf). The equation for rate of conductive heat transfer can be written as

$$\frac{\mathrm{d}Q}{\mathrm{d}t} = \frac{\mathrm{d}T}{\mathrm{d}x} \times k\,A \tag{2.1}$$

where Q is the heat in Joules, t is time in seconds, T is temperature in °C, x is the distance covered during heat transfer, k is thermal conductivity in J/m s °C and A is the area in m². The term "$k\,A$" is conductance, the reciprocal of resistance. Equation (2.1) is known as the Fourier equation for heat conduction.

2.1.2 Heat Capacity and Latent Heat

The transfer of energy during heat transfer happens from higher temperatures to lower temperatures and continues until there is thermal equilibrium in the system. Heat capacity can be

defined as the ratio of the heat added to (or removed from) an object during heat transfer to the resulting temperature change (https://en.wikipedia.org/wiki/Heat_capacity). It is also known as thermal capacity, meaning the amount of energy taken up or given out by a system to reach a particular temperature from its current temperature. Heat capacity is a measurable physical property and its SI unit is Joules per kelvin ($J\ K^{-1}$). It is an extensive property of a system, which means it depends on the size of the system. Thus the amount of heat required by a system to raise its temperature by 1°C is termed its specific heat capacity.

The amount of energy taken up or given out by a system during a constant temperature heat transfer process is termed the latent heat. The latent heat of fusion is the amount of heat required to change the phase of an object or body from solid state to liquid state. In the study of impact of permafrost thawing on the wellbore, specific heat capacity and latent heat play a very important role, since thawing of the frozen soils leads to phase change of ice to water. The amount of radial heat penetration into the frozen soils depends on the specific heat capacity of different soils in the formation. The greater the specific heat capacity of the soil more will be the heat needed to change the temperature, and thus less heat will penetrate further into the formation radially. The rate of permafrost thawing decreases with time primarily because of the latent heat effects. These two thermal properties, along with thermal conductivity, are very important for carrying out a successful thermal analysis for a well-soil system in the Arctic region.

2.2 Behavior of Permafrost around a Wellbore

Permafrost in the North Slope is continuous from the surface. It may or may not contain some unfrozen water zones at greater depth. The thickness of the permafrost can be more than 2000 feet, consisting of different layered soil lithologies of clay, silt, sand and gravel. The continuous radial heat transfer from the wellbore to the surrounding frozen soils leads to many design and operational challenges for developing and producing from an oil well in the Arctic region. Any kind of operations in the Arctic region will disturb the thermal balance of the permafrost and could ultimately end up thawing it. Thaw subsidence is the major problem caused by continuous thawing of permafrost with time. According to Goodman (1978), thaw subsidence happens because of four different but interrelated mechanisms which include melting of excess ice, soil consolidation accompanied by fluid expulsion, pore pressure reduction and stiffness reduction. These four mechanisms are further expanded on below.

2.2.1 Melting of Excess Ice

Melting of excess ice present in the permafrost soil layers is primarily concentrated in near surface permafrost. Excess ice can be present in more than one form: as massive ice bodies or as segregated ice; or second, in the form of ice films around the soil particles. In the North Slope, it is believed that the excess ice is primarily present up to depths of ~50 feet (Goodman, 1978). Though this concept is simple in nature, it should be taken into consideration first while designing an Arctic oil and gas well. Melting of excess ice results volumetric reduction of the soil volume, which may result in the wellbore losing soil support due to the instability of the formation, the wellbore integrity is affected greatly.

2.2.2 Fluid Expulsion Along with Thaw Consolidation

Consolidation of weak thawed soils accompanied by fluid expulsion is also a near surface phenomenon (Goodman, 1978). For this mechanism, the presence of excess ice is necessary; otherwise it would cause a reduction instead of initial increase in pore pressures. As the excess ice melts, it produces pressures exceeding the hydrostatic pressure that causes the pore fluid in the soil to flow out of the thawed zone, leading to consolidation of the thawed soil. Thus melting of excess ice is followed by consolidation of weak thawed soils accompanied by fluid expulsion (Figure 2.1).

2.2.3 Pore Pressure Reduction

According to Goodman (1978), pore pressure reduction is considered the most important mechanism for permafrost thaw subsidence. As the pore ice thaws with time, leading to an increase in pressure due to phase change contraction and fluid expulsion, the fluid pressure inside the pore increases initially and later decreases gradually. It reaches zero in the case of fine-grained soils and a small amount of water head in the case of coarse-grained soils. This pore pressure reduction generates effective stress within the soil grains, causing soil compaction and further generating loads to act on the wellbore. Figure 2.2 gives a brief idea about the soil compaction due to pore pressure reduction, caused by thawing and different natural existing loads (like overburden loads, etc.). The pore pressure reduction is greater in the center and nearly zero at the top and bottom of the permafrost soil layers. It acts across the interface of thawed and

frozen soil zone during radial progression of thaw front with time, further generating loads in the vertical direction.

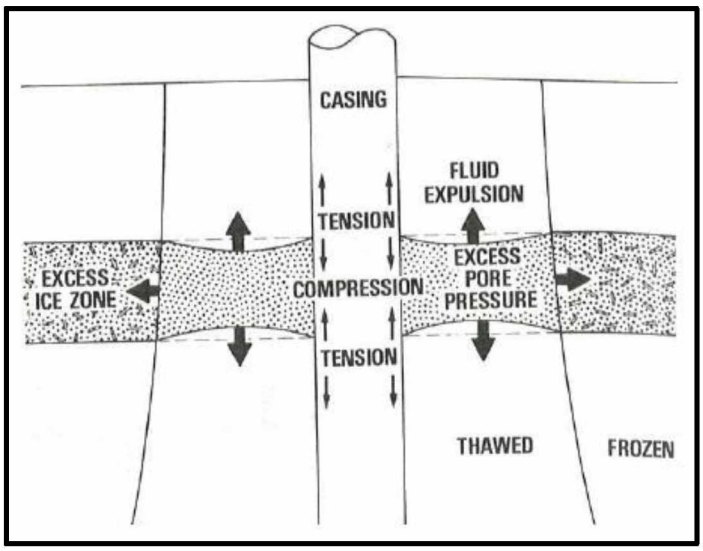

Figure 2.1: Melting of excess ice causing consolidation of thawed soil accompanied by fluid expulsion. (Goodman, 1977)

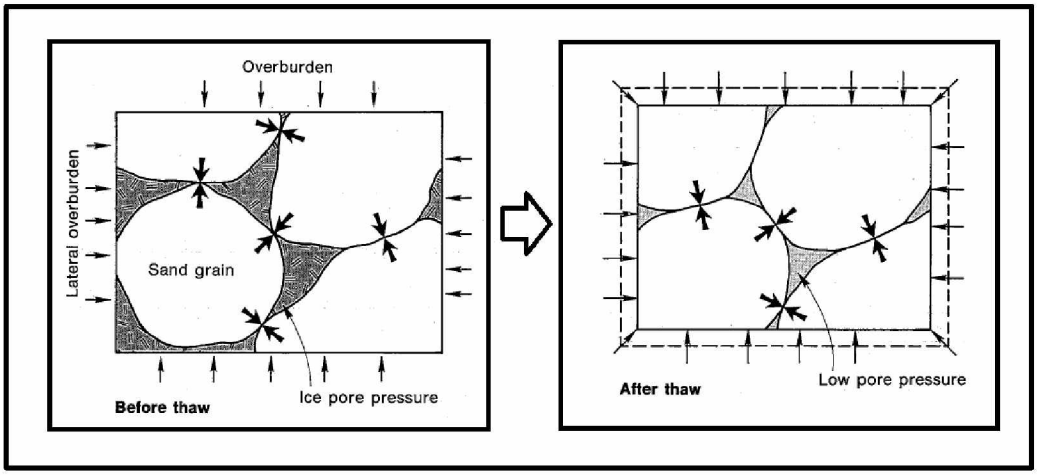

Figure 2.2: Soil compaction due to pore pressure reduction. (Goodman, 1978)

2.2.4 Stiffness Reduction

According to Goodman (1978), stiffness reduction is believed to be the result of all three mechanisms discussed above. As the pore ice melts it causes soil consolidation accompanied by fluid expulsion because of pore pressure reduction. All of these processes cause the soil to become weak and lose strength because the soil loses its support from the pore ice and deforms.

The loads generated by thaw subsidence are very significant and must be considered while designing and developing an oil and gas well in the Arctic region. Vertical deformations and the continuous lateral loads are some of the important factors which induce significant casing strain and must be taken into consideration for wellbore stability.

2.3 Factors Influential towards Permafrost Thaw Subsidence

Vertical settlements or subsidence and horizontal squeezing of soil occur as a result of weak thawed soil being generated due to continuous absorption of heat from the wellbore. According to Matthews and Zhang (2012), the response of thawed soil and the extent to which the frozen soil will thaw radially along the length of wellbore depends on a number of factors:

a. Soil lithology
b. Deposition (geological) history
c. Soil properties
d. Freezing and thawing conditions
e. Thaw discontinuity
f. Design and operation of oil well
g. Well completion design
h. Well spacing
i. Life of the wellbore.

2.3.1 Soil Lithology

In the multilayer permafrost formation, the layering of different soil lithologies and their associated thermal and mechanical properties and drainage conditions post thaw are very significant factors for understanding the nature of loads induced during vertical and horizontal displacements. Compression is generated along the wellbore in the fine-grained soil zone (Figure 2.3) due to phase change contraction, followed by compaction of soil and fluid expulsion into the coarse-grained soil zones above and below it, which generates tension along the wellbore (Figure 2.3) (Goodman, 1978).

The type of soil in the multilayer permafrost formation has a direct impact on soil strength and deformation response during progressive thaw. Due to differences in the depositional environment in the Arctic region, the permafrost soil lithology differs greatly over an area covered by a single large hydrocarbon reservoir (Matthews and Zhang, 2012). This should be an important consideration when deciding the location for a well pad or offshore structure and designing the layout of a well and surface facilities. Segregated ice present in permafrost soils significantly contributes to thaw subsidence behavior. Knowledge about the soil lithology and its depositional history can provide an estimate of the presence of segregated excess ice.

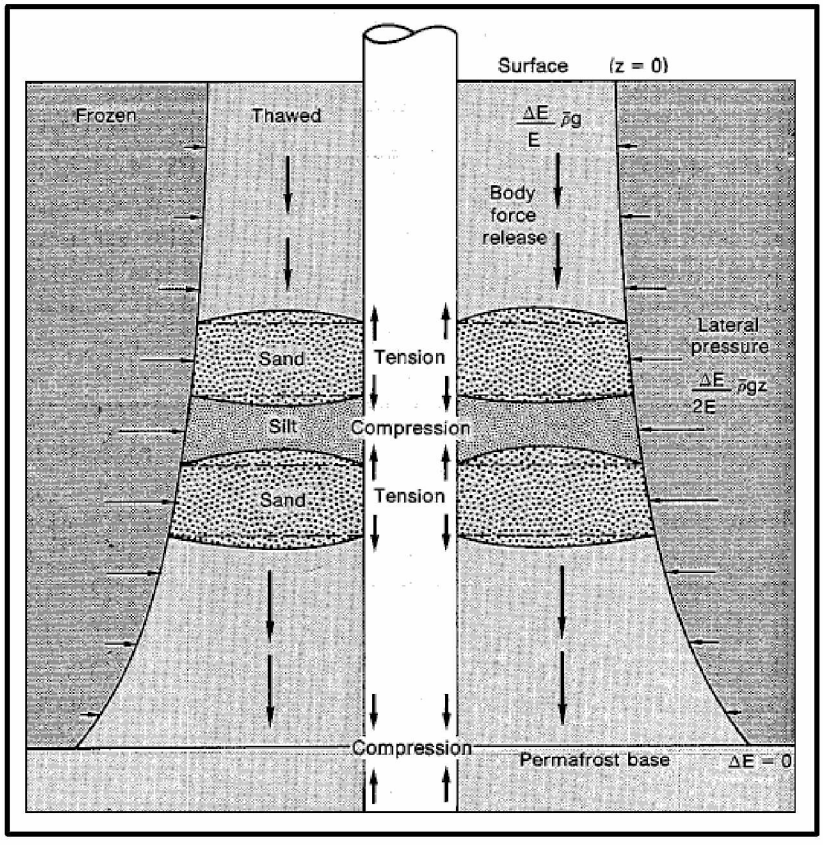

Figure 2.3: Compression and tension forces generated due to difference in soil types. (Goodman, 1978)

2.3.2 Deposition History and Freezing and Thawing Conditions

The presence of pore ice in permafrost contributes to the stability and in-situ strength of the soil. The local depositional and freezing history has an impact on the in-situ consolidation state of different types of permafrost soils. There can be two possibilities under which freezing would

have occurred, first, after the sediments were deposited and consolidated (epigenetic permafrost) or second, along with the sediment's deposition (syngenetic permafrost). If any particular soil zone is being consolidated when it's frozen, or was already frozen before the deposition of the soil above it, then it can be said to be in the underconsolidated state with respect to the existing overburden pressure. Post thaw, the overburden pressure will tend to consolidate the underconsolidated soil zone by compressing it. The densities of fine-grained soils, such as clay or clayey silt depend on the overburden pressure, while those of coarse-grained soils like sands and gravels are not dependent, for greater depths of permafrost. Thus deformation and displacement of soil is greater in the clay and clayey silt soil zones than in the coarse-grained soil zone due to thawing of the underconsolidated fine-grained soils (Smith and Clegg, 1971).

2.3.3 Well Geometry and Spacing

The design (layout) and arrangement of different production and injection wells installed on a single well pad onshore or on a single offshore platform affect the extent of thaw in the multilayer permafrost formation. The amount of heat transfer from a group of wells will have an enormous impact on the frozen soils compared to the impact of heat transfer from one single well. Individual oil wells producing individual thaw bulbs with time, when placed together horizontally, would end up forming a bigger converged thaw bulb. This would cause loss of vertical support at the thawed-frozen interface and further affect the tensile and compressive strain response of the whole system due to the closely spaced oil wells (Goodman, 1978). This results in greater subsidence loads due to loss of support and compaction of the surrounding soft thawed soils due to excess heat input from a group of wells (Matthews and Zhang, 2012). Thus, spacing of producing oil wells can alter the nature of thaw settlement significantly.

2.3.4 Thaw Discontinuities

Unfrozen water is believed to be present in frozen soils. This is due to the salinity of pore water causing a freezing point depression leading to unfrozen water in the pores of the soil even at temperatures of 30°F (Matthews and Zhang, 2012). The presence of unfrozen water affects the in-situ stress state and thermal properties of the permafrost soil. Such variations in the layered permafrost formations and in the thermal properties cause an increase in the wellbore strains. Effects due to reduction in pore pressures and further stiffness reduction tend to act horizontally,

resulting in a compressive squeeze in the vertical direction (Goodman, 1978). The presence of unfrozen water is mainly influenced by the salt ions in the pore fluid, total pore pressure, differences in soil grain size and soil type (Matthews and Zhang, 2012).

2.4 Behavior of Permafrost Soils upon Thaw

Coarse-grained and fine-grained soils have different freezing and thawing characteristics and post thaw deformation responses. According to Matthews and Zhang (2012), coarse-grained soils, being highly permeable in nature, tend to freeze under open drainage conditions at the existing in-situ freezing rate. Because of this, there is not much excess ice formed within them and the void ratio (porosity) and effective stresses tend not to change upon freezing. Upon thawing, again due to free drainage conditions, the void ratio and effective stresses remain unchanged. However, when a layer of highly permeable coarse-grained soil is between two layers of low permeability fine-grained soils (Figure 2.4), upon thaw under closed drainage conditions it will receive water from the top and bottom, which will decrease the soil's effective stresses. This happens mainly due to reduction of pore pressure (Section 2.2.3) in the fine-grained soils as pore fluid tends to flow from fine-grained soil to coarse-grained zones to achieve equilibrium.

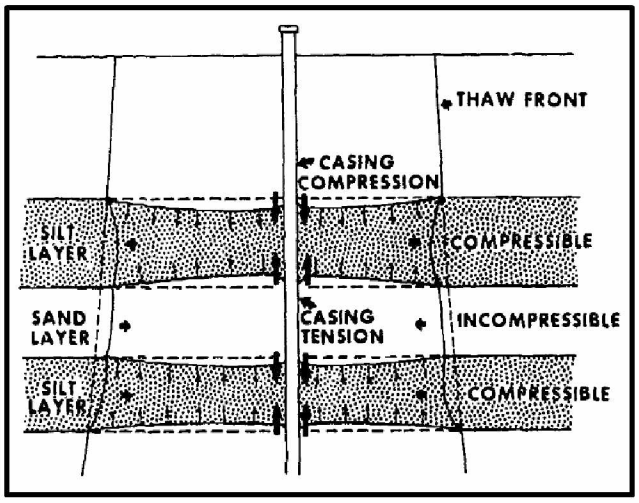

Figure 2.4: Behavior of coarse-grained soil vs fine-grained soil upon thaw. (Mitchell and Goodman, 1978)

Fine-grained soils tend to form ice lenses due to their fluid-retaining characteristics because of low permeability. Upon freezing, under open drainage conditions, they suck in water from the

surrounding coarse-grained soil and freeze just behind the freezing front. Even at great depths, segregated ice (ice lenses) is formed when there is a balance between the freezing rate and the water supply. An open drainage condition and a sufficient supply of water lead to the growth of ice lenses. In a closed drainage system, the probability of forming ice lenses is less, though they can form from water already present in the soil.

Mostly thawing of fine-grained soils occurs under closed drainage conditions. This is due to the fact that they have very low permeabilities compared to coarse-grained soils. Due to pore pressure reduction, due to melting of pore ice, there is a phase change contraction that causes a decrease in volume of the fine-grained soils. This is also because of high compressibility of fine-grained soil compared to coarse-grained soils. Initially there is an increase in the pore water pressure, causing them to swell or deform under undrained conditions. After the thawing period, the pore water pressure gradually reduces, increasing the effective stresses and decreasing the void ratio. In the case of fine-grained soils under open drainage condition, there is comparatively more thawed soil deformation or consolidation than under closed drainage conditions.

2.5 External and Internal Freezeback

Multilayer permafrost soil thaws due to drilling and production operations. However, if a well is shut in for a period of time after drilling or after a period of hot oil production, the heat transfer from the wellbore to the surrounding frozen soil decreases gradually. Because of this, the thawed permafrost tends to refreeze to achieve thermal equilibrium. When the outside thawed soil freezes again, it produces significant amounts of pressure on the wellbore, which can cause serious damage to the casing string and crack the outside cement layer. These pressures are generated because the thawed soil refreezes, due to which there is a volumetric or phase change expansion wherein the extra volume tries to forcibly fit in the system in order to achieve equilibrium. This generates a large load on the wellbore because of the enormous heave pressure due to soil expansion. The refreezing of permafrost does not recreate the same state of the soil as it was prior to thawing. This is an irreversible process wherein refreezing does not recover the soil consolidation caused by thawing. Freezeback pressures increase gradually as the thawed soil refreezes with time. The thawed permafrost soil does not need to refreeze completely to generate massive amounts of pressure on the wellbore (Goodman, 1978). The casing damage can also be caused by freezing of the fluids inside the wellbore. Annular fluids and excess water left in the

drilling mud post drilling due to improper mixing freeze, which impacts the inner strings directly. This is known as internal freezeback. It is known that pressures up to 10000 psig can be generated by internal freezeback and up to 2000 psig in the lower permafrost by external freezeback (Davies et al., 1979).

2.6 Thaw Subsidence Loading

The different vertical, horizontal and other interactive forces in the well-soil system (due to four mechanisms discussed in section 2.2) generate large amounts of loading along the wellbore due to variation in lithology and well geometry/spacing. Figure 2.5 shows most of the forces acting on the wellbore due to thawing of ice-rich permafrost soil. Thaw subsidence is not a stress-induced problem; rather, it is a strain-induced problem. The stress is a result of thawing of permafrost, soil consolidation, and displacement induced strain effects on the casing. The casing strain effect is controlled by the permafrost soil deformation (Goodman, 1977). According to Goodman (1977), phase change contraction induced casing strain is only due to excess ice melting in the near surface region of the permafrost formation. The volumetric reduction tends to create void space in the soil zone, causing it to slump because of the weight of the soil (overburden pressure), and also uplifting the underlying soil due to the reduced stress state in the void space. Both of these actions compress the casing.

Consolidation of thawed soil with fluid flow occurs mainly in the underconsolidated soil zone, which is frozen and contains excess ice. This also accounts for the post thaw interactive forces between the fine-grained and coarse-grained soil layers. It is a process in which excess pressures are generated post thaw, causing pore fluids to move in order to achieve equilibrium in the soil system. The excess ice present in the soil pores should be more than ~9% of the pore space to have the initial excess pore pressure for fluid expulsion, or else there would be a direct reduction of pore pressure with no fluid expulsion. Even if there is not much excess ice present, the soil would still try to consolidate/deform upon thaw because of its underconsolidated state prior to thawing. Thus soil instability or displacement is due mainly to the initial excess pore fluid pressure and/or underconsolidation states of frozen soil. It decreases the effective stresses in the soil system, causing loss of shear support and bearing capacity of the soil.

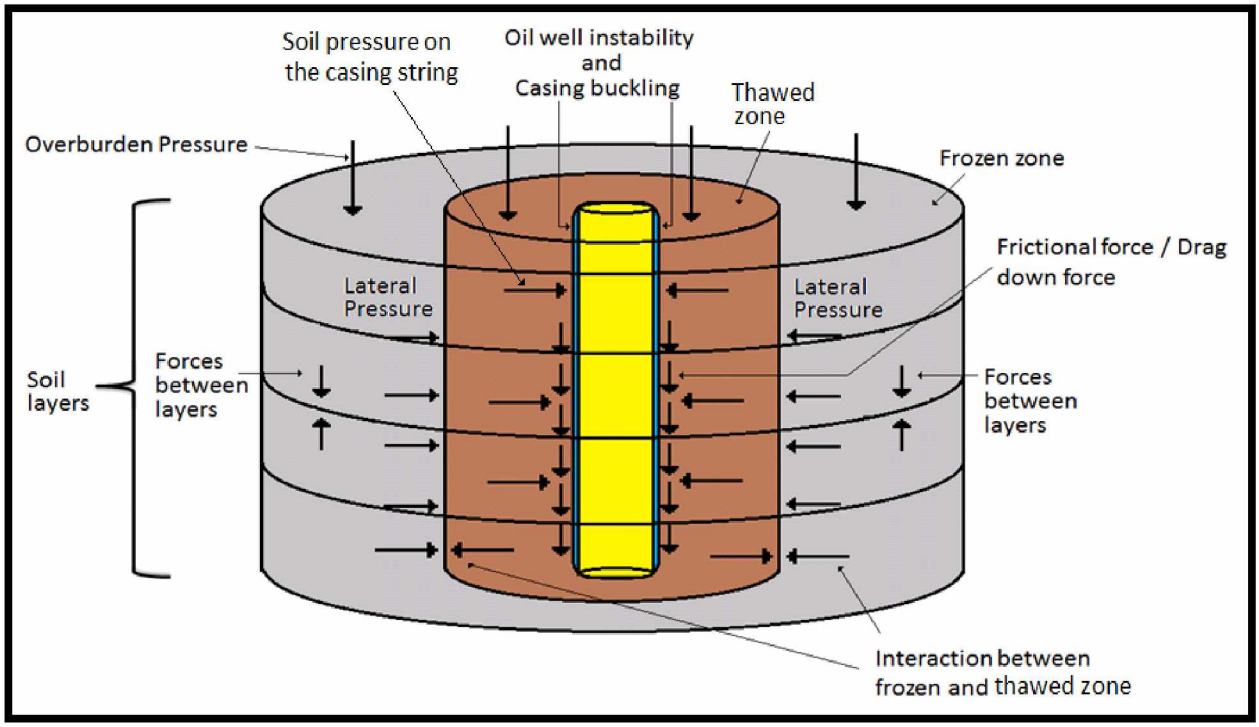

Figure 2.5: Different pressure forces acting on the casing string in the thawed zone.

The thaw settlement effects due to reduction in pore pressure are believed to be significant in the consolidated soil zone or in nearly compacted soil, mainly in the deep permafrost zone. The deep permafrost zone can be considered consolidated because it was deposited and compacted prior to freezing. Thus the presence of low permeability fine-grained soils would bind the flow of water between soil layers (Goodman, 1977), creating conditions for concentrated pore pressure reduction (Figure 2.6). The mechanical properties of thawed and frozen permafrost soils are different and because of it stiffness reduction causes soil deformation and further subsidence problems due to the effect of gravity. This is because thawed soils are weak and/or soft and can thus deform easily. Stiffness reduction is mainly a result of loss of shear support from pore ice. This is because as the pore ice melts, the soil in the underconsolidated state consolidates. Stiffness reduction can lead to complex loading conditions across the fine-grained and coarse-grained soil layers in permafrost formations (Figure 2.3) with varying lithology and some underconsolidated soil (Goodman, 1977).

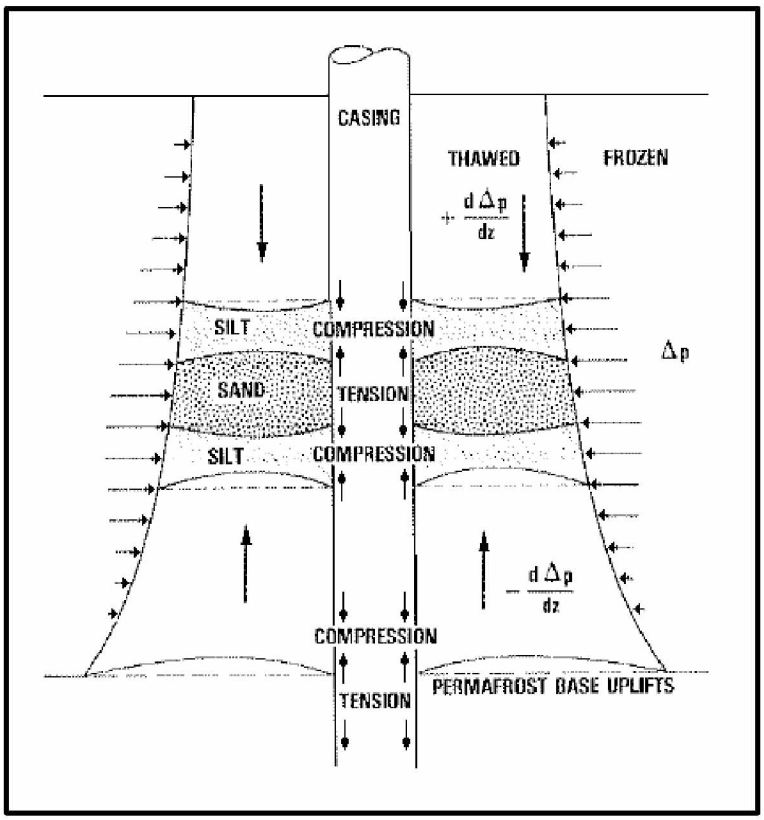

Figure 2.6: Loading caused by pore pressure reduction. (Goodman, 1977)

2.7 Summary of Mechanisms and Factors influencing Permafrost Thaw Subsidence

All four mechanisms responsible for thaw settlement induce continuous casing strain with alternating compression and tension forces on the casing string depending upon the lithology of the permafrost. Phase change contraction and post thaw soil consolidation occurring in the soil zone would cause compression forces to act on the adjacent casing and tension forces in the zones above and below it. Stiffness and pore pressure reduction causes inward pressing of the thawed-frozen interface due to alternating tension-compression forces. The nature of interactive forces between soil layers and the increasing casing strains depend mostly on soil type and variations in thermal and mechanical properties. Lateral deformation of soil due to inward squeezing forms a vertical thaw front, causing sloughing of soil in an unsupported drilled hole or generating lateral pressure on the casing.

Phase change contraction and thaw consolidation with fluid expulsion occurs mainly in the near surface region, which is rich in excess ice and underconsolidated, whereas pore pressure and stiffness reduction occur in the deep permafrost regions where the soil zones are consolidated or nearly compacted. Vertical body force loads are generated by pore pressure and stiffness reduction, which make the thawed soil 50% heavier (Goodman, 1977) and generate continuous lateral loads because of inward pressing of the thawed-frozen interface. The magnitude of loads generated by pore pressure and stiffness reduction can be of the same order.

2.8 Previous Work Described in the Literature

Couch et al. (1970) defined a mathematical model for describing the heat conduction and convection process between a well consisting of a maximum of four casing strings and the surrounding permafrost. The model's main product was the time-dependent temperature distribution around a production well assuming two-dimensional radial-vertical heat transfer. The model took into consideration not only the radial heat transfer but also the vertical heat exchange within a multilayer permafrost formation. It also took the latent heat of fusion into consideration for modeling the phase change of ice to water. The model was used for testing different completion schemes and in decision making of appropriate insulation requirements for production tubing. Results calculated were for a 1400 -foot permafrost section with insulation for the top 700 feet of the tubing.

Smith and Clegg (1971) did detailed modeling of the unsteady state heat flow causing permafrost thawing with production of hot oil. They took into consideration the dependence of thermal and mechanical properties on the heat transfer process and the resulting thaw settlement, respectively. They modeled the time-dependent heat conduction process in different permafrost soils by making a two-dimensional axisymmetric model, including different permafrost characteristics. They modeled thaw subsidence and did analytical calculations of the stresses generated during the radial movement of the thawed soils. Their simulation work was based on an assumption that the permafrost thawing depends on the temperature difference between the wellbore and the surrounding soil, the thermal properties of different permafrost soils and the well completion design. The simulation results showed a rapid rate of thawing for the initial 20 years of production followed by a comparatively slow rate of thawing.

The study involved a few other important considerations for soil deformation and movement, such as, the soil contains segregated ice, it is in a underconsolidated state relative to the overburden, interstitial ice carries a certain fraction of the overburden and tries to stabilize the soil matrix, and the soil contains low permeability zones with poor water supply. The well design had a 20 inch diameter of 94 lb/ft casing until 750 feet followed by a 13 3/8 inch diameter of 72 lb/ft casing up to 2350 feet, both cemented to the surface. Along with this it had a 7 inch diameter oil string insulated with 2.5 inch polyurethane foam until 750 feet depth. Calculations for this design resulted in a bell-shaped thaw profile with body force of 50 lb/ft^3 due to thawing from 750 to 1600 feet depth and then linear body force until 1800 feet depth. Casing stresses due to soil movement were calculated to be 25000 lbf/in^2 tensile stresses at a depth of 750-800 feet and 28000 lbf/in^2 compressive stresses at the permafrost base. If insulation is extended for the entire well, it would result in lower casing stresses, 1500 lb/in^2 tensile stress at 1200 feet and 5000 lb/in^2 compressive stress.

Davies and Boorman (1973) discussed in detail the field experiment carried out by BP Alaska at Prudhoe Bay. The experiment involved drilling two wells, namely, well A and well B, and then circulating hot oil at an inlet temperature of ~190 °F for a period of 12 months. At frequent time intervals during the 12 month period, the temperature distribution, thaw radius, thaw settlement, casing strains and freezeback were analyzed. The design of two wells is given in Table 2.1. At the end of the 12 month period, the surrounding frozen sandy soils thawed up to ~11 feet with negligible casing damage. Well A exhibited soil settlement at a depth of 300 feet and well B at a depth of 650 feet. Not much evidence of casing strains was noticed in the upper part of both the wells, but there was small soil displacement below 700 feet in both wells.

Table 2.1: Design of wells for the BP Alaska Field experiment (Smith and Clegg, 1971)

Information	Well A	Well B
$13\frac{3}{8}$ in surface casing set at	73 ft	73 ft
Hole size—$12\frac{1}{4}$ in to	2400 ft	2700 ft
$9\frac{5}{8}$ in N-80 47 lb/ft casing set at	2108 ft	2483 ft
Cemented from total depth to	surface	2013 ft
$2\frac{3}{8}$ in tubing set at	1997 ft	1980 ft
Base of Permafrost	1850 ft	1850 ft

Merriam et al. (1975) followed the mathematical model prepared by Couch et al. (1970) and modified it by taking into consideration the heat flow inside of a casing. Their work concentrated on the thermal performance of insulated well-casing systems. The main purpose was to understand the thawing behavior of frozen soils with respect to different well-casing designs and development schemes. Due to variation of thermal properties with temperature and depth, the heat transfer process becomes more complex in the well-soil system. Results based on their model were for two different cases, insulated and uninsulated oil wells. Assuming 32°F as the thawing temperature for permafrost, thaw radii were calculated and plotted against each other for comparison. The model focused mainly on the heat flow characteristics of different insulation materials and aimed to identify an optimum insulated-casing design that would cause minimum thaw even at elevated oil flowing temperatures.

Ruedrich et al. (1978) described the casing strain results of a field test conducted by ARCO-Exxon Co., USA. The soil tends to compact on thawing and thus is subjected to high stress levels. The compaction depends on soil type, stress state prior to thaw, response of pore pressure and extent of thawed region. The field test involved a compact five-spot pattern of wells circulating a mixture of ethylene glycol-water at ~190°F with a rate of 1-1.5 bbl/min. The test site was very close to that of the BP Alaska field test because the lithology of the permafrost was already known. The thaw radius generated during the field test was equivalent to that generated by the end of 20 years of oil production. The maximum compressive strains generated were 0.13% and maximum tensile strains were 0.08%. The near surface soil displacements were on the order of tenths of a foot.

Mitchell and Goodman (1978) did a sensitivity analysis for three important factors which contribute to the thaw subsidence problem; pore pressure, thaw radius and lithology of permafrost.. Based on results for thaw subsidence effects through the field study done by Atlantic Richfield Co. and Exxon Co. USA (Ruedrich et al., 1978), they made an analytical model. In order to improve the accuracy of the model, they focused on different input parameters. The sensitivity study was mainly concentrated on the input parameters. They describe the mechanics of thaw subsidence in three parts: 1) the loads acting on the frozen and thawed parts of the soil; 2) the soil's mechanical response to the loads; 3) the casing's reaction to the soil deformation. Based on the sensitivity analysis results, compressive strains are more than

the tensile strains. Multilayered permafrost is responsible for producing tensile strains and compressibility ratio is one of the most important mechanical properties for the thaw settlement problem. Furthermore, compressibility strain tends to increase at a uniform rate with thaw radius and tensile strain tends to decrease at a slower rate with thaw radius.

Lin and Wheeler (1978) made a thermal model for predicting thawing behavior of different permafrost soils for different well completion designs. Their model was a modified version of the thermal model by Couch et al. (1970) and Merriam et al. (1975). They took the flow or production of a mixture of fluids through the pipe into consideration, while the older models only considered production of oil through the pipe. The results obtained for thaw behavior from the thermal model showed a good match with the different field results by ARCO/Exxon Co (Ruedrich et al., 1978). Later the model was applied to look into the effectiveness of different insulating schemes for the production wells.

Sengul and Brigham (1983) developed a numerical model for predicting the extent of thaw of permafrost soils. A computer model was used to apply the numerical model and get predictions for thaw radii for different permafrost soils. The numerical model generated results for heat transfer by conduction, taking into account the phase change due to latent heat. They plotted dimensionless thaw radii against dimensionless time and developed a correlation for predicting thaw radius by assuming a constant temperature of the well.

Xie (2009) did a detailed analysis of thaw subsidence and presented a numerical methodology for understanding the thaw settlement problem using Abaqus, a finite element analysis platform. The suggested methodology comprised four different analyses, namely, wellbore hydraulic and heat transfer analysis, geothermal analysis, geomechanical analysis and soil deformation analysis. These analyses were applied for both single and multiple well designs. The analysis was successful in establishing a relationship between different factors like operating conditions, formation thermal and mechanical properties, well completion design, soil deformation and displacement and casing deformation. The proposed methodology can be used with a great level of confidence for decision making and optimizing well completion design in the Arctic.

Xie and Matthews (2011) presented a detailed methodology for modeling and studying casing loading and deformation conditions occurring due to the major thaw subsidence problem. Their methodology was based on a five-step process:

1) Developing a permafrost lithology model, which included studying the geological characteristics of the permafrost and different properties of frozen soils in the multilayer permafrost formation.
2) Wellbore heat transfer analysis, which included the study of the process of heat exchange between the wellbore and the surrounding permafrost soils.
3) Geothermal analysis, which included quantification of thaw extent with time for each individual soil layer in the multilayered permafrost.
4) Geomechanical and soil deformation analysis, which included quantification of soil stresses, post thaw soil displacement and thaw settlement or surface subsidence due to progressive thawing.
5) Casing/formation interaction analysis, which included studying the loading effects on the casing integrity and on the serviceability of the designed well-casing system.

CHAPTER 3 OBJECTIVE OF THE STUDY

Permafrost thaw subsidence is an observed issue affecting current oil wells in Alaska's North Slope region. It not only affects the wellbore in the subsurface, but also has a severe impact on surface facilities. The main objective of this study was to understand permafrost thaw subsidence and the resulting formation instability of production wells at Alaska's North Slope by studying well-soil systems in the Arctic and the changes occurring within them with time during thaw settlement. The study was focused mainly on gaining a better perspective of the complex interaction between wellbore and soil during progressive thaw. Due to lack of data for the deeper permafrost layers, the mechanisms causing thaw subsidence are not yet well understood. Following are some of the summarized objectives addressed during the study:

a. Understanding and testing characteristics of different types of soils, that is, fine-grained (like clay and silt) and coarse-grained (like sand) soils, with respect to thawing and refreezing behavior of ice-rich permafrost.
b. Understanding the effect of layering of different soil types on the mechanisms causing thaw settlement. Multilayer permafrost formations interact with the casing differently depending on the adjacent zone of soil type.
c. Understanding and testing different factors affecting thaw settlement like lateral and vertical pressure development with time, pore pressure response, post thaw soil consolidation and ice content in different soil types.
d. Understanding the effect of different thermal and mechanical parameters on the thawing of ice-rich permafrost with time, the generation of vertical and horizontal loads, and the stress-strain characteristics of the ice-rich permafrost.

This study was divided into two sections, experimental work and computer modeling work. Two different experimental approaches (Figure 3.1), one-dimensional consolidation and three-dimensional physical scale test, were employed to study thaw subsidence mechanisms in three different types of soils, namely, clay, silt and sand. The computer modeling work (Figure 3.2) involved integrated thermal and mechanical analysis to understand permafrost thaw subsidence induced instability effects on casings. COMSOL Multiphysics™ was used to run simulations for the computer modeling work.

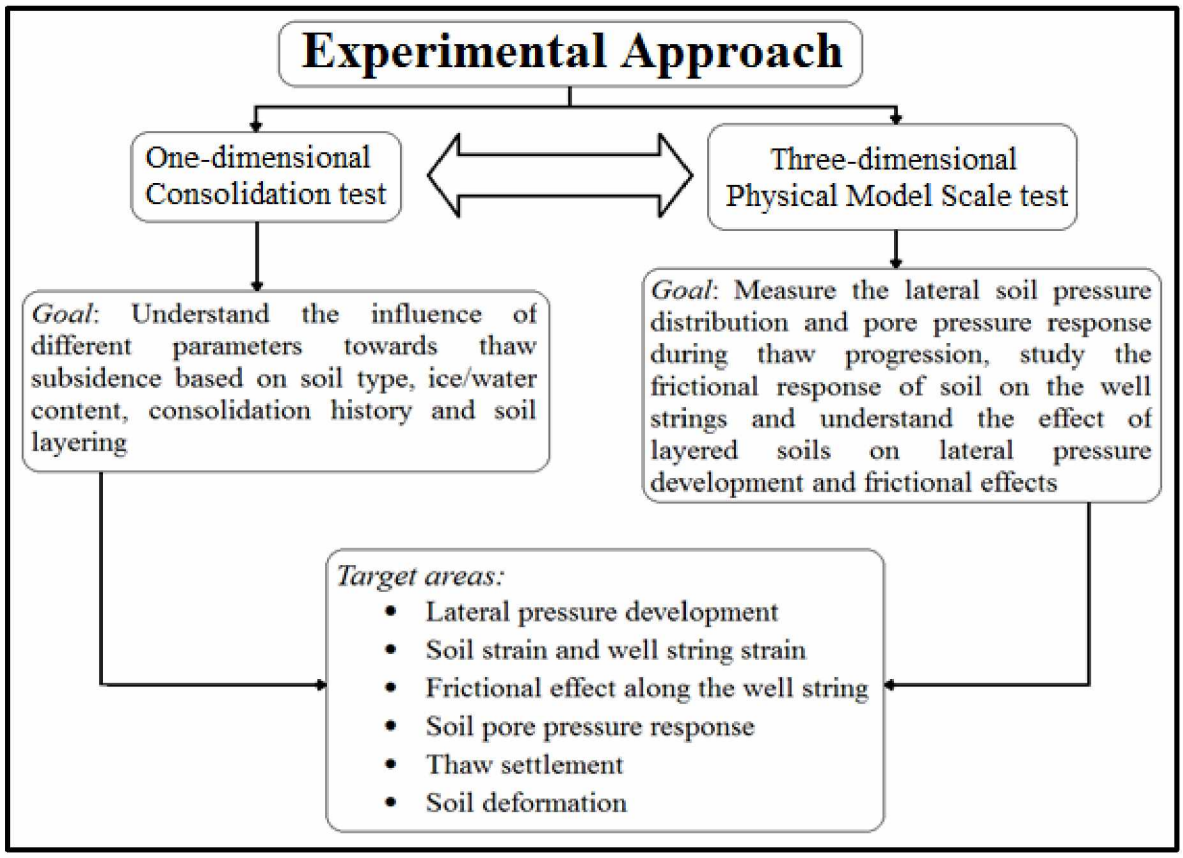

Figure 3.1: Objective for the experiment approach.

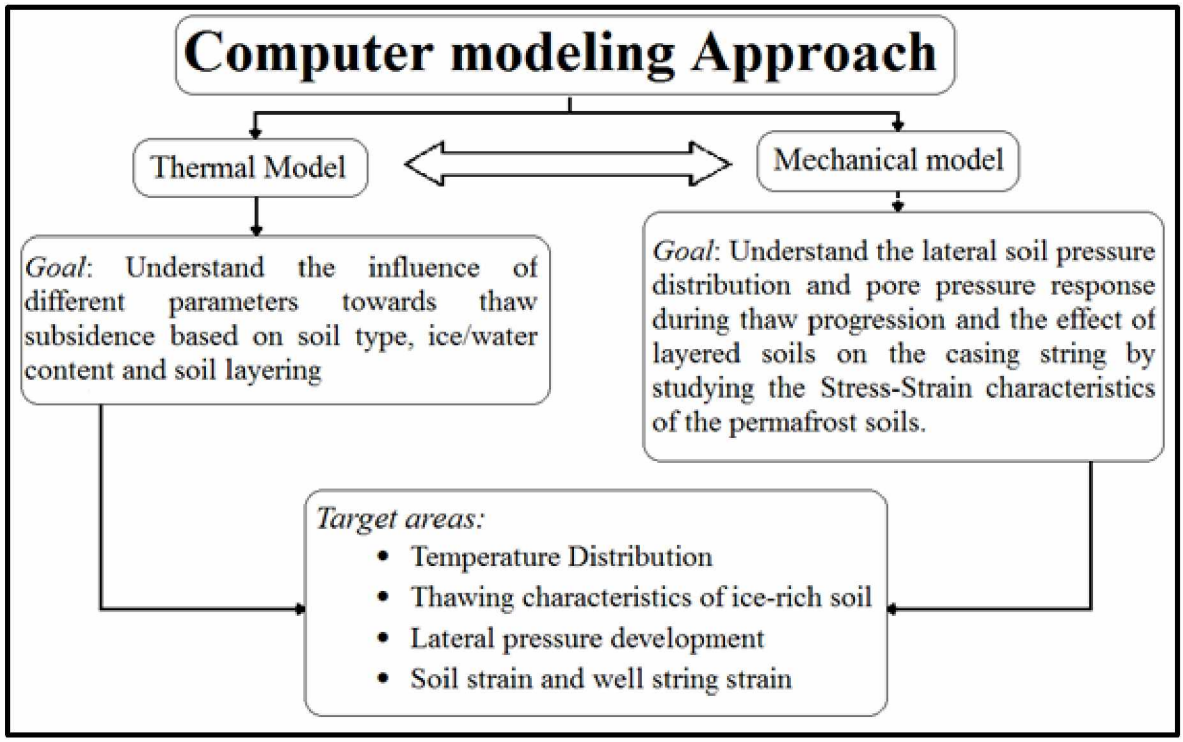

Figure 3.2: Objective for the computer modeling approach.

CHAPTER 4 EXPERIMENTAL APPROACH TO UNDERSTAND THAW SUBSIDENCE

This chapter explains in detail the entire experimental study of permafrost thaw subsidence. Two different experiments were planned and designed to understand the effect of various factors on the thaw settlement problem, such as vertical and lateral pressure, pore pressure, soil strain and casing strain, frictional effect along the well string, soil type and soil deformation. The primary goal of the entire experimental study was to gain a better understanding of the complex interaction between soil and well systems and changes occurring within them with time during progressive thaw. A one-dimensional consolidation test and three-dimensional physical scale test were custom designed for the experimental study.

4.1 Understanding and Testing of Soil

Both the experimental tests involved three types of soil; clay, silt and sand. All three soils were obtained from different sources. Clay was obtained from a mining pit at the Usibelli Coal Mine in Healy, Alaska. It was underlying coal seam #6 in the Suntrana Formation, the coal-bearing group of the Nenana Coal field. The coal was brought to the laboratory in the form of claystone and was broken down after saturating it with water. The silt obtained was aeolian Fairbanks silt from the UAF Campus. Sand was obtained from a commercial source where it was the byproduct of a commercial gravel washing operation. The sites from where the clay and silt were obtained are shown in Figure 4.1 and 4.2.

Figure 4.1: Site from where Fairbanks silt was obtained.

Figure 4.2: Site from where clay in the form of claystone was obtained.

4.1.1 Testing of Soil Part #1: Sieve Analysis and Hydrometer Analysis

Different tests were performed on all soil types to understand their characteristics. These tests included gradation tests and hydrometer analyses, Atterberg limit tests and frost heave tests. Sieve analysis, also known as the gradation test, is a grading method or procedure for understanding the variation in particle size distribution of a granular material. The soil's performance in different scenarios depends mainly on the type of particle and the variation of different particle sizes present. The sieve analysis test involved the separation of particles on the basis of shape, size and quantitative determination of mass of the different size particles present. This test uses a square opening sieve criterion for the determination of different soil particle grades ranging from 75 millimeters to 75 micrometers. The test was important for understanding the subsurface drainage system. Certain engineering properties of soil, like hydraulic conductivity, compressibility and shear strength, are related to the particle size gradation of soil. The ASTM D6913 (Particle-Size Distribution (Gradation) of Soils Using Sieve Analysis procedure) testing procedure was followed to conduct the sieve analysis test. The set of sieves used were #30, #40, #50, #100, #140, #170 and # 200, as shown in Figure 4.3. At the end of the test, the soil sample passing through the #200 sieve was collected in a plastic zip-lock bag to

prevent the soil from absorbing any moisture from the atmosphere. The sample was later used for hydrometer analysis to determine the gradation of finer particles.

Figure 4.3: Set of sieves used for gradation test.

Hydrometer analysis, also known as the sedimentation method, of soil was done for determining the grain size distribution of the soil sample that passed through the #200 sieve. It was used for calculating the percentage of clayey or silty soil particles present in the sample. The soil sample was added to a solution (Figure 4.4) of deionized water and a dispersing agent (Sodium Hexametaphosphate solution) to avoid the formation of aggregates by neutralizing certain cations like Ca^{++}, Al^{3+} and Fe^{3+}. This method is based on Stoke's law, taking into account the rate of sedimentation of particles suspended in solution of deionized water and dispersing agent The ASTM D422 (Hydrometer Analysis of Fine soil) testing procedure was followed to conduct the test.

Figure 4.4: Hydrometer analysis using ASTM D422.

4.1.1.1 Results for Sieve Analysis and Hydrometer Analysis

Plots shown in this section (Figure 4.5, 4.6, 4.7, 4.8 and 4.9) are the results obtained for the particle size distribution tests conducted on five samples of different types of soil. The results were calculated by combining the data obtained from sieve analysis and the hydrometer analysis test. The data for the sieve analysis and hydrometer tests is given in Appendix A-1. The following two equations were used for the purpose of processing the results obtained from hydrometer analysis:

$$P = \left[\frac{1000 * Gs * P10}{Ms}\right]\left[\frac{R-1}{Gs-1}\right] \tag{4.1}$$

$$D = K\sqrt{\frac{L}{T}} \tag{4.2}$$

where

P = percentage of soil in suspension, %

Gs = specific gravity of soil particles

P10 = percent of original soil sample which passes No.10 sieve

Ms = dry mass of soil, gm

R = hydrometer reading

D = diameter of soil particle, mm

K = constant depending on solution temperature and specific gravity of the soil (Table A-2)

L = effective depth, equal to the distance from the surface of the suspension to the level at which the density of the suspension is being measured, cm (Table A-1)

T = time of hydrometer reading, min.

The percent of the original soil sample passing through the No.10 sieve was considered to be 100% because all the samples passed through it after air-drying and breaking down using a hammering tool until most of the sample particles broke apart.

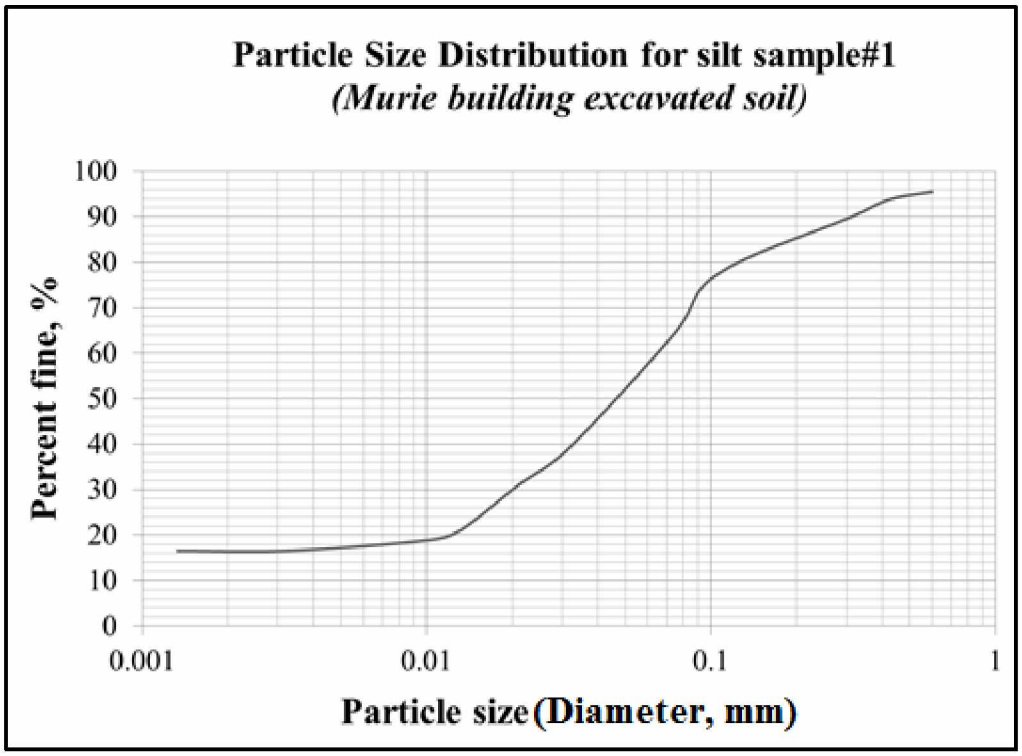

Figure 4.5: Particle Size Distribution for silt sample#1. (Murie building excavated soil)

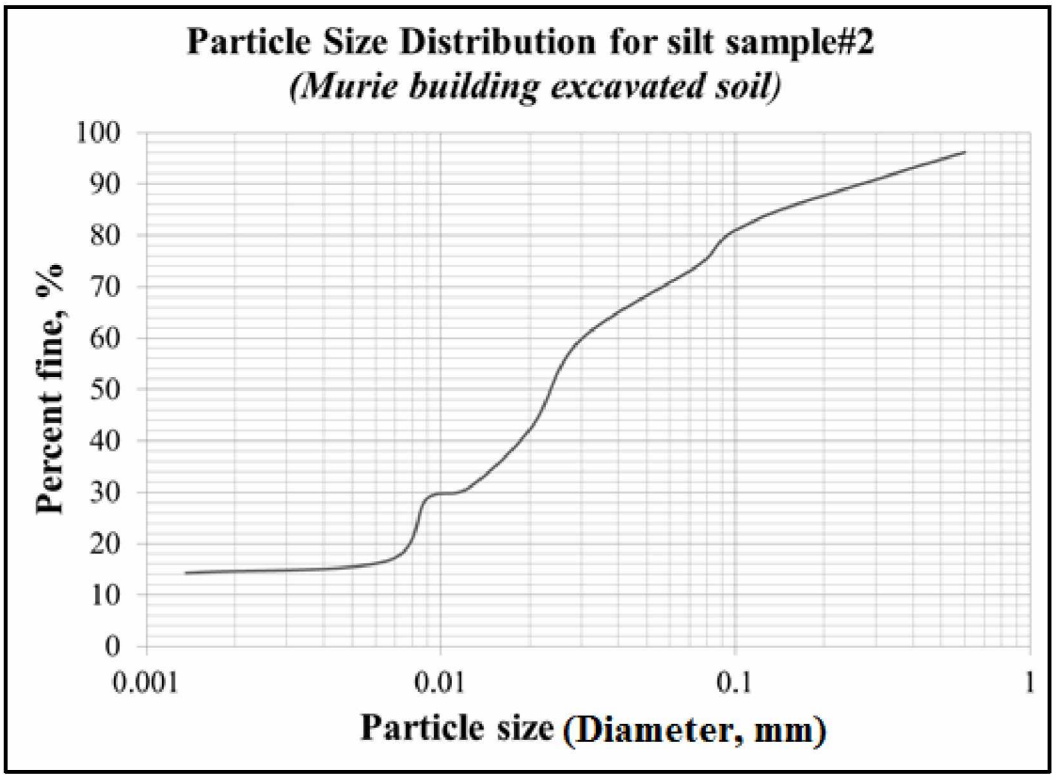

Figure 4.6: Particle Size Distribution for silt sample#2. (Murie building excavated soil)

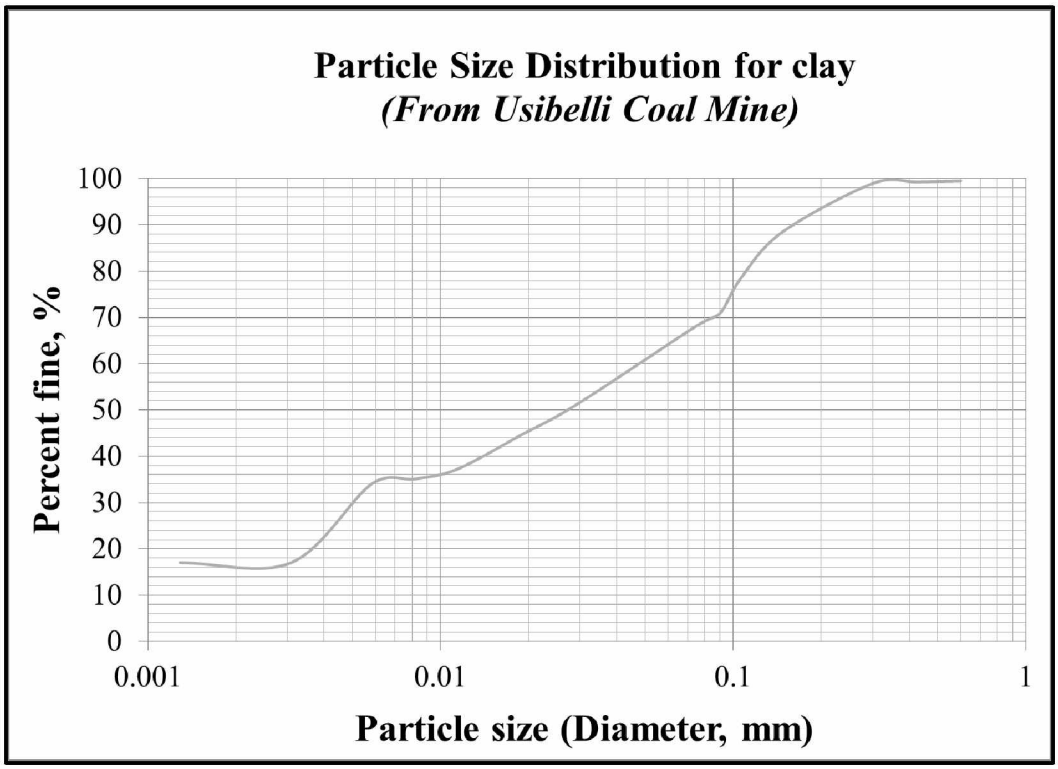

Figure 4.7: Particle Size Distribution for clay. (From Usibelli Coal Mine)

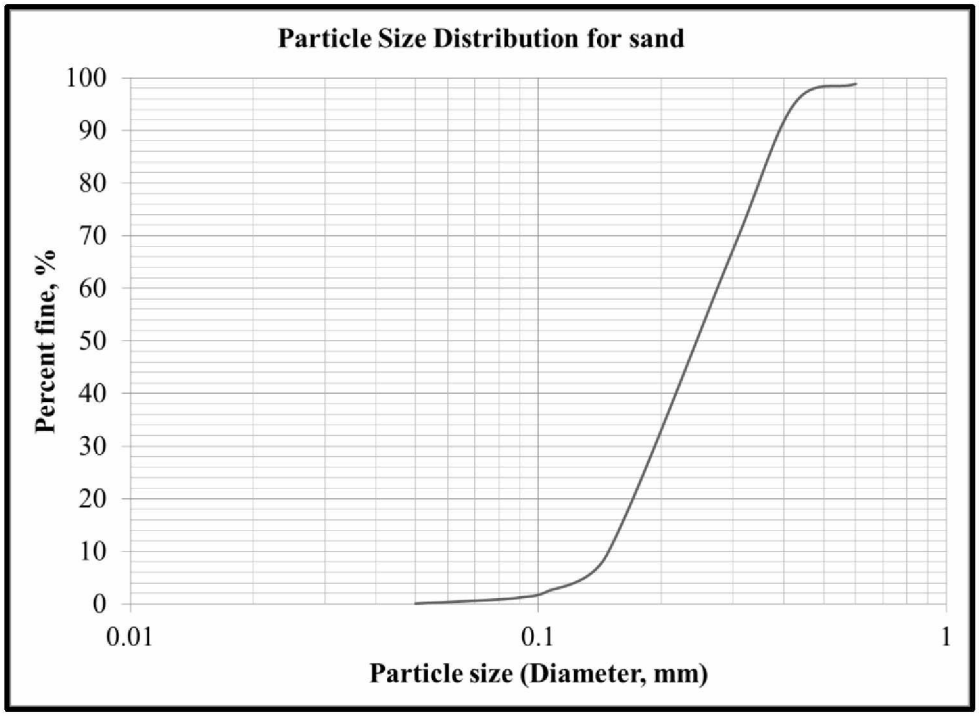

Figure 4.8: Particle Size Distribution for sand.

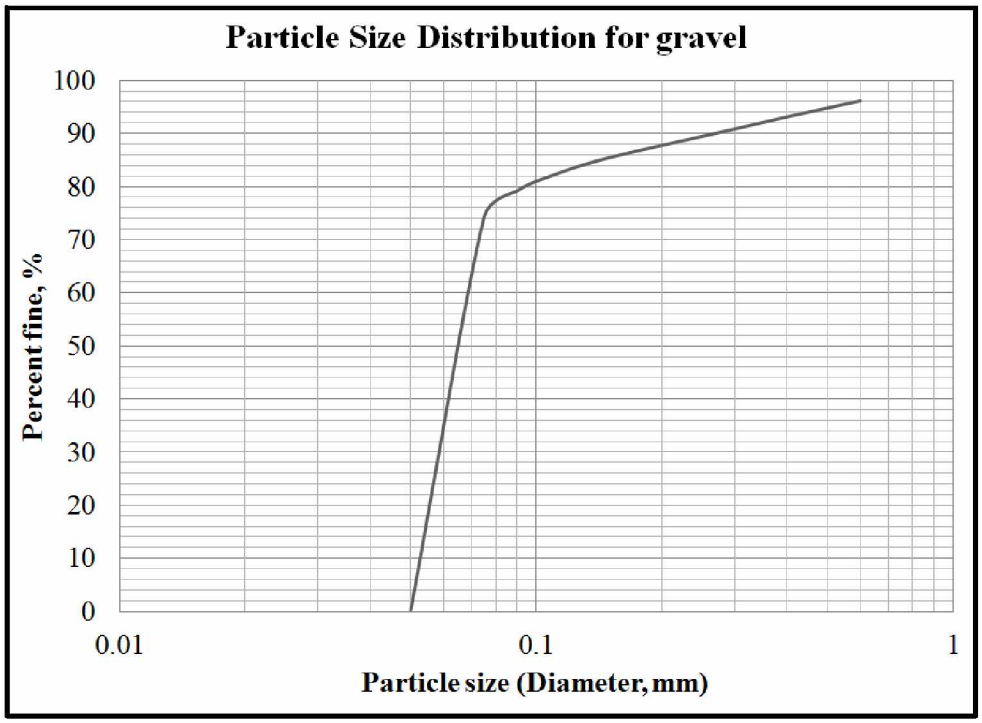

Figure 4.9: Particle Size Distribution for gravel.

4.1.2 Testing of Soil Part #2: Atterberg Limit Tests

Water content is defined as the quantity of water contained in a material or the percentage of water by volume present in a material. Water content can range from 0 to the maximum value of porosity of the material (Shur, 2014). Water content is calculated by using the following equation:

$$W, \% = \frac{Wwt - Dwt}{Dwt - Cewt} * 100 \quad (4.3)$$

Where

W = Water content expressed in %

Wwt = Wet weight of the material

Dwt = Dry weight of the material

Cewt = Weight of empty container.

Atterberg limit tests include the shrinkage limit test, liquid limit test and plastic limit test. These tests are done in order to know the critical water content of a material, which in this study was soil. Depending on the water content of the soil, it can be said to appear in four different states, namely, solid, semi-solid, plastic and liquid. With each state the consistency and behavior of the soil changes, along with its engineering properties. Thus, on the basis of the results obtained from these different Atterberg tests, boundaries between individual states can be well defined for understanding the behavior of soil under different conditions. These tests were performed mostly for fine-grained soils, as they are known to expand or shrink with variation in their water or moisture content.

The liquid limit is the water content value of the soil where its behavior changes from plastic to liquid, i.e., it starts behaving like a liquid with the ability to flow. It is obtained by following the ASTM D4318 testing procedure. This testing procedure involves the use of the Liquid Limit Device, a mechanical device comprising a cup made up of brass suspended from a carriage such that its drop can be controlled. The base of this device is made up of a block of resilient material. A groove (Figure 4.10) is made in the soil sample placed in the brass cup with a standard tool.

The groove is 0.52 inches or 13.5 millimeters wide. According to the standard procedure, the water content value of the soil at which, after 25 blows, the two sides of the groove made in the soil sample meet or touch each other for a distance of approximately 0.5 inches, defines the liquid limit of the soil.

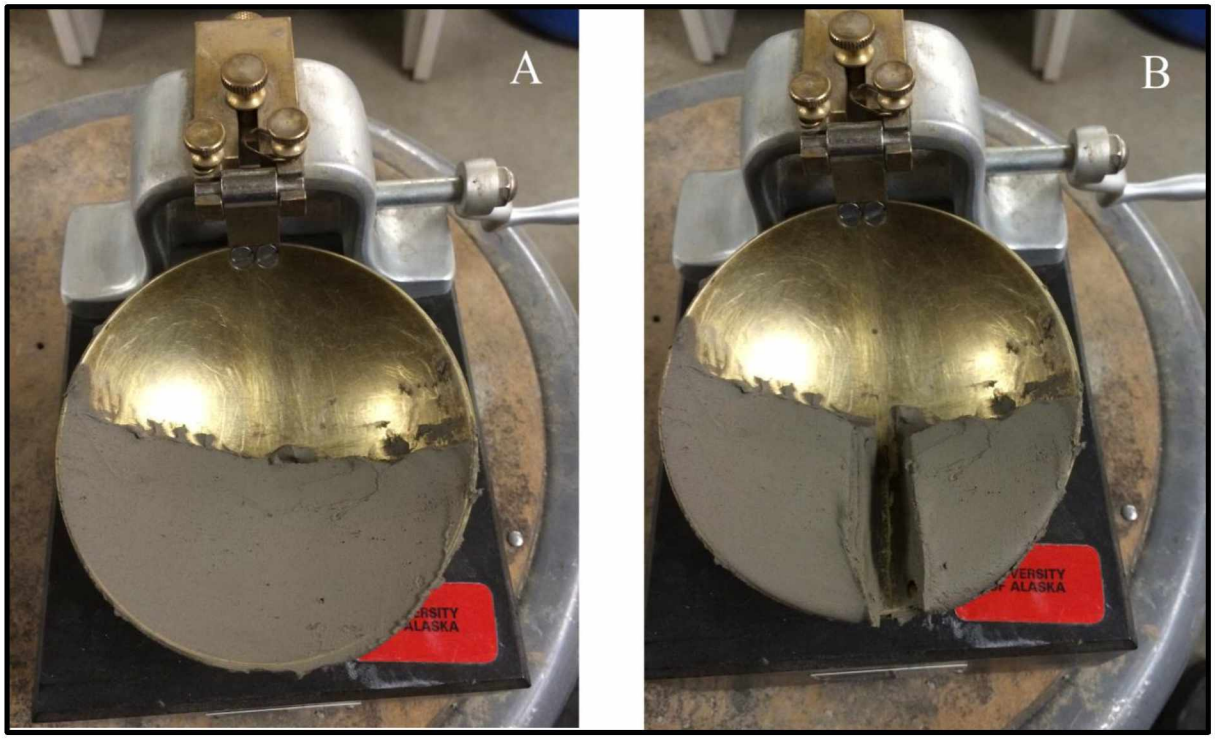

Figure 4.10: (A) Brass cup with soil sample (clay) and (B) Brass cup with soil sample (clay) with groove.

The plastic limit is the water content value of the soil where its behavior changes from semi-solid to plastic. Similar to the liquid limit, the plastic limit is obtained by following the ASTM D4318 testing procedure. The soil sample is rolled on a flat hard surface, forming thread-like portions. If the thread from the soil sample can be rolled up to ~3.2 mm or ~1/8 inch, then the current water content is the plastic limit value for the soil sample. Both tests needed to be repeated for the purpose of confidence in the value of water content for that particular limit Once the tests were completed, small portions of wet soil samples were taken in containers and dried overnight in an oven (Figure 4.11 and 4.12) for the calculation of water content.

Figure 4.11: (A) Portions of soil sample (clay) collected in containers for liquid limit test and (B) threads of soil sample (clay) collected in containers for plastic limit test.

Figure 4.12: Soil samples kept in the oven overnight for air drying.

4.1.2.1 Results for Liquid limit Test and Plastic limit Tests

The results of the two Atterberg limit tests are summarized in Table 4.1. The tests were performed only on fine-grained soils (clay and silt). There were two different samples of silt (Sample A and Sample B) and one sample of clay (Usibelli Coal Mine clay). MI-Gel was added to Sample A silt and Usibelli clay to increase their water retaining characteristics. The MI-Gel was added at constant increments in fixed proportions (5%, 10%, 15% and 20%). The MI Gel was mostly Wyoming clay and was believed to absorb water and swell. This was necessary for the next step of the study, the frost heave test, where each type of soil was tested for its heaving characteristics on freezing. Both tests were repeated several times until desired values of water content were obtained. Sometimes it was difficult to obtain exactly 25 blows for the liquid limit test. All the data obtained from the liquid limit test where the number of blows was close to 25 was plotted in MS Excel and equations were obtained from trendline that was used to approximate the water content value for 25 blows.

Table 4.1: Summary of all Atterberg limit tests conducted

Sr. No	Soil type	Liquid limit, %	Plastic limit, %
1	Silt sample A	43.66	31.58
2	Silt sample B	26.40	25.00
3	Usibelli clay	39.04	33.33
4	Usibelli clay + 10% MI Gel	41.00	27.00
5	Usibelli clay + 15% MI Gel	74.08	35.00
6	Usibelli clay + 20% MI Gel	67.20	32.00
7	Silt sample A + 5% MI Gel	32.14	25.00
8	Silt sample A + 10% MI Gel	39.25	32.00
9	Silt sample A + 15% MI Gel	55.63	24.00
10	Silt sample A + 20% MI Gel	62.06	32.25

Based on the results obtained from the tests (Figure 4.13 and 4.14), the addition of 10% and more MI Gel did increase the soil's capacity to absorb and retain more water for both silt and clay. This was an important factor for the final three-dimensional physical scale test, because the

soil needs to heave for it to form segregated ice distribution for the thaw settlement effect to be visible. The data from repeated Atterberg limit tests is given in appendix A-1.

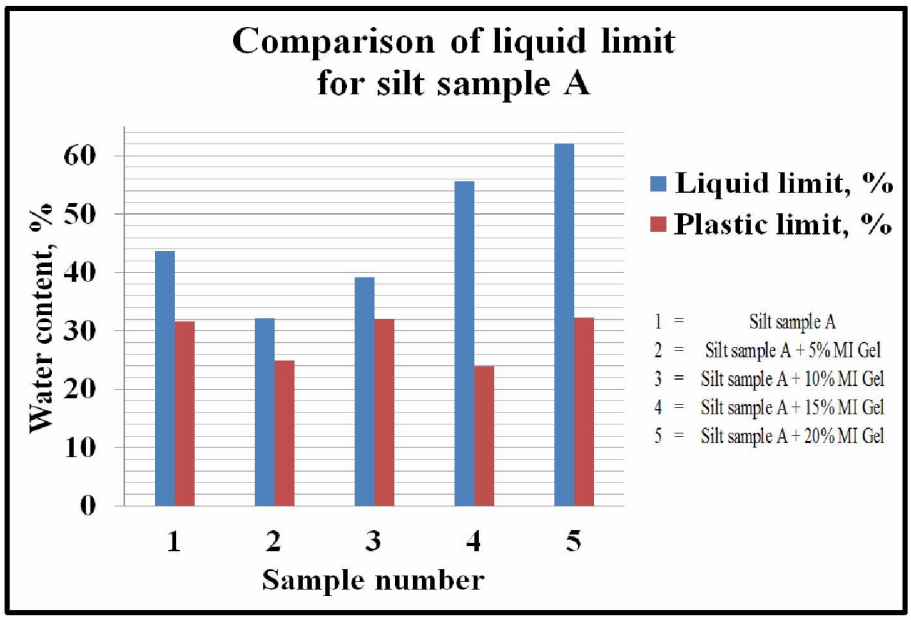

Figure 4.13: Comparison of liquid limit for silt sample A for addition of MI-Gel.

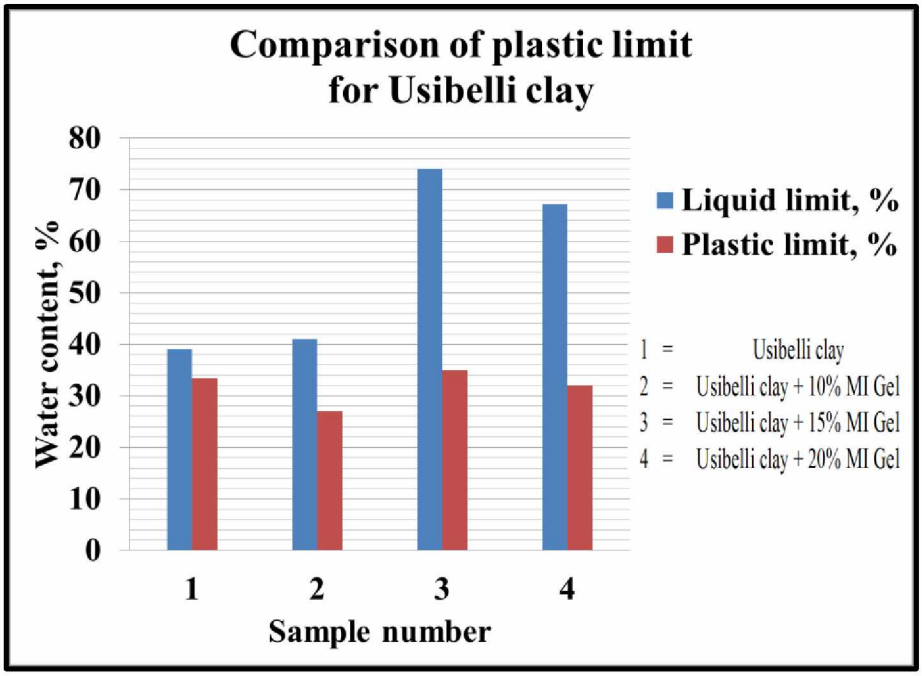

Figure 4.14: Comparison of plastic limit for Usibelli clay for addition of MI-Gel.

4.1.3 Testing of Soil Part #3: Soil Consolidation and Layer Test

The purpose behind this part of soil testing was to look at the layering effect of different soil types. This was an important step towards deciding the layering scheme for the final three-dimensional physical scale test, which consisted of 6 different layers of soil. Four acrylic cylinders of different diameters were used to look at the interaction of different soils with each other when they are layered under slightly oversaturated conditions. All the cylinders were placed in a tub filled with a sand layer of thickness 3 inches (Figure 4.15). The cylinders were undisturbed and were under observation for a period of 2 days. Each acrylic cylinder had a different layering and thickness scheme of different soils, as shown in Figure 4.16. The initial data for layering and thickness and data collected at the end of the test for each cylinder is shown in Appendix A-1.

Figure 4.15: Tub with layer of sand of thickness = 3 inch and four acrylic cylinders.

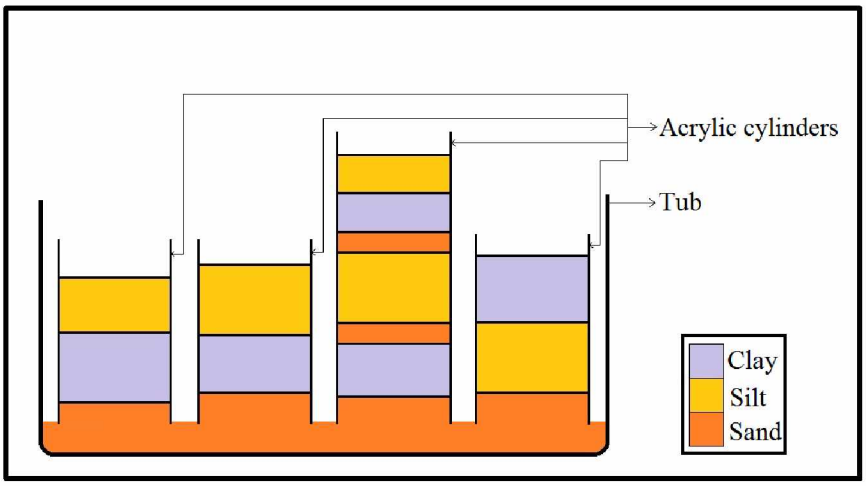

Figure 4.16: Schematics of Soil consolidation and Layering test.

Figure 4.17: Cylinder #3 at the end of test. (After 2 days)

After 2 days of consolidation under atmospheric pressure, the soil was removed from each cylinder and visual observations were made which aided in making final decisions for the layering scheme of the three-dimensional physical scale test. Based on visual observations, sand never consolidated in any of the four cylinders. Clay and silt were significantly consolidated in cylinder #3 due to the weight of the overlying soil layers. In cylinder #4, which had equal thicknesses of clay and silt, clay submerged completely into silt and was difficult to differentiate (Figure 4.18). In other cylinders there was some amount of submergence of silt into clay, or vice-versa, due to different thicknesses of silt and clay (Figure 4.19(B)). In cylinders #1, #2 and #4, silt and clay did not significantly consolidate compared to cylinder #3 (Figure 4.19(A)).

Figure 4.18: Cylinder #4 showing complete submergence of clay and silt.

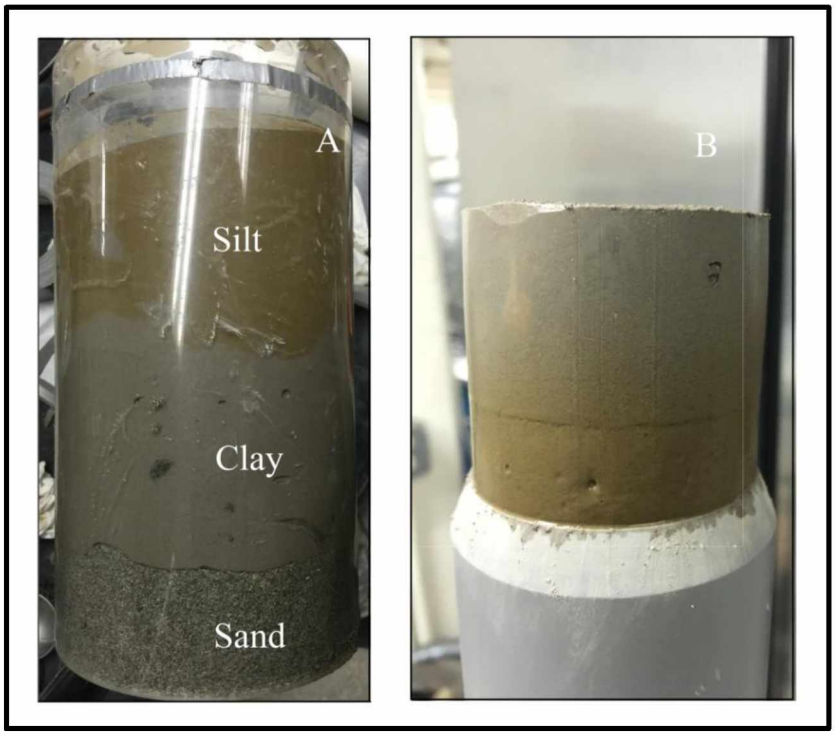

Figure 4.19: (A) Cylinder #2 showing consolidation of clay and silt at the end of the test and (B) Submergence at the interface of silt and clay in cylinder #2.

4.1.4 Testing of Soil Part #4: Frost Heave Test

Frost heave is defined as "the upward or outward movement of the ground surface (or objects on, or in the ground) caused by the formation of ice in the soil" (Page no. 28, R. O. van Everdingen, 1998). The frost heave test was the main part of soil testing. Different soils were tested to observe their frost heaving action. The aim was to understand the water intake characteristics for different soil types. Samples tested were clay, silt sample A, and a silt sample with added MI Gel. Out of all the samples tested, clay was the only soil that heaved on its own (Figure 4.29). Silt did not heave significantly on its own (Figure 4.27), but heaved slightly after the addition of MI Gel (Figure 4.28). Two different cells were used for testing frost heave behavior, namely, Japanese cell (Figure 4.22) and Laval cell (Figure 4.25).

The main aim was to look at the ice distribution in each soil type when subjected to freezing conditions. It is important for fine-grained soil to form segregated ice (ice lenses) for it to heave. Particle size distribution tests and Atterberg limit tests were performed to get an initial idea about the soil's water retention. Only after the soil has heaved due to formation of segregated ice could the effect of thaw settlement be studied efficiently. Thus it was important to check about the frost heaving action of the soil samples used in the study beforehand. The results for the frost heave test are shown in Figures 4.27 and 4.29 for silt sample A and Usibelli clay, respectively. Silt sample A with added MI Gel did not show significant change in its frost heaving characteristics, as shown in Figure 4.28. Figure 4.30 shows the Usibelli clay soil sample at the end of the frost heave test with segregated ice distribution within it.

4.1.4.1 Preparation of Soil Sample

The soil samples used in both the cells for the frost heave test were prepared in an acrylic cylinder or consolidation cell. The cell had two openings, one at the top to apply vacuum pressure and one at the bottom to let the excess water flow out. The soil samples were prepared by the following procedure:

1. The soil was oversaturated with distilled and deionized water. It was allowed to soak in the water for a period of 4 to 5 days to obtain uniform water distribution.
2. The saturated soil sample was mixed well in slurry form, with water content greater than the liquid limit of the soil. This was done to obtain uniform particle size distribution.

3. The slurry was then put in the consolidation cell (Figure 4.20) and later was kept under vacuum conditions for around 24 hours (depending on the sample).
4. Pressure was applied over the soil in the consolidation cell for less cohesive soil types (Figure 4.21).
5. After a period of more than 36 hours, aluminum tubes with beveled edges on one side were used for cutting through the soil to obtain cylinder soil samples for the frost heave tests. The size of the sample was different for both cells.
6. Later, the soil samples were plastic wrapped along with the tubes, then stored in an airtight container until the time of testing.

Figure 4.20: Consolidation cell used for preparing soil samples for frost heave test.

Figure 4.21: Pressure being applied on the consolidation cell.

4.1.4.2 Japanese Cell

The Japanese cell used for the frost heave test (Figure 4.22) was manufactured at the Hokkaido University in Japan. It consisted of a custom designed refrigeration system whose temperature can be controlled and monitored with the help of a control panel attached to the outside of the refrigerator. The design of the cell used for holding the soil sample is shown in Figure 4.24. The refrigerator consisted of the following parts:

1. Stainless steel frame
2. Acrylic cylinder (60.0 mm diameter)
3. Circular plate with vertical rod and horizontal arm
4. Measurement system
    a. Platinum Resistance Temperature Detector (RTD)
    b. Keyence LK-081 Laser (30 mm range, 0.003 mm resolution)
    c. Validyne DP-10 differential pressure transducer
    d. PolyScience Model 1167 programmable circulating baths
    e. PID (Proportional, Integral, Derivative) control logic device (data logger)
5. Upper and lower pedestal
6. Flow lines for water and anti-freeze fluid.

The stainless steel frame was used to hold all the other equipment in place. The circular plate was used to apply pressure (overburden pressure) on the soil sample by placing weights on it (minimum of 9.1 KPa). The vertical rod attached to the circular plate transferred the applied overburden pressure to the upper pedestal on top of the soil sample. The horizontal arm attached to the circular plate was used to check the soil sample's heaving behavior with the help of the Keyence LK-081 Laser. The RTD was installed for checking the temperature of the two pedestals over the testing period. The Validyne DP-10 differential pressure transducer was used to monitor the amount of the water entering the system from the lower pedestal.

The PolyScience Model 1167 programmable circulating baths were used for maintaining the temperature of the upper and lower pedestals. The pedestals were designed to allow the circulation of antifreeze fluid from the temperature baths. The PID (Proportional, Integral,

Derivative) control logic device, the data logger, was used to record the real-time data from the cell and transfer it to the computer for further processing. The upper pedestal could be moved in the axial direction (up/down) and allowed the upward/downward movement of soil sample upon heaving. The fixed lower pedestal was the source of water to the soil sample through a porous metal surface. There were different flow lines for water and anti-freeze fluid, as shown in Figure 4.23. The water was constantly provided to the soil sample through a burette of 50 cc capacity placed outside of the cell. A thin layer of sand was put in the acrylic cylinder before placing the cylindrical soil sample from the consolidation cell in it. This was done to ensure the proper supply of water over the entire circumference of the sample. 1. The average core volume obtained at the end of the test was ~170 cc.

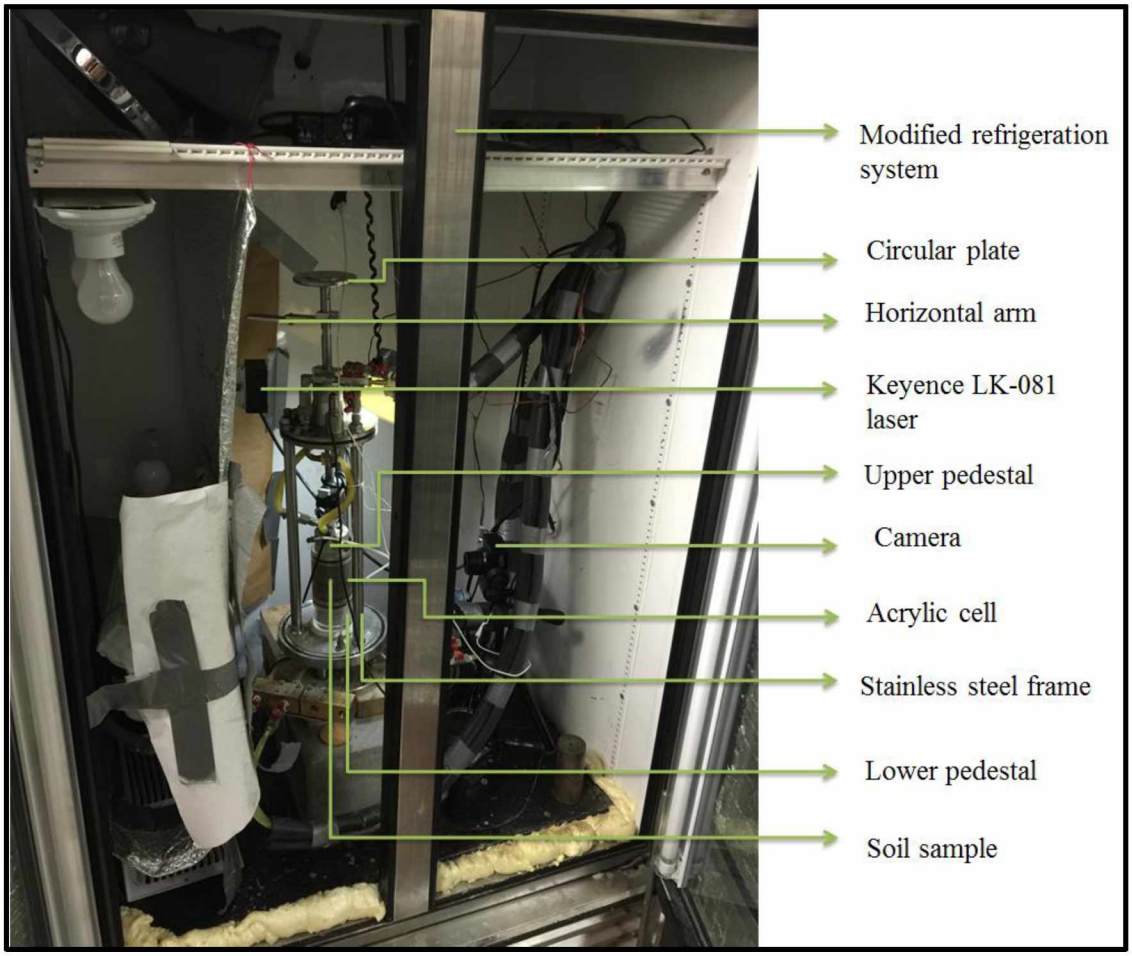

Figure 4.22: Japanese cell used for frost heave test.

The test was run in such a manner that the soil sample had a continuous supply of water from a connection attached to the lower pedestal. A constant temperature gradient was maintained along the length of the soil sample. This was achieved by setting fixed temperatures for the upper and lower pedestal with the help of programmable temperature baths. Thus the freezing front went from the top to the bottom of the soil sample and the water front went from the bottom to the top. Whenever these two fronts met, ice lenses were expected to form, resulting in frost heaving of the soil. The experiments performed on this cell were based on previous work conducted by Dr. Darrow (2007) in the Department of Civil Engineering at the University of Alaska Fairbanks.

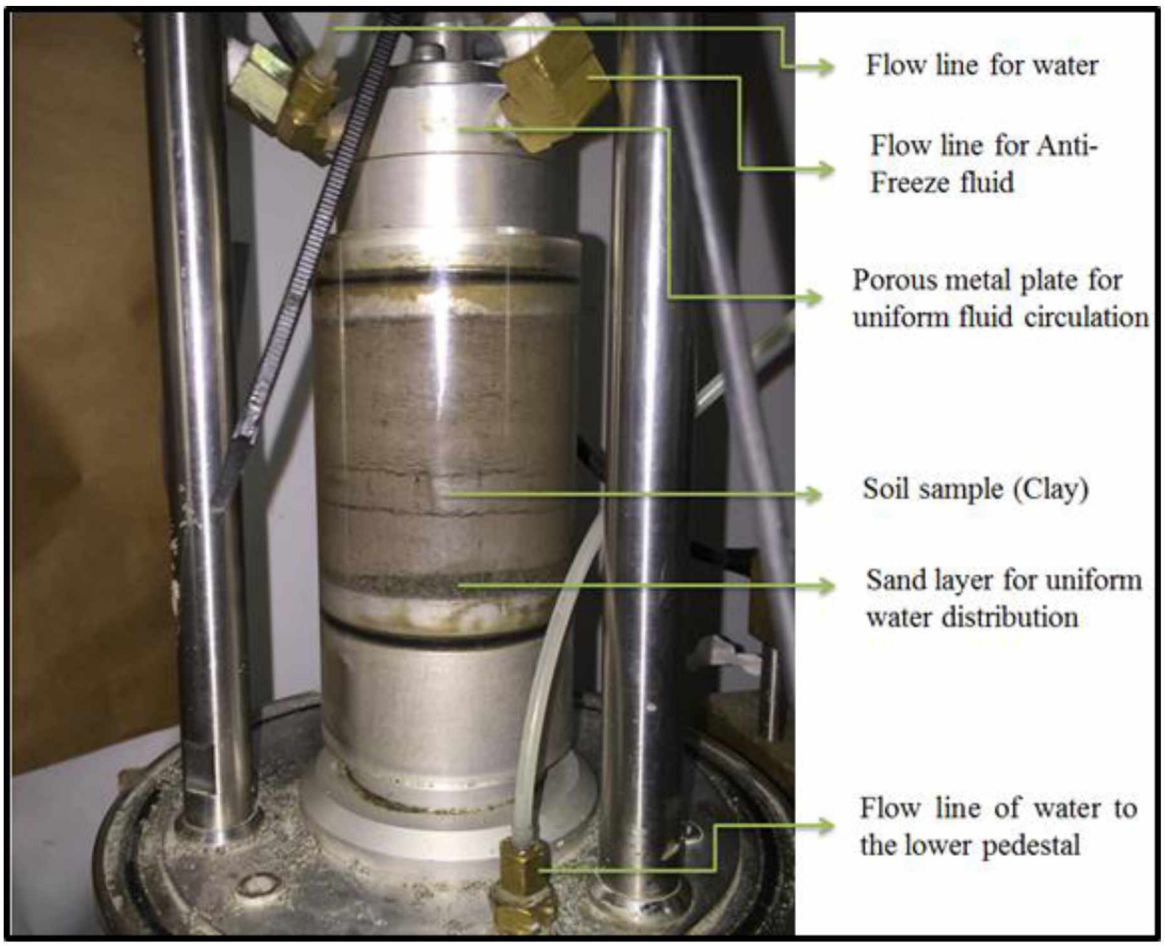

Figure 4.23: Acrylic cell connected to different flow-lines during the frost heave test.

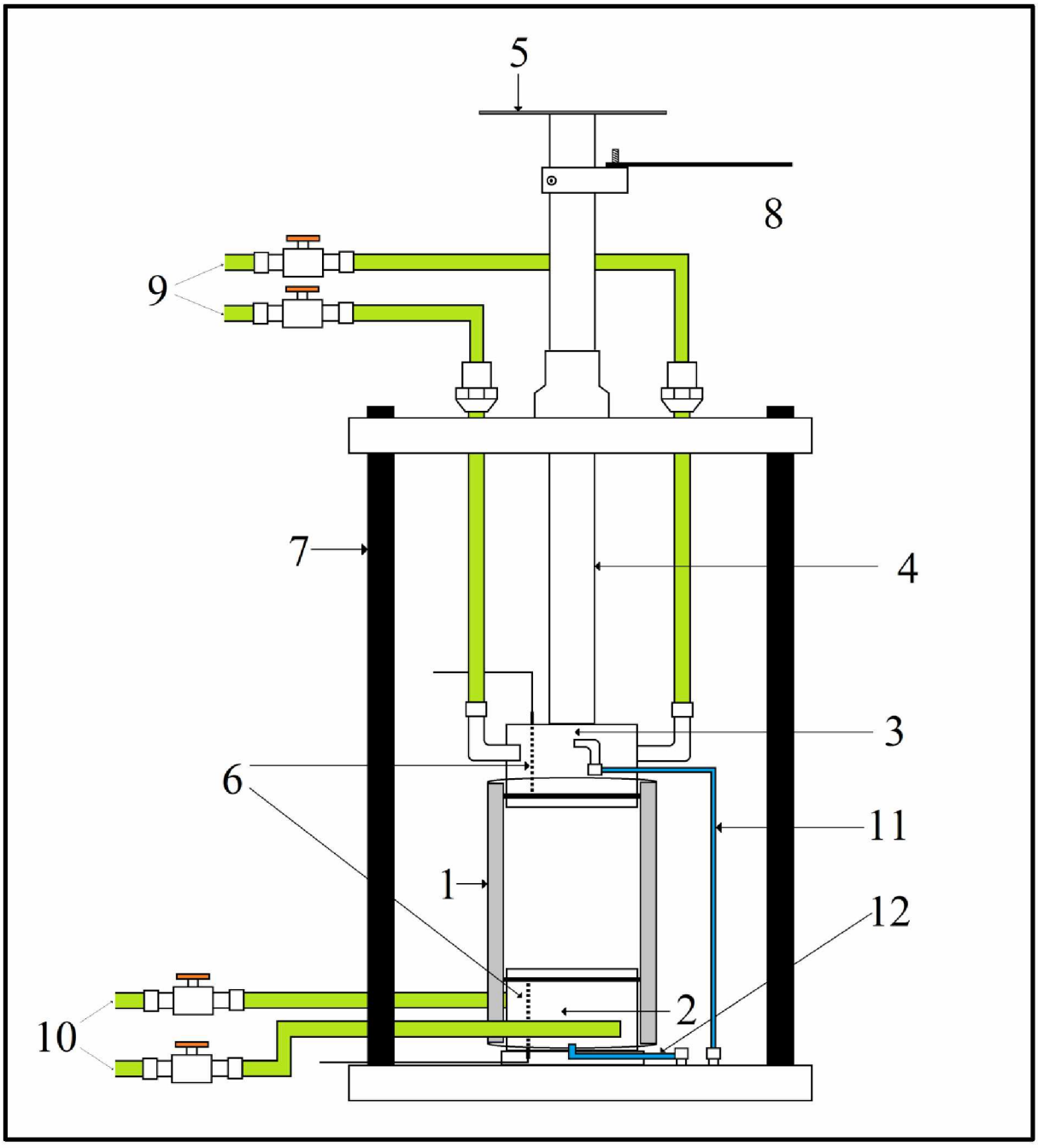

Figure 4.24: Schematic of Japanese frost heave cell from inside: (1) Acrylic cylinder; (2) Lower pedestal; (3) Upper pedestal; (4) vertical rod; (5) Circular plate; (6) Platinum RTDs; (7) Stainless steel frame; (8) Horizontal arm; (9) Flow-line for antifreeze fluid to upper pedestal; (10) Flow-line for antifreeze fluid to lower pedestal; (11) Water outlet from upper pedestal and (12) Water inlet to lower pedestal.

4.1.4.3 Laval Cell

The Laval cell used for the frost heave test (Figure 4.25) was manufactured at the University of Laval, Canada. The design of the refrigeration system for the Laval cell was similar to that of the Japanese cell. The only difference between both setups was the design and size of the cell in which the soil sample was tested. The design of the cell used for holding the soil sample is shown in Figure 4.26. The refrigerator consisted of the following parts:

1. Stainless steel frame
2. Thick-walled high strength plastic cylinder (101.2 mm diameter)
3. Measurement system
    a. Platinum Resistance Temperature Detectors (RTD)
    b. LVDT (Linear Variable Differential Transformer) (50 mm range, 0.1 mm resolution)
    c. Validyne DP-10 differential pressure transducer
    d. PolyScience Model 1167 programmable circulating baths
    e. PID (Proportional, Integral, Derivative) control logic device
    f. Thermocouple
    g. Thermistor (7)
4. Air pressure manifold
5. Upper and lower pedestal
6. Piston (for upper pedestal)
7. Flow lines for water and anti-freeze fluid

An air pressure manifold was used to apply pressure (overburden pressure) to the upper pedestal through a vertical rod, i.e., to the piston. A Platinum RTD was used to check the temperature at the top of the soil sample over the testing period. It was placed inside the upper pedestal (Figure 4.26). To monitor the heaving or thawing of the soil sample, Linear Variable Differential Transformer (LVDT) was used. A thermocouple was attached to the bottom of the cell, on the lower pedestal, to monitor the temperature at the bottom of the soil sample during the test. Thermistors were used for getting real-time data for the change in temperature due to thawing or freezing along the length of the soil sample with time. They were very helpful in getting an understanding of the frozen-unfrozen boundaries in the soil sample. Seven thermistors were used for monitoring the temperature along the length of the soil sample. Water was provided to the

soil sample through a burette of 100 cc capacity placed outside of the cell. The plastic cell had a layer of insulation wrapped around it to avoid any heat exchange with its surroundings, as shown in Figure 4.25. The Average core volume obtained at the end of the test was ~1600cc. The experiments performed on this cell were based on previous work conducted by Dr. Matthew Dillon (2012) in the Department of Civil Engineering at the University of Alaska Fairbanks.

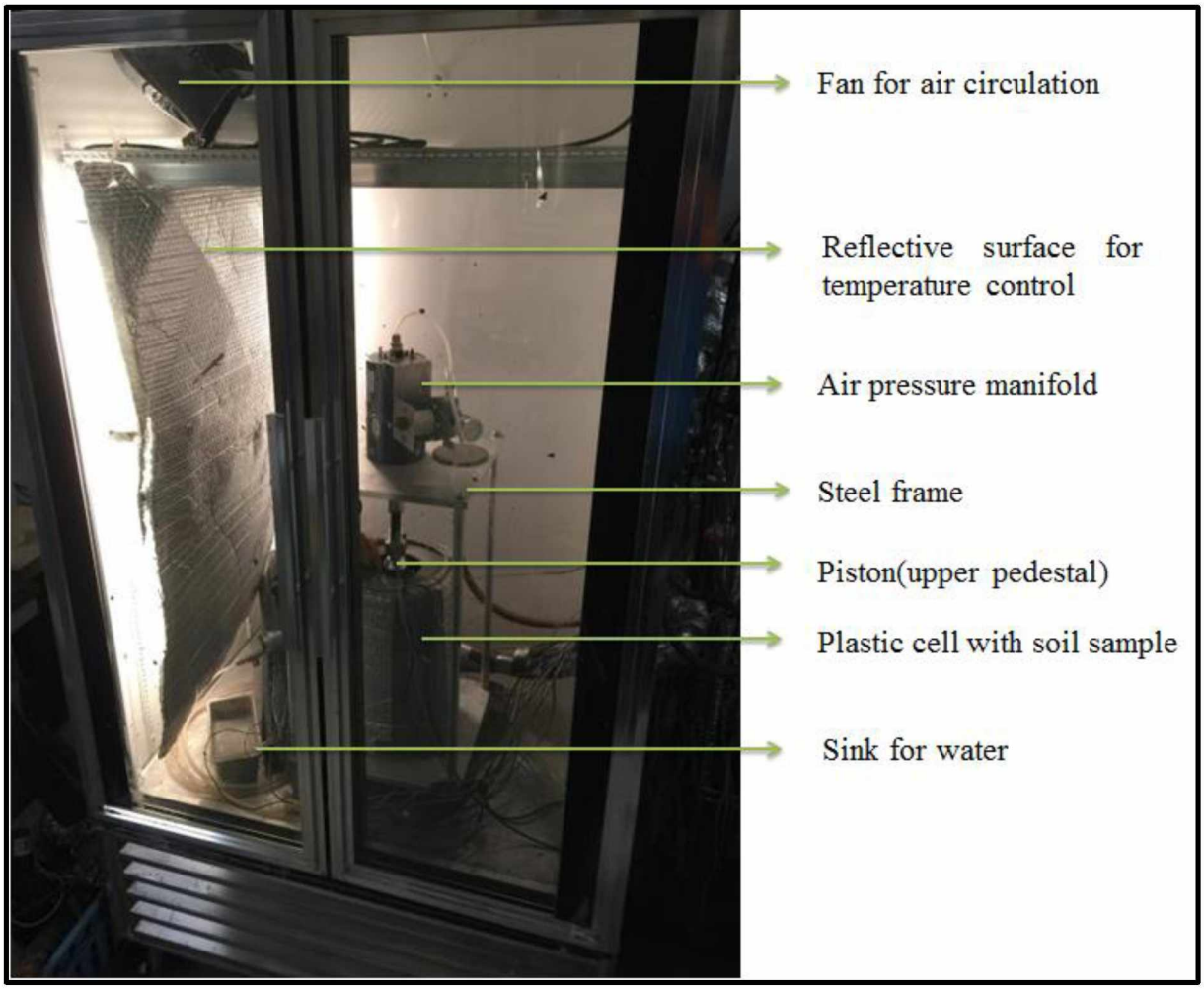

Figure 4.25: Laval cell used for frost heave test.

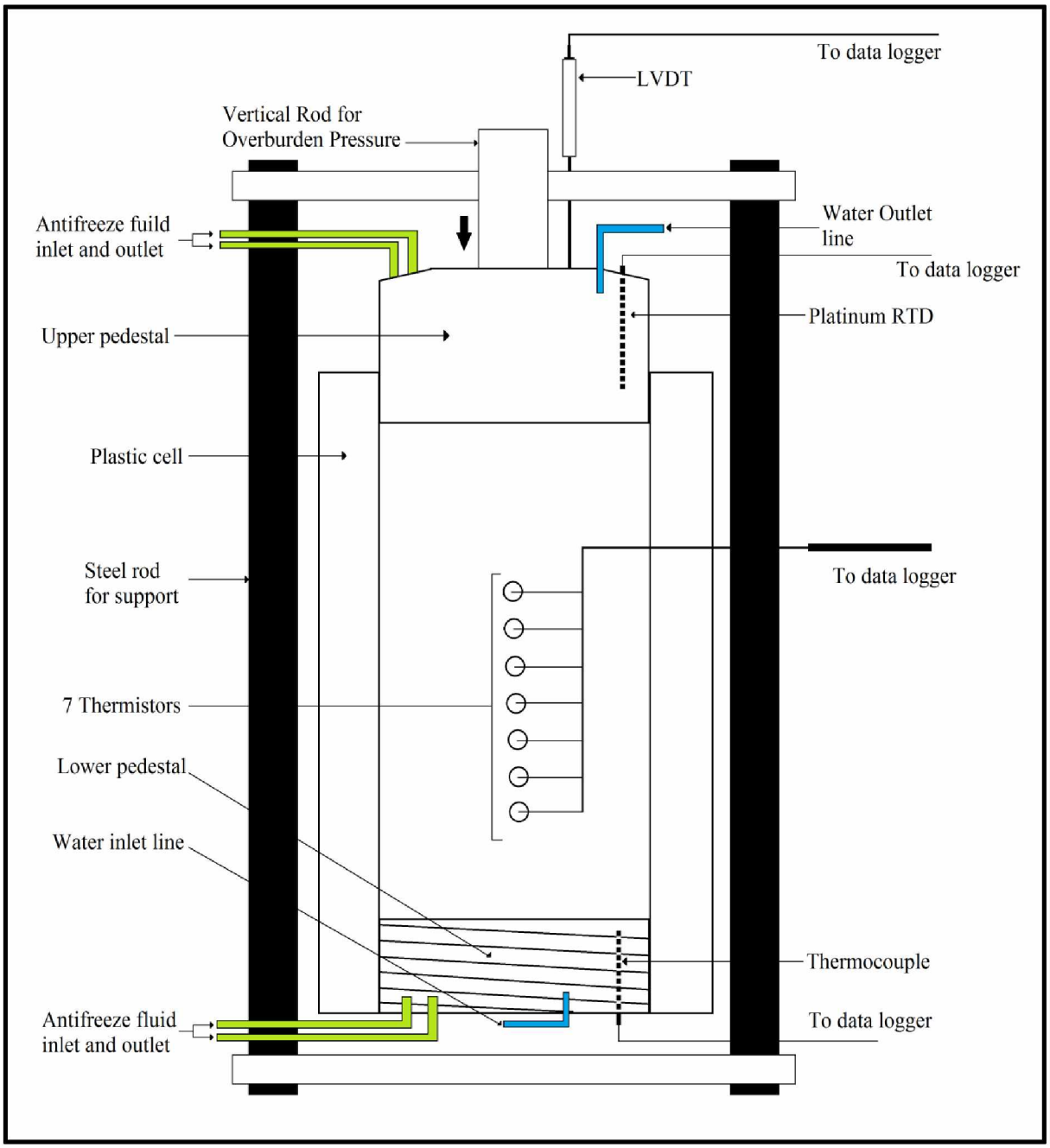

Figure 4.26: Schematic of Laval cell used for frost heave test.

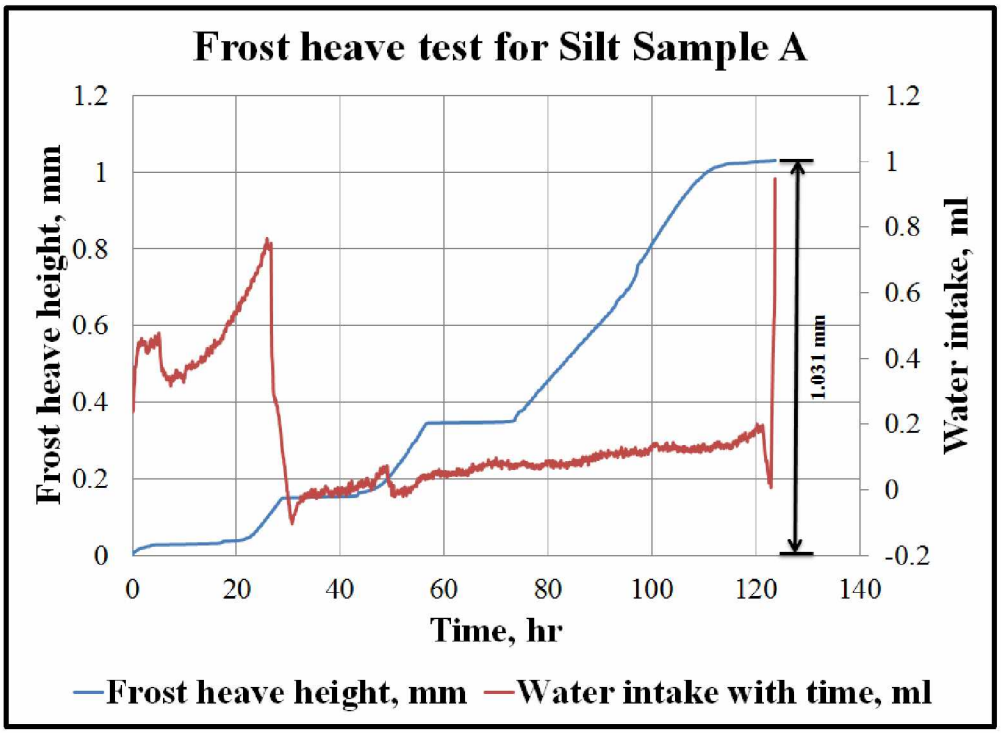

Figure 4.27: Frost heave test results for silt sample A.

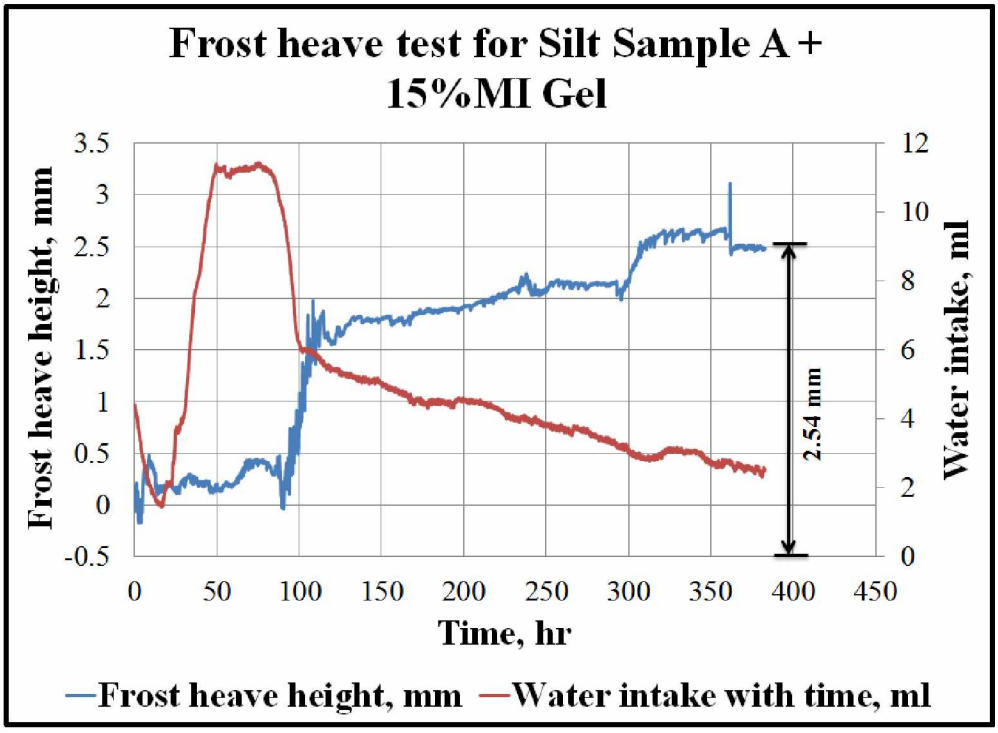

Figure 4.28: Frost heave test results for silt sample A + 15% MI Gel.

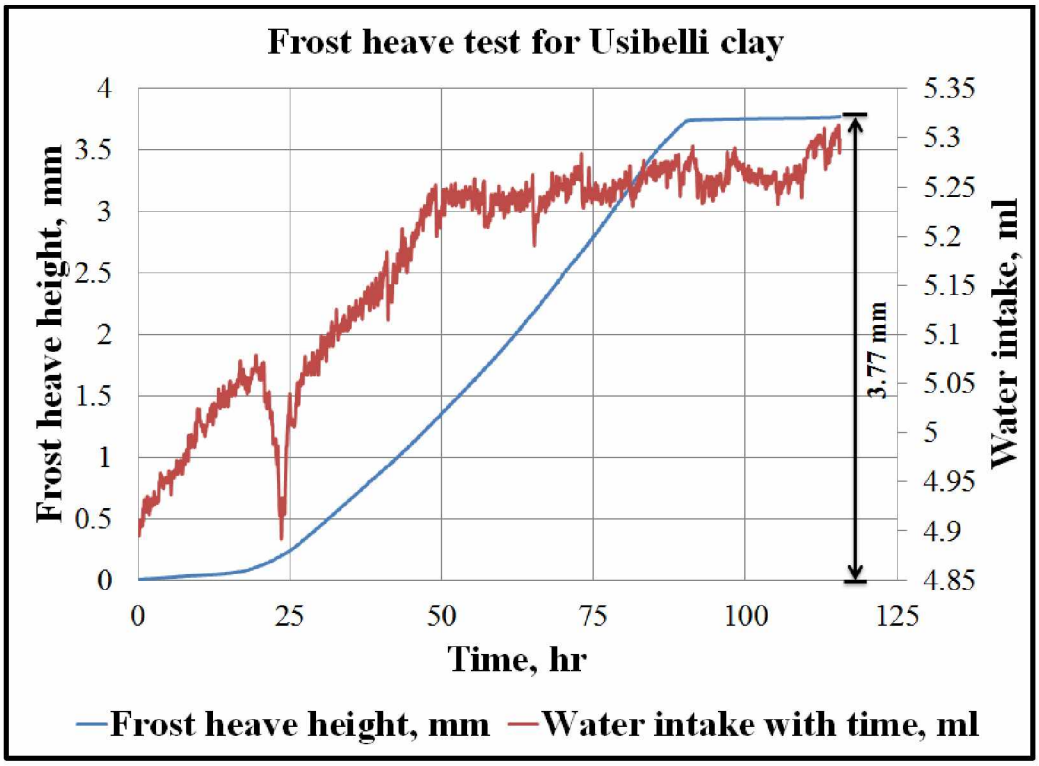

Figure 4.29: Frost heave test results for Usibelli clay.

Figure 4.30: Usibelli clay soil sample (frozen) at the end of the frost heave test along with segregated ice distribution within it.

4.2 Three-Dimensional Physical Scale Test

The three-dimension physical scale test involved understanding thaw settlement through simulating a scaled model for a portion of the well-soil system. The main objective behind this test was to measure the lateral soil pressure distribution and pore pressure response during thaw progression in layered soils and gain an understanding of post thaw frictional response of soil on the well strings. The test involved both thermal and mechanical analyses in a three-dimensional perspective. The idea was to understand the reaction of the soil with respect to strain effects on multiple wells and the changes in its stress state when changing from a frozen to a thawed state. The areas/parameters targeted in this testing approach were lateral soil pressure development, pore pressure response, soil strain and well string strain, frictional effects upon well string along its length, soil consolidation/deformation and thaw settlement.

The test was conducted in a large custom built polycarbonate cell with dimensions of 3.28 feet x 6.25 feet x 4 feet, as shown in Figure 4.31. The cell was located in a large cold room whose temperature could be controlled per the requirements of the test. The cell was equipped with twelve custom designed aluminum cold plates, six at the top and six at the bottom, whose temperature was controlled by antifreeze fluid circulating through them via four Lauda Integral XT150 precision control programmable recirculating refrigerated baths. These baths were placed outside of the cold room. The cell was built to accommodate 60 to 80 ft^3 of soil. Pressure was applied from top of the cell to simulate overburden pressure with the help of an air folded flexible diaphragm. The diaphragm was attached to a rigid steel structure which was fitted around the cell for support. The steel structure was designed to apply a maximum pressure of 50 psi, nearly equal to 84000 lbf, with the help of the diaphragm.

Different measurement systems were built and/or installed for measuring upward/downward movement of the soil, strain, pressure and temperature. For measuring the frost heave action (upward and/or downward movement) of the soil, 10 Omega linear voltage displacement transducers were fitted at the top of the cell, as shown in Figure 4.32. The temperature of the cold plates was monitored with time by thermistors attached to them. Thermistor strings were made, consisting of 4 thermistors, each at different spacing. For monitoring the change in temperature with time within each soil layer, 32 thermistors were installed in each soil layer (Figure 4.33), except for the bottommost soil layer, which had 4 thermistors installed in it

(Figure 4.34). For the measurement of vertical and horizontal pressure development, 8 null pressure transducers (NP) were custom built. The arrangement and placement of all 8 NPs is shown in Figure 4.35. Each transducer had a strain gauge attached to the stainless steel diaphragm of the NP and one thermistor installed on its circumference, as shown in Figure 4.36. The strain data from the NP was processed by National Instruments Labview software.

The working principle of NP was that whenever the soil changed its state, from frozen to thawed or vice versa, the diaphragm of the NP would experience strain effects due to deflection caused by the pressure response from the soil. The strain data would be processed by the software, which would send a control signal to the electro-pneumatic (E/P) controller through a PID loop. The control signal causes the E/P controller to apply a back pressure on the diaphragm of the NP, causing it to return to its initial position (null position = zero deflection). The back pressure applied is the air pressure from an air dryer tower passed through an air filter prior to entering the E/P converter. The amount of back pressure applied was the measure of the pressure response from the soil due to its change of state on the diaphragm of the NP. The amount of back pressure was monitored by the Omega PX309 pressure transducers. All the measuring sensors were well calibrated before installing them in different soil layers.

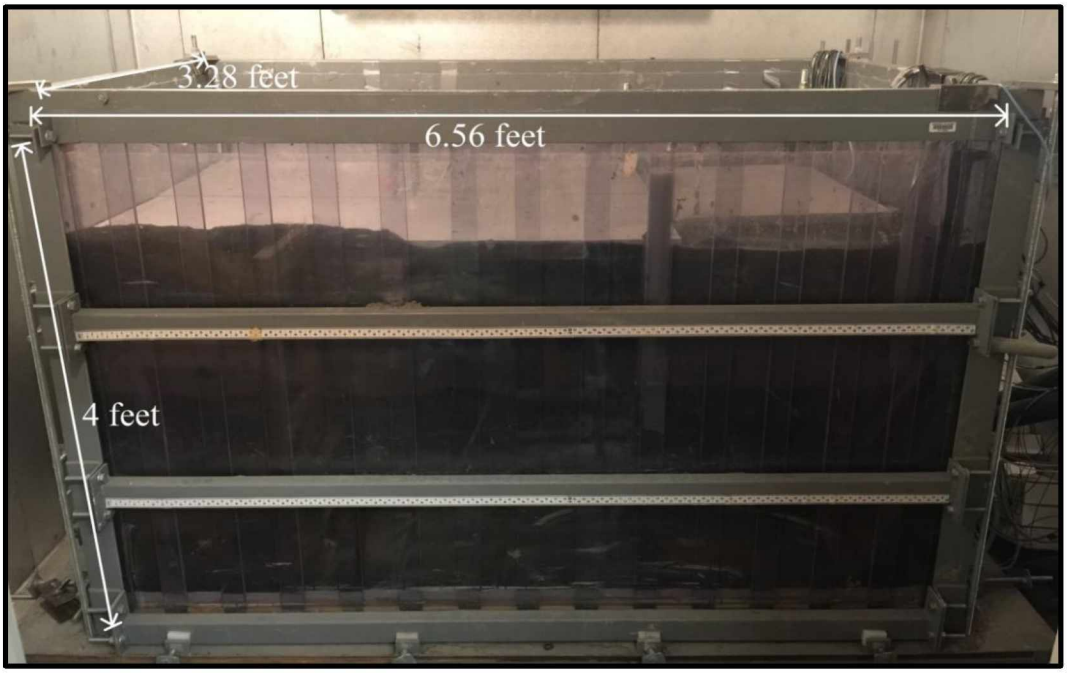

Figure 4.31: Large custom built cell used for three dimensional physical scale tests.

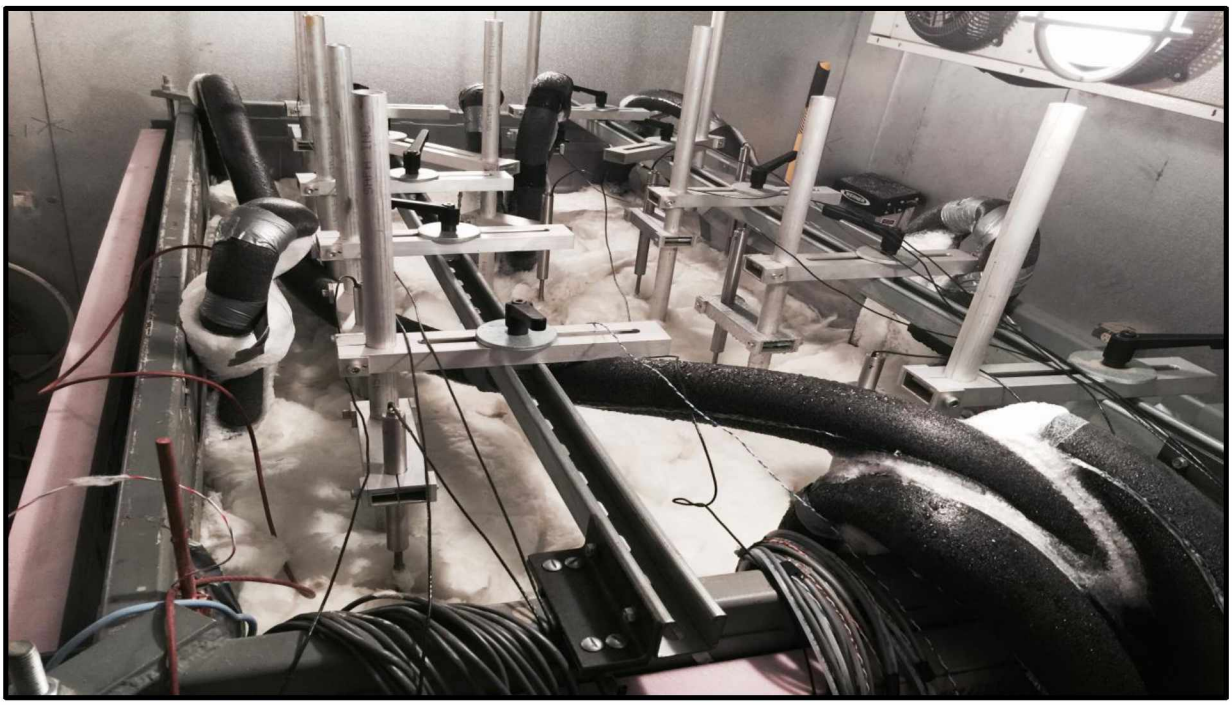

Figure 4.32: 10 Omega linear voltage displacement transducers (LVDT) installed on the top of the cell.

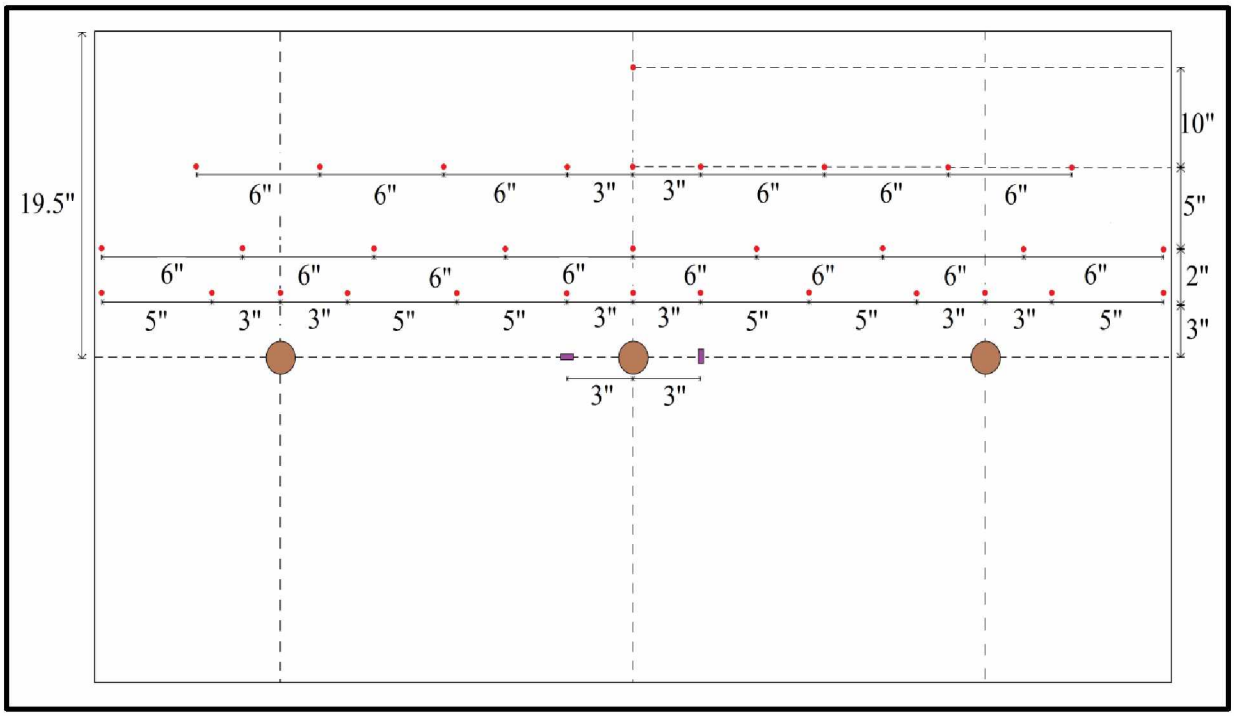

Figure 4.33: Thermistor arrangement for soil layers #2, #3, #4, #5 and #6.

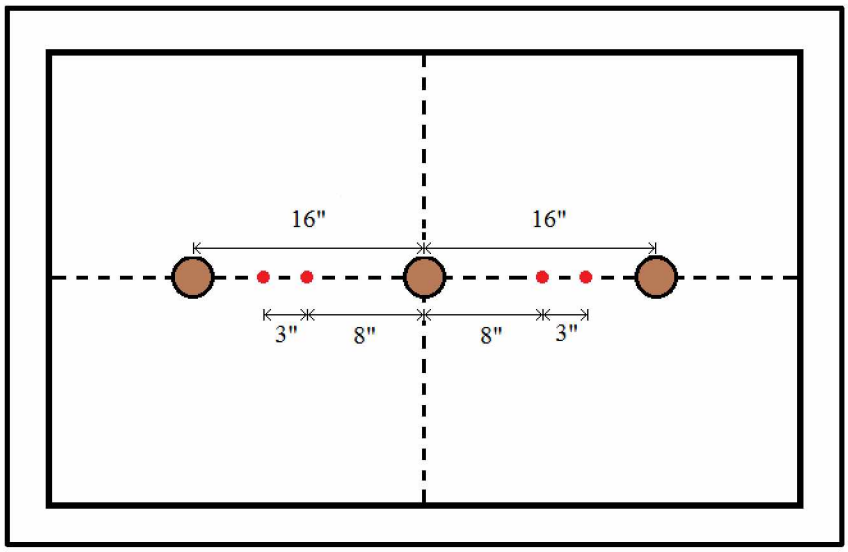

Figure 4.34: Thermistor arrangement for soil layer #1 (sand).

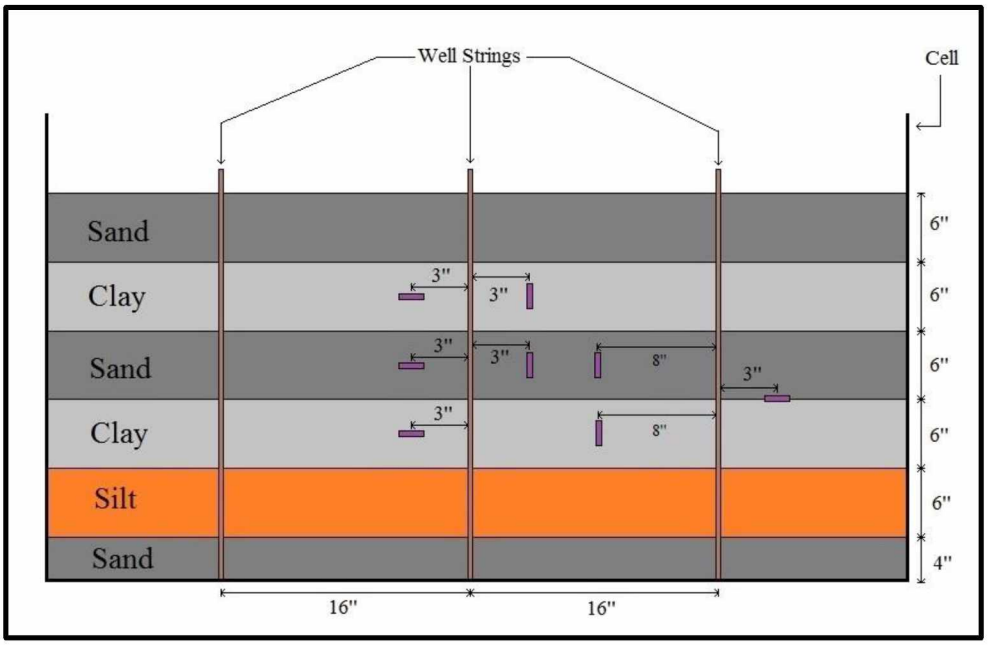

Figure 4.35: Arrangement and placement of null pressure transducer.

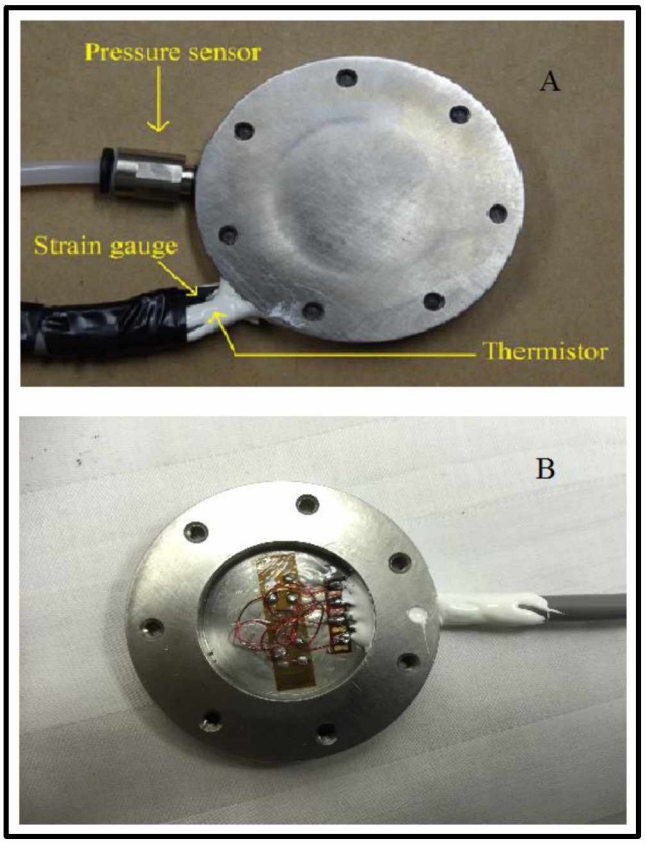

Figure 4.36: (A) Null pressure transducer from outside and (B) Null pressure transducer from inside.

The cell comprised six layers of different types of soil; clay, silt and sand. The layering and thickness scheme for different soils is shown in Figure 4.35. Based on the results of different soil tests (section 4.1), it was decided to fill the cell with three layers of commercial sand, two layers of Usibelli clay and one layer of silt sample A. Since the soil needed to heave upon freezing and only Usibelli clay showed the heaving action when subjected to freezing conditions compared to silt sample A (Figure 4.27, 4.28 and 4.29), clay was considered over silt to represent the fine-grained soil and sand for coarse-grained soils in the study. Since frost heave action is possible when there is a segregated ice distribution within soil, it is also important to observe the thaw subsidence due to melting of ice lenses upon thawing. It was necessary to have alternate layers (Figure 4.35) of fine-grained soil (clay and silt) and coarse grained soil (sand) in order to observe the tension and compression responses of different soil types on the well strings, as stated in the scientific literature.

Figure 4.37 shows the entire setup for the three-dimensional physical scale test. Along with the cell, an acrylic cylinder was placed next to the cell inside the cold room. The purpose of this acrylic cylinder was to ensure a constant supply of water to the cell during the freezing period of the soil. A 100-gallon tank of processed RO water was placed outside the cold room. Thus there was a constant supply of water from this tank to the acrylic cylinder and later to the cell during the testing period. The acrylic cylinder was well equipped with an electric pressure control switch which allowed backfilling of water in the cylinder with time from the outside tank. The amount of water consumed/given out by the soil during the freezing period was measured by monitoring the height of the water column inside the acrylic cylinder. This was achieved with the help of a Validyne differential pressure transducer.

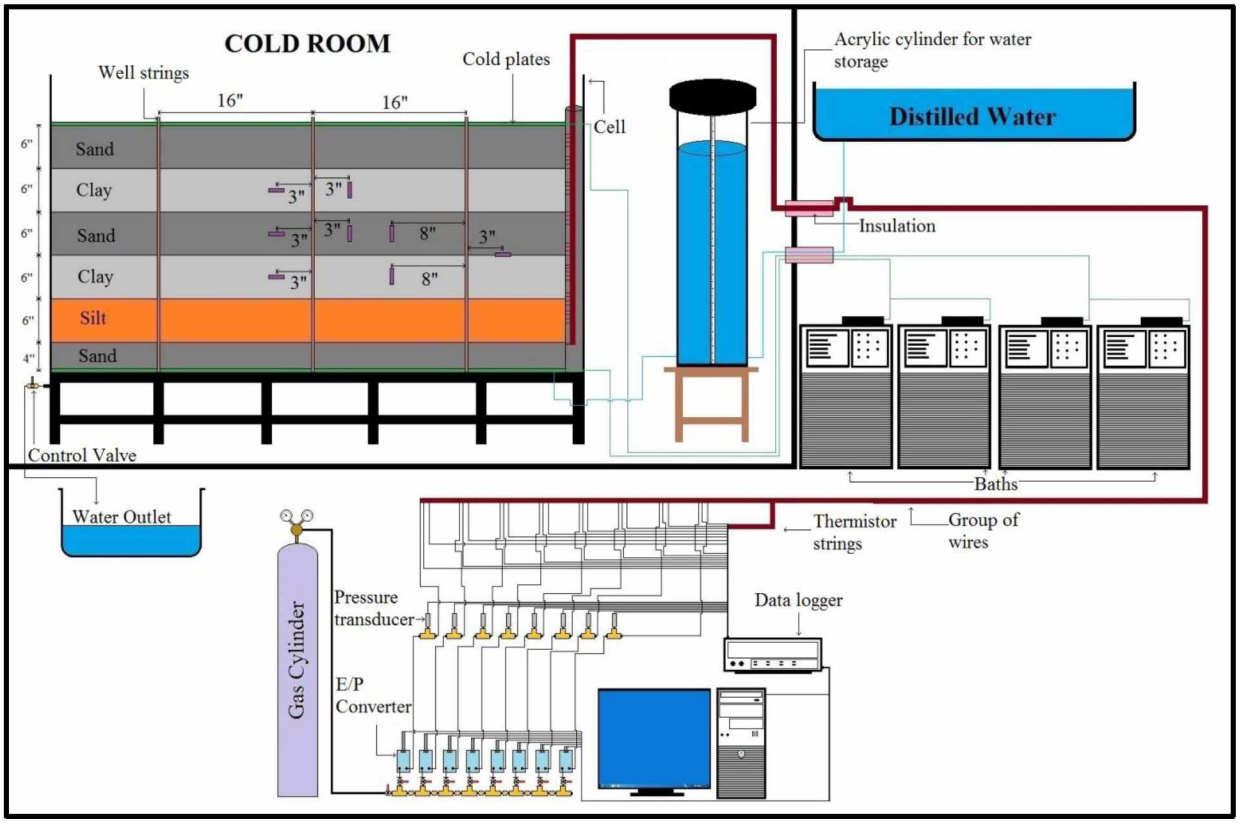

Figure 4.37: Schematic of three dimensional physical scale test including all the instrumentation and control setups.

All the NPs were placed at different orientations and locations in soil layers #3, #4 and #5 (clay, sand and clay from the bottom) to monitor and measure the vertical and horizontal soil pressure response, as shown in Figure 4.38. The cell was completely loaded with different soil layers along with all the measuring sensors and a frost heave test was conducted to monitor the functionality of the whole setup. The frost heave test ran for a period of 40 days. The aim of the test was to look at the frost heave capability for a layered soil system and further measure the tension-compression response for different types of soil with time upon freezing and thawing through the installed different measuring sensors. A constant temperature gradient was maintained along the vertical length of the cell during the test, with top plate at a lower temperature compared to the bottom plate. The source of water to the cell was from the bottom and the freezing front moved from top to bottom. The temperature inside individual soil layers was constantly monitored with the help of the thermistors installed in each soil layer (Figure 4.39). This also helped track the movement of the freezing front with time by assuming the freezing temperature of soil to be 32°F.

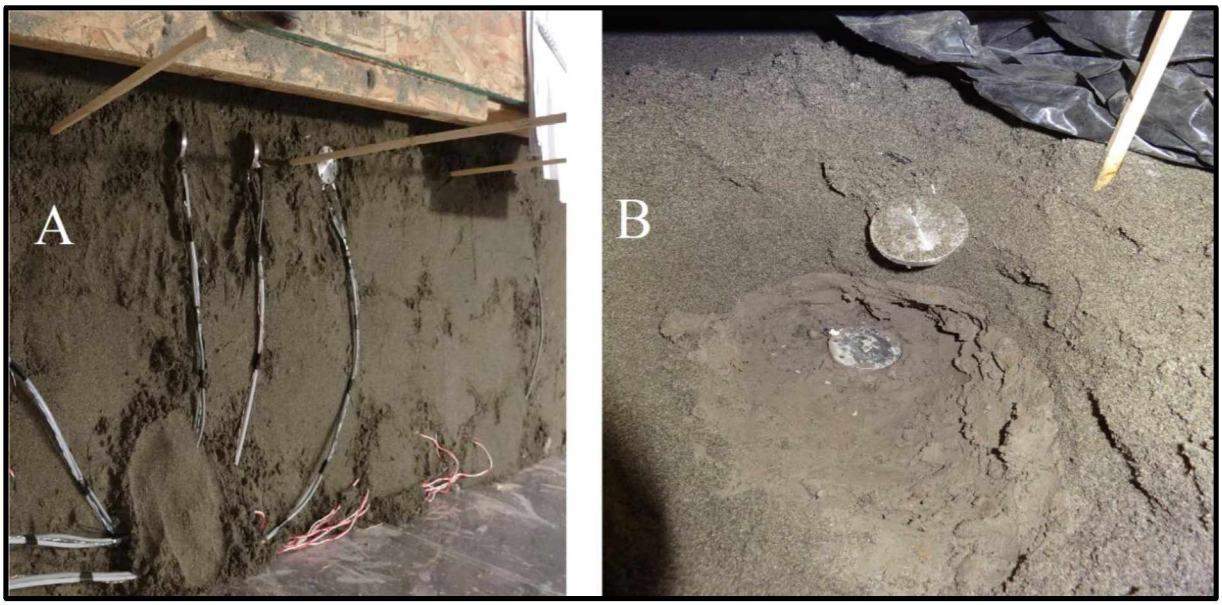

Figure 4.38: (A) Null pressure transducer installed at the different locations in different orientations around a well string* in a single layer of soil (sand) and (B) Null pressure transducer installed at the different layers of soils (sand on the top and clay in the bottom). *Wooden stick represents the well string in the picture

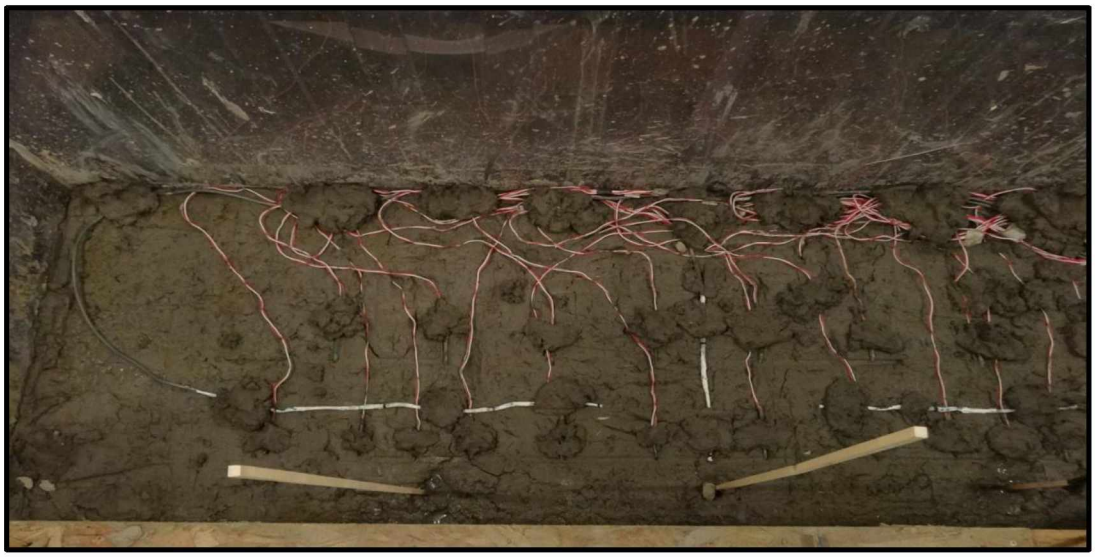

Figure 4.39: Placement of thermistor strings in the soil layer.

The results from frost heave test are shown in Figures 4.40, 4.41 and 4.42 for different NP sensors and for the thermistors (installed in each respective NP) installed in clay layer #5, sand layer #4 and clay layer #3. Based on the calibration data it was observed that approximately 7 micro-strain (7×10^{-6}) was equal to 1 psi. Strain data was converted to pressure data and plotted in these figures. The backpressure system was not functioning correctly; therefore strain was used to calculate soil pressure in the examples. As seen in these figures, the initial (at time = 0 hours) high pressure response was because of the weight of the overlaying soil. As the freezing front passed through the sensor, the soil tend to freeze causing it to change its state. The freezing of the soil caused the frost heave due to volumetric increase of the soil's mass. There was an initial compression which caused the deflection of the sensor's diaphragm as a result of the frost heave. As shown in Figure 4.40 and 4.42, the initial increase in the pressure was because of the initial compression from the soil's mass. Later the pressure drops with time as the soil tried to achieve an equilibrium state after the freezing front has passed through it. In Figure 4.41, the pressure response from sand did not change much because it is a coarse-grained soil and believed not to exhibit heaving on freezing. The sudden high response for NP3 in Figure 4.41 was believed to be a result of malfunctioning of the sensor. The pressure response from clay layer #3 was less than that shown by clay layer #5. This was because it was much deeper as compared to clay layer #5, which resulted in smaller freezing rate for clay layer #3. Figure 4.43 shows the formation of ice lenses which caused the frost heave of soils.

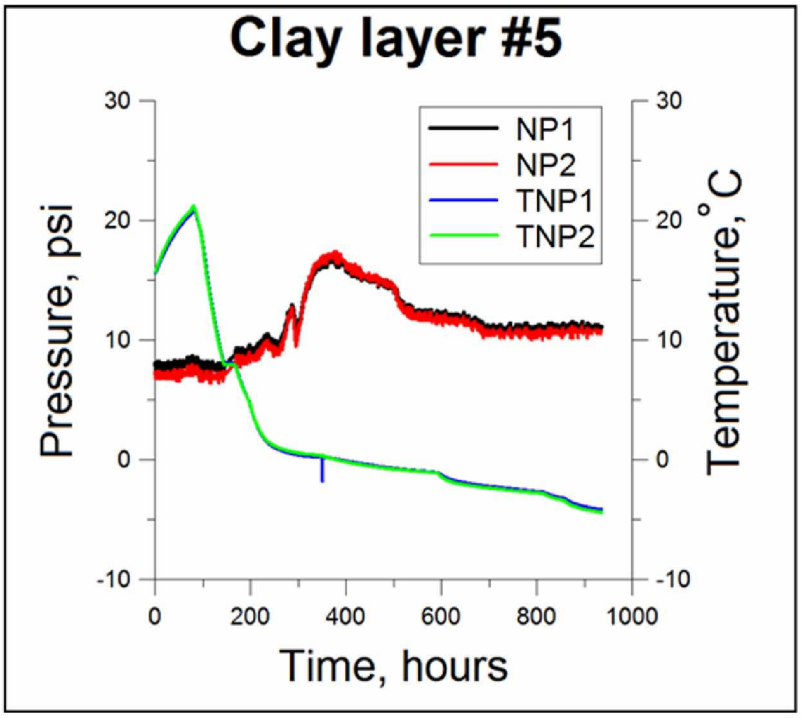

Figure 4.40: Strain data from frost heave test in the large cell for clay layer #5.

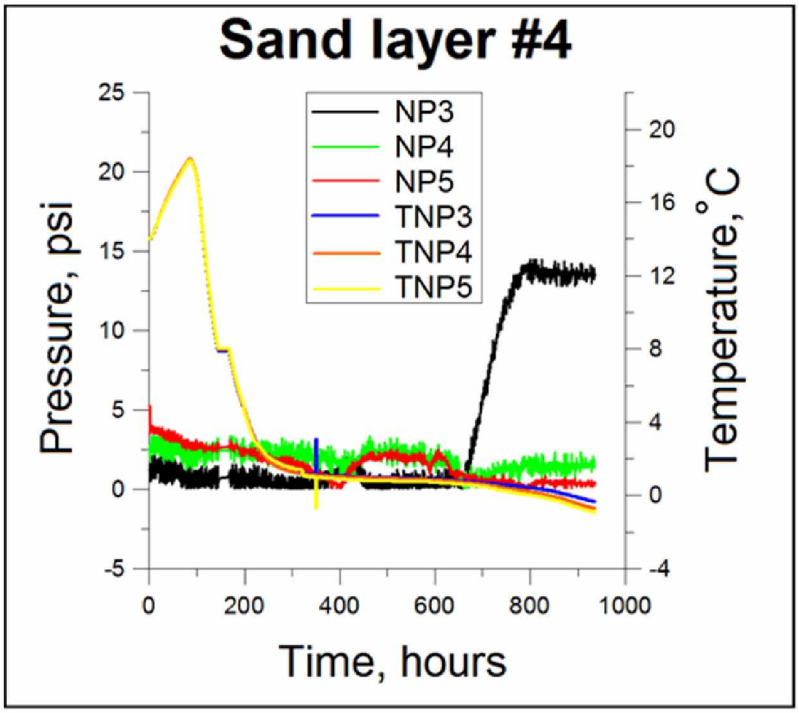

Figure 4.41: Strain data from frost heave test in the large cell for sand layer #4.

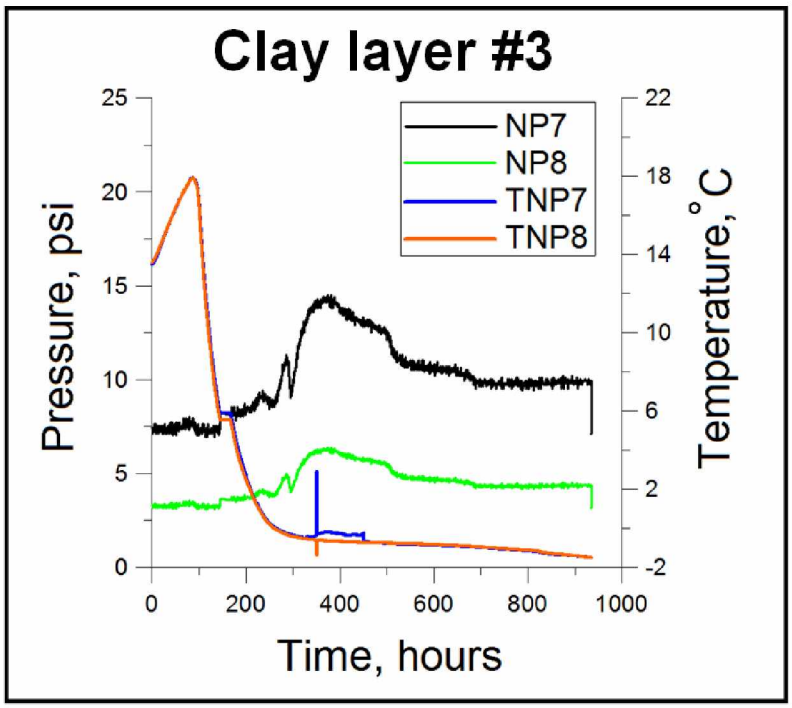

Figure 4.42: Strain data from frost heave test in the large cell for clay layer #3.

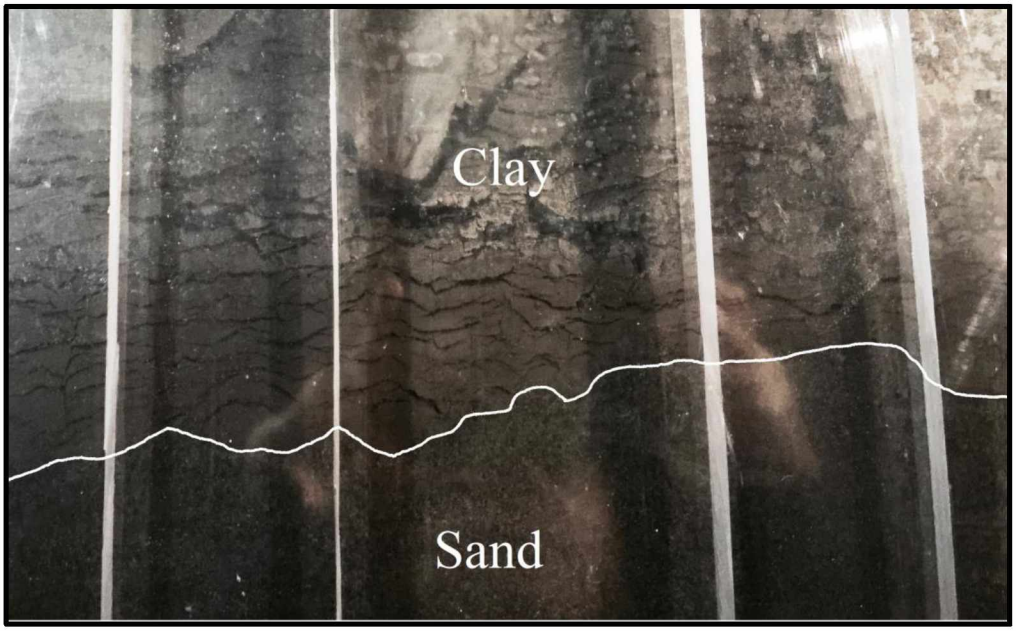

Figure 4.43: Formation of ice lens at the end of the frost heave test conducted in the large cell. (White line drawn shows the clay-sand interface)

Based on the results obtained from each individual NP, the soil pressure response was successfully monitored with time. The layered soil system absorbed ~42.83 gallons (~162.13 Liter) of water total for a period of 40 days. Additional soil data obtained at the end of the test is given in the appendix in Table A-39.

4.3 One-Dimensional Consolidation Test

The one-dimensional consolidation test aimed towards understanding the influence of different parameters on thaw subsidence: soil type, ice/water content, consolidation history and soil layering. The parameters that can be targeted in this test approach are lateral soil pressure development, soil pore pressure response, consolidation pattern, frost heaving action and thaw settlement. The test would be conducted in a custom designed and built acrylic cylinder, as shown in Figure 4.44. The test was designed for direct measurement of lateral soil pressure response in frozen and thawed states and pore pressure response from soil during thawing. Due to its transparent body, soil consolidation and thaw settlement with time will be visible directly.

Figure 4.44: Custom designed and built acrylic cylinder along with its components for one-dimensional consolidation test.

The cell was designed to handle pressures up to 500 psi. The upper and lower pedestals shown in Figure 4.44 can be connected to two external programmable temperature baths which will be circulating antifreeze fluid through them for temperature control. The pedestals can be set at desired temperatures which will aid in achieving the desired temperature gradient along the vertical length of the soil sample during the test. This will be required for creating freezing and thawing conditions for the cylindrical soil sample inside the cylinder. This will help in studying the post thaw consolidation pattern upon thaw settlement with time. Samples obtained from the frost heave test conducted in the Laval cell can be used for this test. The design of the cell has two null pressure transducers on its side, as shown in Figures 4.45 and 4.46. The working principle of these is the same as that explained in section 4.2. The pore water pressure response can be monitored at the top, bottom and center of the soil sample. The setup is equipped with two air diaphragm control high pressure regulators connected to a high pressure nitrogen gas cylinder, for the two null pressure transducers to increase the air pressure from 100 psi to 1000 psi, if needed. The PID control signal goes through the E/P controller and then to the air loaded high pressure regulator for applying the appropriate back pressure. Figure 4.47 shows the schematic for the one-dimensional consolidation test approach and Figure 4.48 shows the actual view of the whole setup.

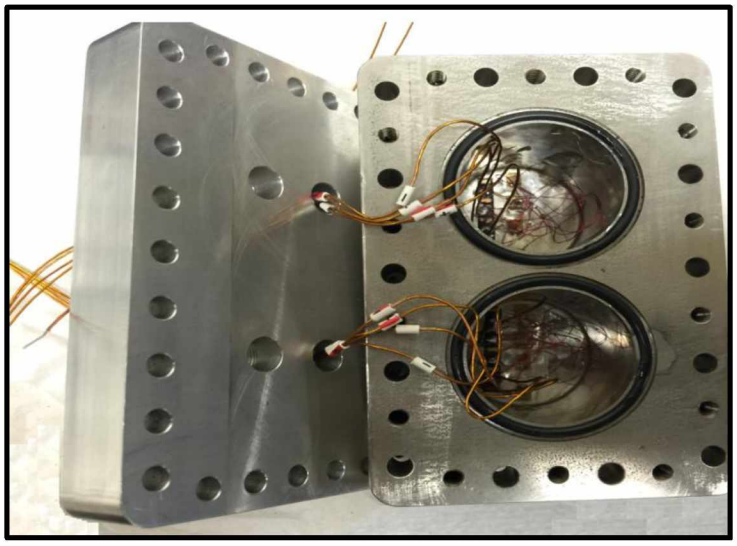

Figure 4.45: Null pressure transducer from inside for the one dimensional consolidation test.

Figure 4.46: One dimensional consolidation cell with two null pressure transducers attached to its side.

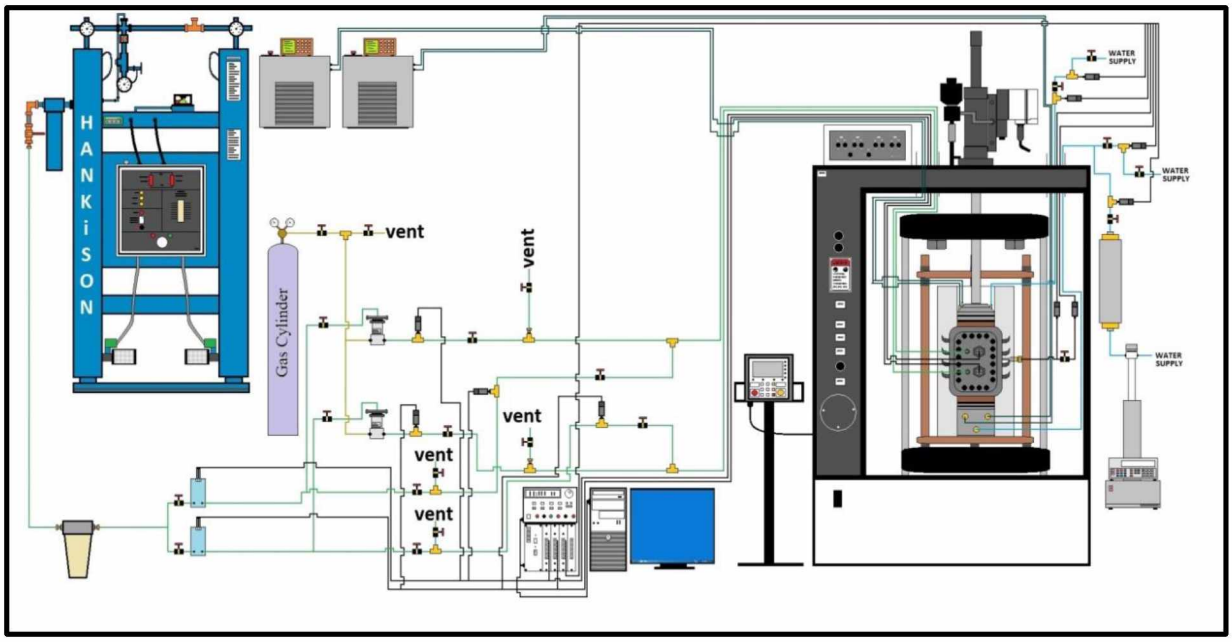

Figure 4.47: Schematic of one-dimensional consolidation cell with all the instrumentation.

Figure 4.48: One dimensional consolidation test actual setup.

Soil samples were not tested on this experimental setup because the setup was not completely ready at the time of writing this thesis. But the real time data obtained from this test can be compared with the data obtained from the three-dimensional physical scale test. This can help in developing correlations among different factors and understanding the different mechanisms causing thaw subsidence problems.

CHAPTER 5 COMPUTER MODELING APPROACH TO UNDERSTAND THAW SUBSIDENCE

The completion practices of a conventional oil and gas well vary greatly when compared to those of an Arctic region oil and gas wells. More than 35 years of production of hot oil from Arctic oil and gas wells has potentially resulted in continuous thawing of surrounding permafrost. In order to better understand the principles regarding the effects of thawing of different frozen soils, the constant radial heat exchange between the wellbore and the surrounding frozen soils and between different layers of frozen soils was modeled in COMSOL Multiphysics™. A two dimensional axisymmetric geometry computer model was made in COMSOL Multiphysics™ for thermal analysis and a two dimensional geometry computer model for mechanical analysis. The thermal analysis was conducted using only the "Heat Transfer in Solids *(ht)*" module and the mechanical analysis was conducted using the "Heat Transfer in Solids *(ht)*" and the "Solid Mechanics (solid)" module of the software.

5.1 Thermal Analysis

Thermal analysis included studying and understanding thawing of ice-rich soils and refreezing behavior of the thawed soils with time. Different soil types were taken into consideration and peat was considered for the active layer. Based on the literature review (section 2.7) certain aspects of the thawing behavior of ice-rich soils were targeted and studied in this analysis. Previous work was compared to the simulation results obtained for different scenarios.

5.1.1 Base Model for Thermal Analysis

A two-dimensional axisymmetric model of a 28 feet section of the wellbore was designed in the heat transfer module of the software, as shown in Figure 5.1. The simulation work initially involved working on a base model. It consists of different components of a conventional oil and gas well, including tubing, casing and cement layer. The modelled soil system was composed of a 10 feet of active layer followed by 6 feet of three individual layers of clay, silt and sand from top to bottom. The purpose behind building a base model was to look at the effect of different thermal properties or input parameters on the thawing and refreezing behavior of the frozen soils and to calibrate the approach for application to the larger more realistic model. The amount of thawing and the final thaw radius for a particular period of time would depend strongly on the

soil properties, especially the thermal properties of the soil. Figure 5.2 shows the actual size of the model along with the thermal insulation boundary taken into consideration for simulation runs. Figure 5.3 shows the zoomed in image of the oil well configuration and Figure 5.4 shows the meshing considered for the simulation run. An extremely fine mesh was considered for the simulation. Thermal properties considered for the tubing, annular fluid, casing and cement are listed in Table A-41 in the Appendix.

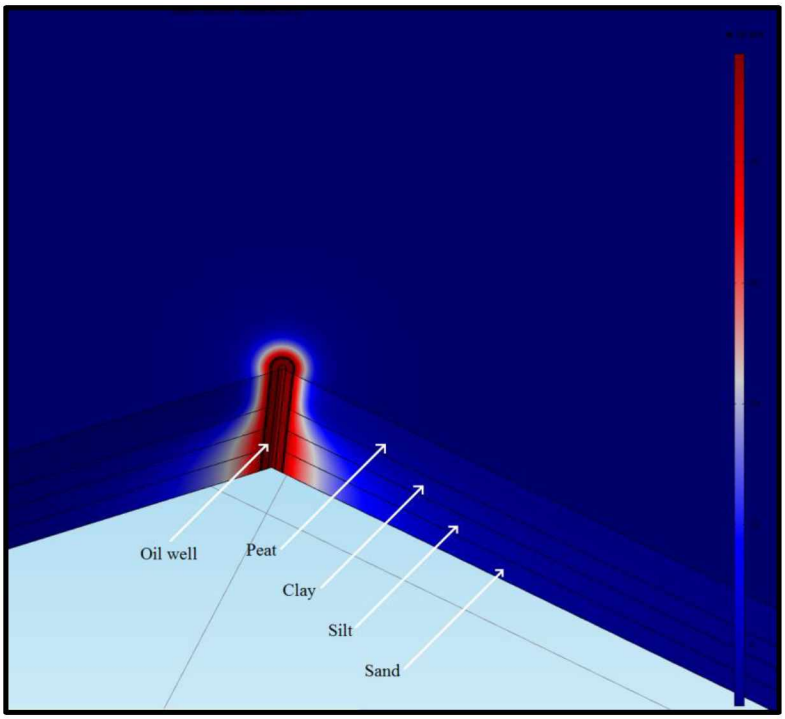

Figure 5.1: Base model post simulation run showing different layers of soil.

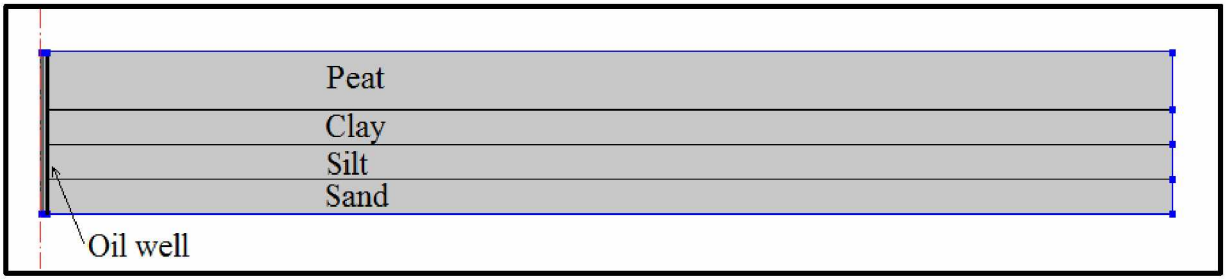

Figure 5.2: Base model layout showing the thermal insulation boundary. (Blue line)

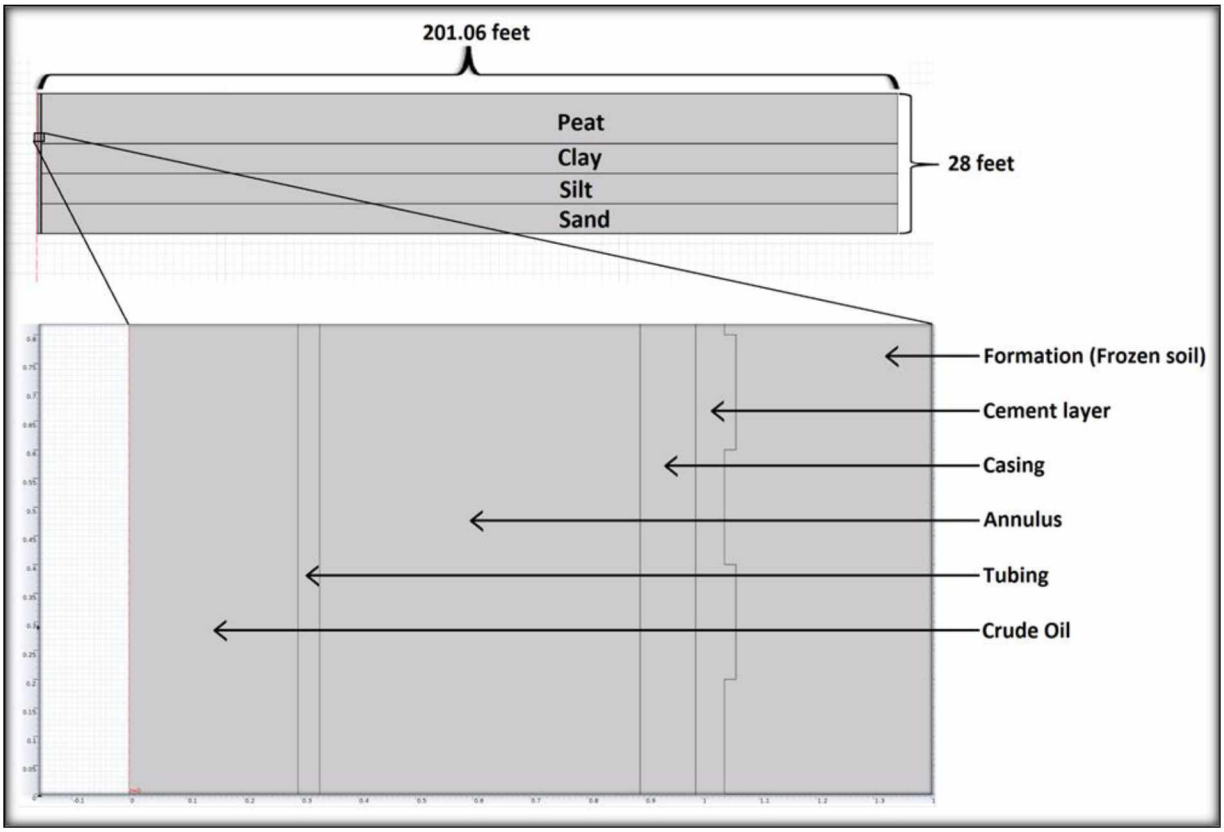

Figure 5.3: Zoomed in image of the oil well configuration in the base model.

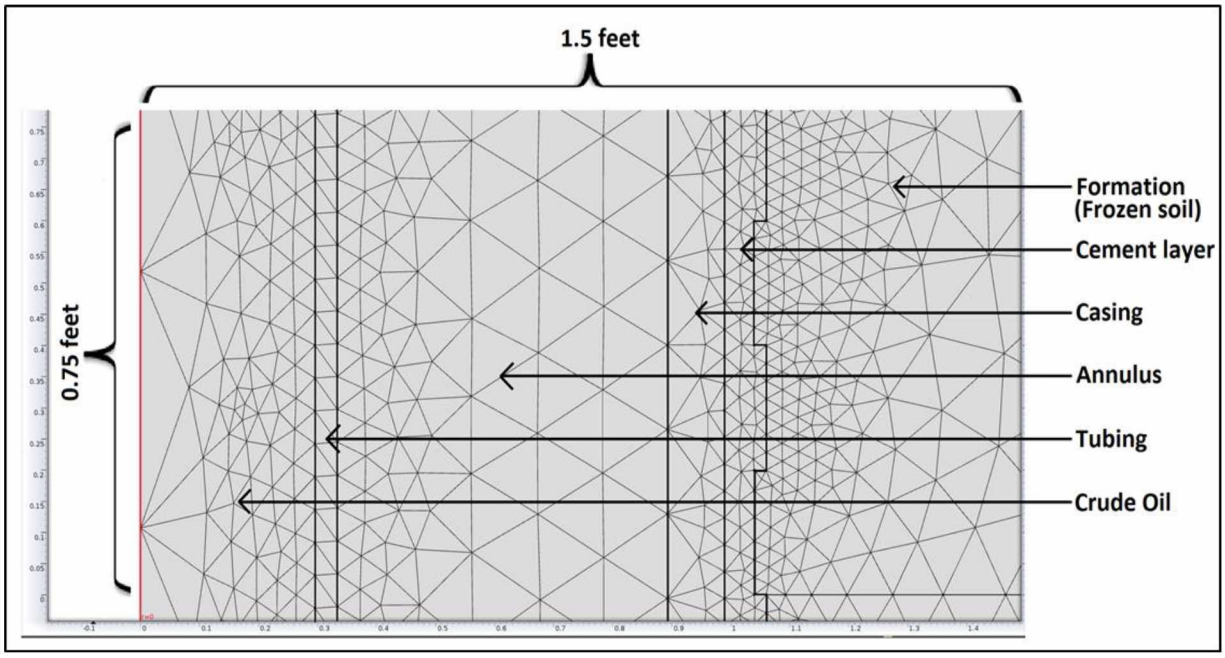

Figure 5.4: Fine mesh considered for simulation run in the base model.

5.1.1.1 Input Parameters and Assumptions for Thermal Analysis

The main aim behind the base model was to look at the effect of varying thermal properties on the final thaw radius. For the thermal properties of different types of soils, temperature dependent empirical correlations were used. The empirical correlations were obtained from the plots shown in Figures A-5 to A-11 in the Appendix. To date, most of the simulation work was conducted by assuming constant values for different thermal properties to analyze thaw radius. Using temperature-dependent empirical correlations differentiates this analysis from the previous simulation work and the results obtained were later compared to those discovered for thaw radius in the scientific literature.

The entire thermal analysis followed three assumptions: (1) the initial temperature of the permafrost formation was 23°F; (2) there was no heat exchange at the boundary of the frozen soils; and (3) soil freezing temperature was 32°F. The temperature at the boundary had no effect on the thawing process of the frozen soils and the only source of heat was the oil well (Figure 5.2). This assumption also considers having an infinite permafrost formation in radial direction. The initial temperature for the permafrost formation was assumed to be 23°F on the basis of Figure A-12 in the Appendix, where the average value was obtained from a Prudhoe Bay area subsurface temperature profile.

5.1.1.2 Results and their Validation for Base Model

Simulations were conducted for a period of 45 years where the heat input from the wellbore was during the initial 30 years and for the latter 15 years there was no heat input from the wellbore (shut-in period for well). Thaw radius was analyzed for all the soil types at different time periods. This was achieved by observing the horizontal temperature distribution at various soil depths from the center of the wellbore. The region where temperatures exceeded 32°F was considered the thawed region according to assumption (3). Along with thaw radius, the effect of different parameters on thaw radius was also analyzed. The input values for oil flowing temperature and soil's initial temperature were changed periodically. This was done to compare the simulation results to data from current literature under similar conditions. Figure 5.5 shows the post simulation model layout.

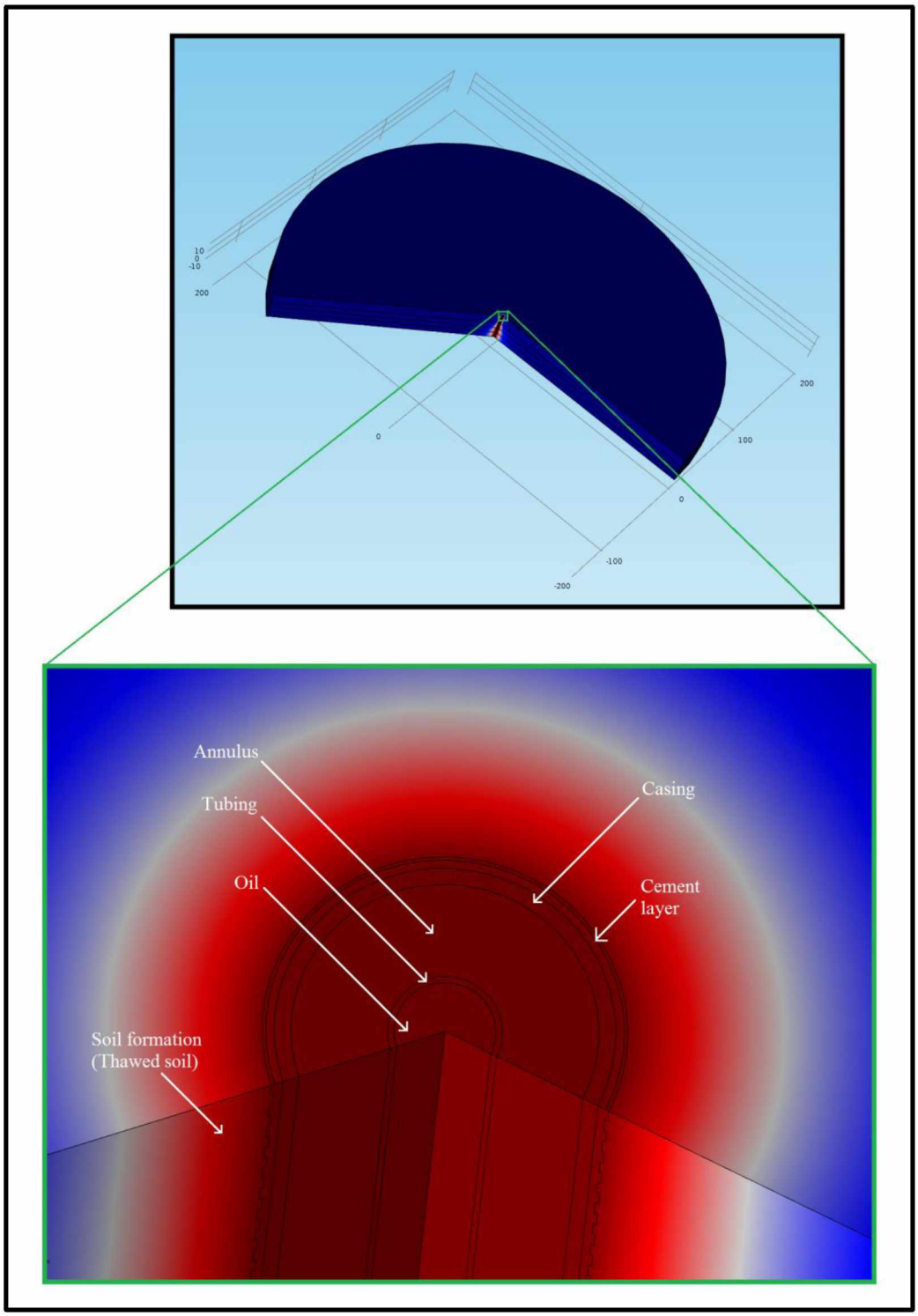

Figure 5.5: Post simulation model layout for base model.

A sample run was conducted on the base model to check the applicability of empirical correlations to modeling of the heat transfer process between the wellbore and the surrounding frozen soils. The simulation was conducted by assuming an oil flowing temperature of 120°F and the whole geometry was assumed to be at 23°F initially. Figures 5.6, 5.7, 5.8 and 5.9 show the horizontal temperature distribution from the center of the well during the heat transfer period for soil types peat, clay, silt and sand, respectively. Figures 5.10, 5.11, 5.12 and 5.13 show the horizontal temperature distribution from the center of the well when there is no heat input from the well (shut-in period of the well). Thus the assumption was that hot oil is flowing through the wellbore for the first 30 years and then it is a well shut-in period (or refreezing period) for the next 15 years.

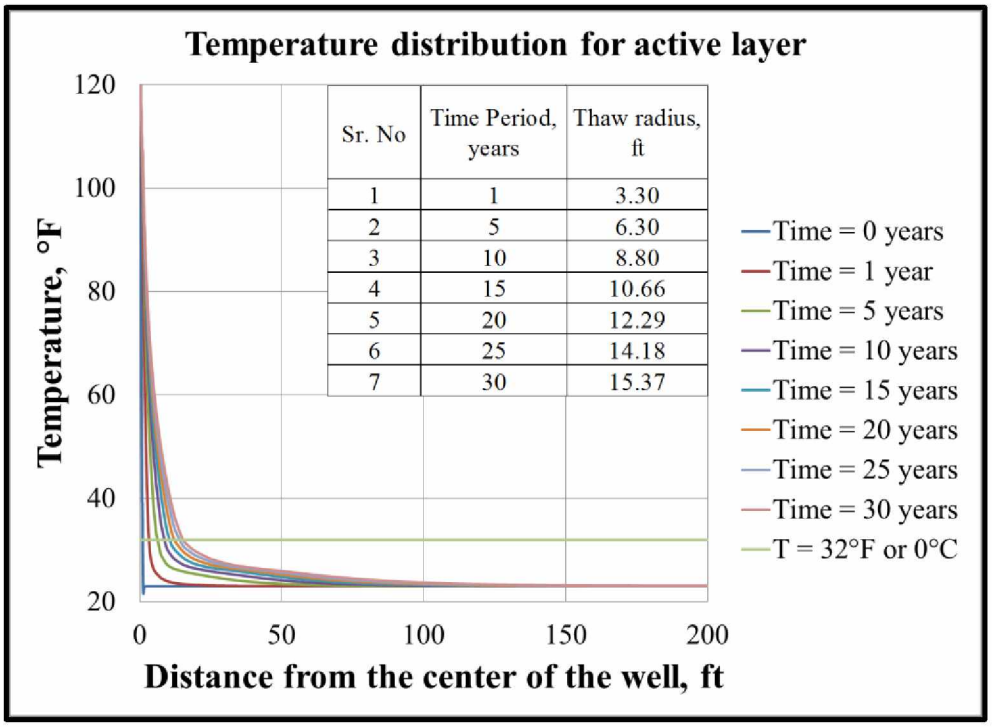

Sr. No	Time Period, years	Thaw radius, ft
1	1	3.30
2	5	6.30
3	10	8.80
4	15	10.66
5	20	12.29
6	25	14.18
7	30	15.37

Figure 5.6: Radial temperature distribution with incremental time period for peat (active layer) during thawing period.

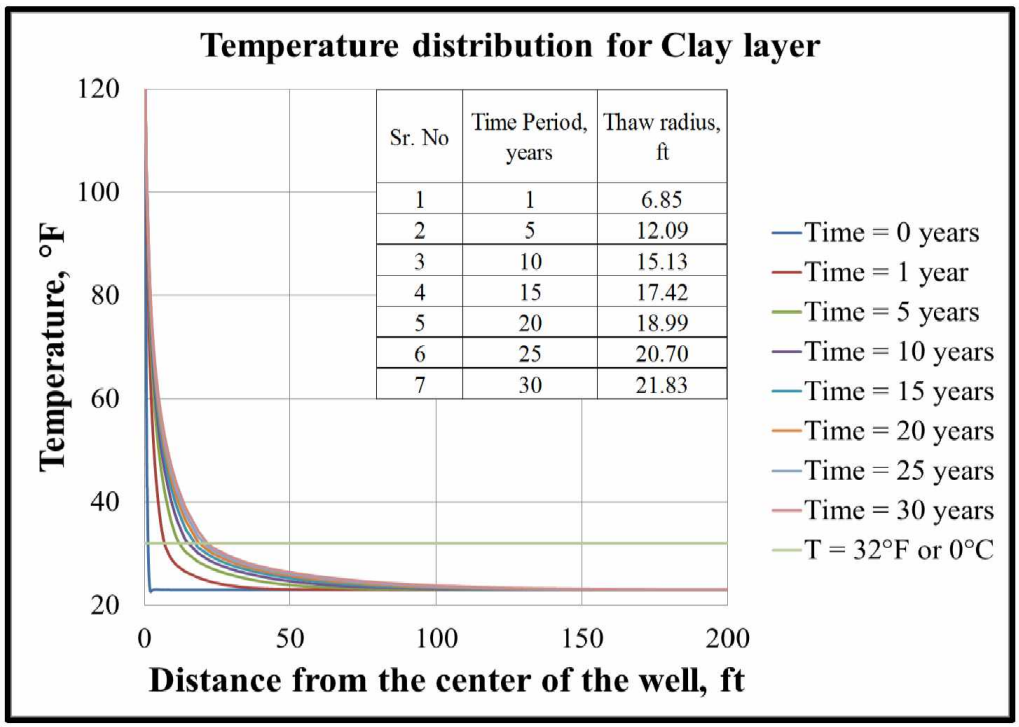

Figure 5.7: Radial temperature distribution with incremental time period for clay during thawing period.

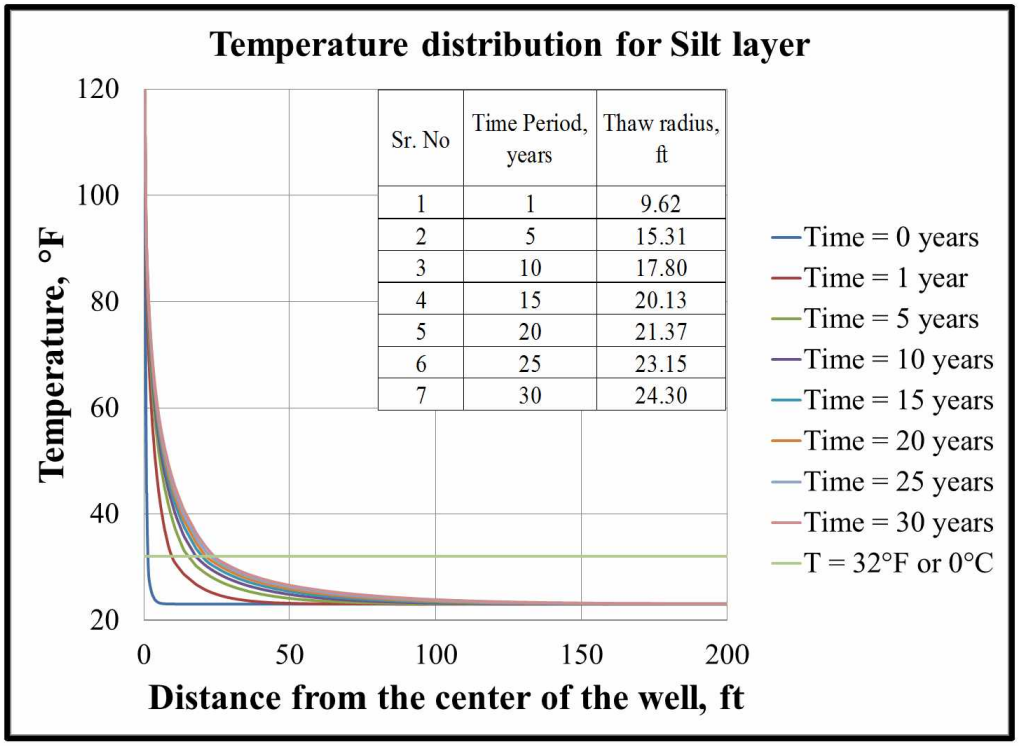

Figure 5.8: Radial temperature distribution with incremental time period for silt during thawing period.

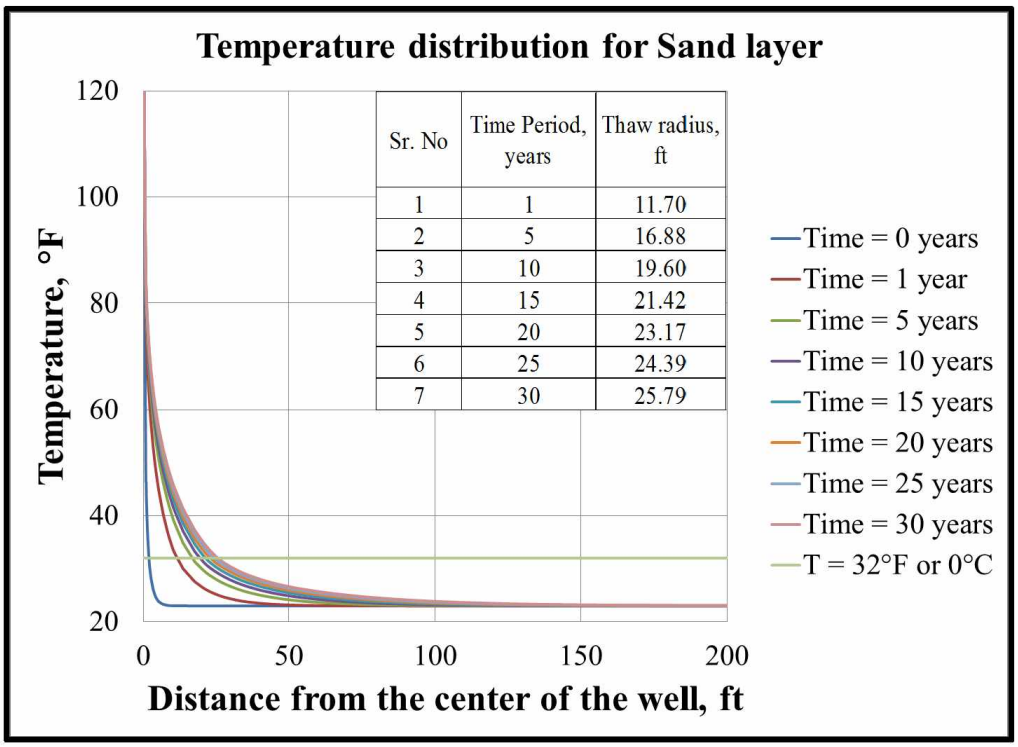

Sr. No	Time Period, years	Thaw radius, ft
1	1	11.70
2	5	16.88
3	10	19.60
4	15	21.42
5	20	23.17
6	25	24.39
7	30	25.79

Figure 5.9: Radial temperature distribution with incremental time period for sand during thawing period.

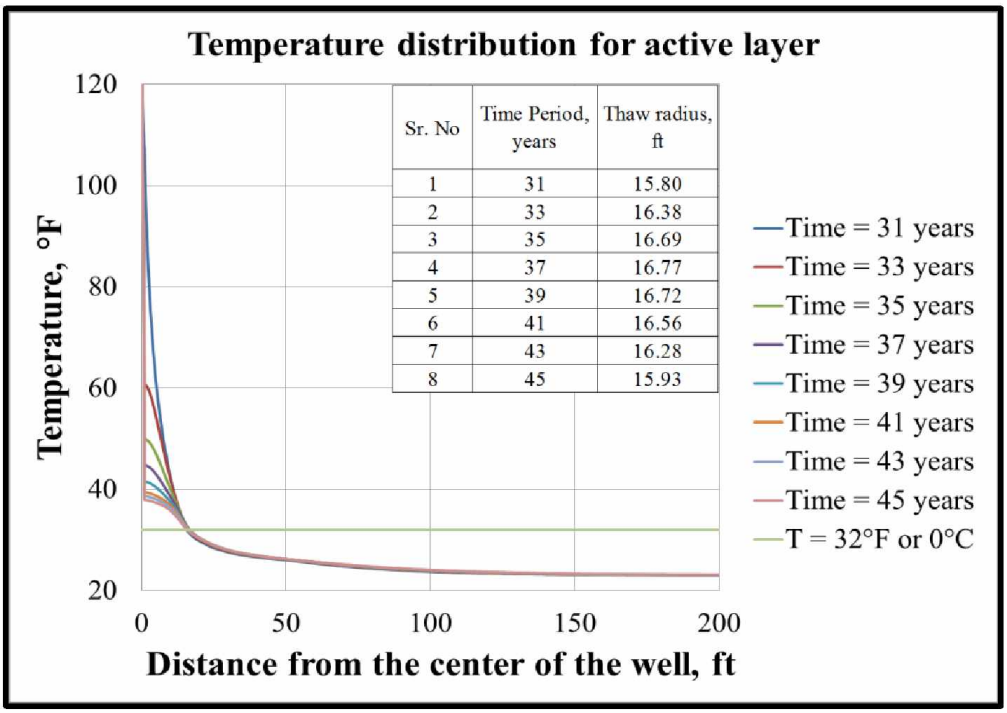

Sr. No	Time Period, years	Thaw radius, ft
1	31	15.80
2	33	16.38
3	35	16.69
4	37	16.77
5	39	16.72
6	41	16.56
7	43	16.28
8	45	15.93

Figure 5.10: Radial temperature distribution with incremental time period for peat (active layer) during refreezing period.

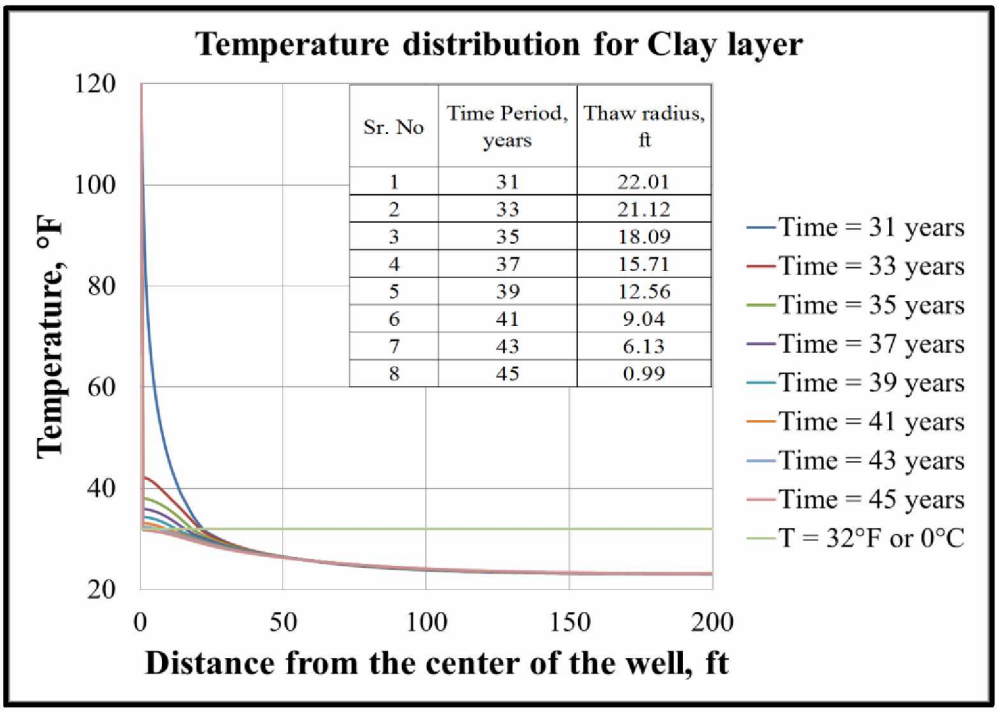

Sr. No	Time Period, years	Thaw radius, ft
1	31	22.01
2	33	21.12
3	35	18.09
4	37	15.71
5	39	12.56
6	41	9.04
7	43	6.13
8	45	0.99

Figure 5.11: Radial temperature distribution with incremental time period for clay during refreezing period.

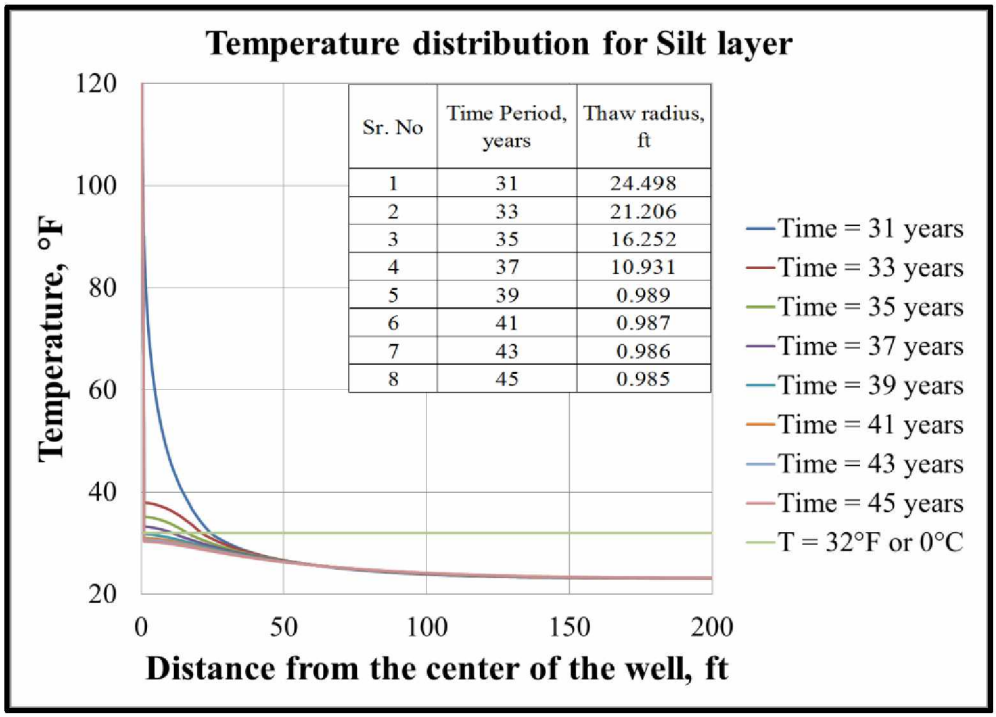

Sr. No	Time Period, years	Thaw radius, ft
1	31	24.498
2	33	21.206
3	35	16.252
4	37	10.931
5	39	0.989
6	41	0.987
7	43	0.986
8	45	0.985

Figure 5.12: Radial temperature distribution with incremental time period for silt during refreezing period.

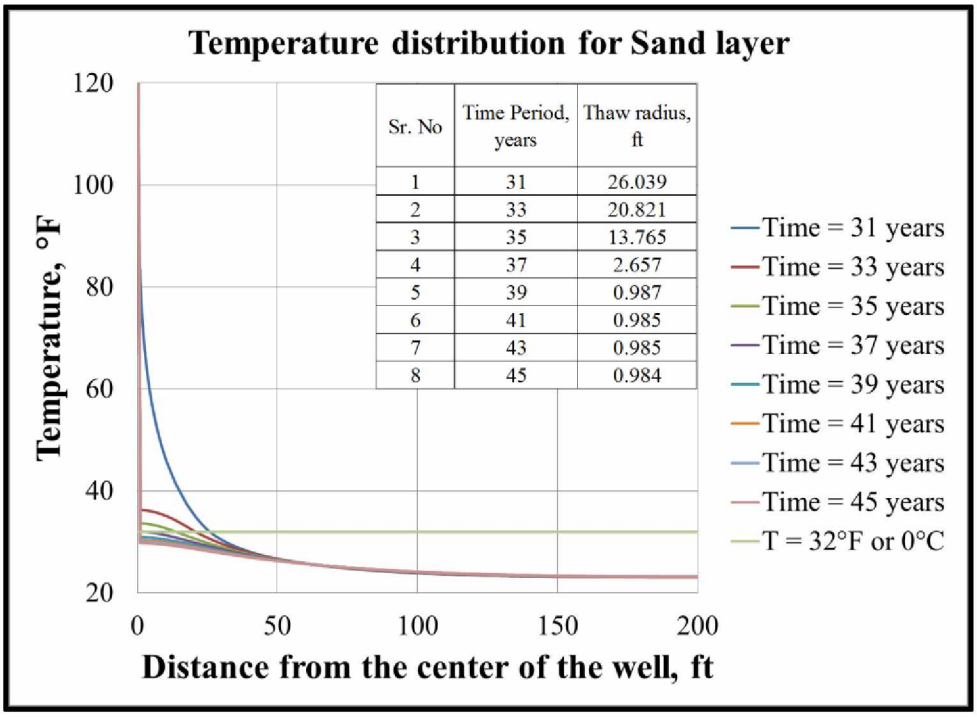

Sr. No	Time Period, years	Thaw radius, ft
1	31	26.039
2	33	20.821
3	35	13.765
4	37	2.657
5	39	0.987
6	41	0.985
7	43	0.985
8	45	0.984

Figure 5.13: Radial temperature distribution with incremental time period for sand during refreezing period.

Figures 5.14 and 5.15, show the change in the thermal properties with temperature at the end of 30 years of thawing for different soil types. Since latent heat was taken into consideration, there is a sudden increase for the temperature range 26.33°F to 37.13°F (or -3.15°C to 2.85°C or 270K to 276K) for heat capacity in Figure 5.14. Sand, being a coarse-grained soil, has a very low water content compared to other fine-grained soils like clay and silt, thus there is not much increase in heat capacity for sand, as shown in Figure 5.14. All the results for the sample simulation runs are summarized in Table 5.1. Figure 5.16 shows the thawing behavior for different soil types during the thawing period and Figure 5.17 shows the thaw radius during the refreezing period. In Figure 5.16, sand thawed the most because it had less water content compared to other three soil types . This is due to the latent heat effect, wherein the phase change of ice to water absorbs more heat resulting into a decrease of the rate of heat transfer. In Figure 5.17, clay, silt and sand all refreeze completely except for peat. This is mainly because peat is believed to have insulation properties compared to other soil types. Surface freezing was not taken into account in the model. Thus the base model exhibited good results after using the empirical correlations for temperature dependent thermal properties of soil.

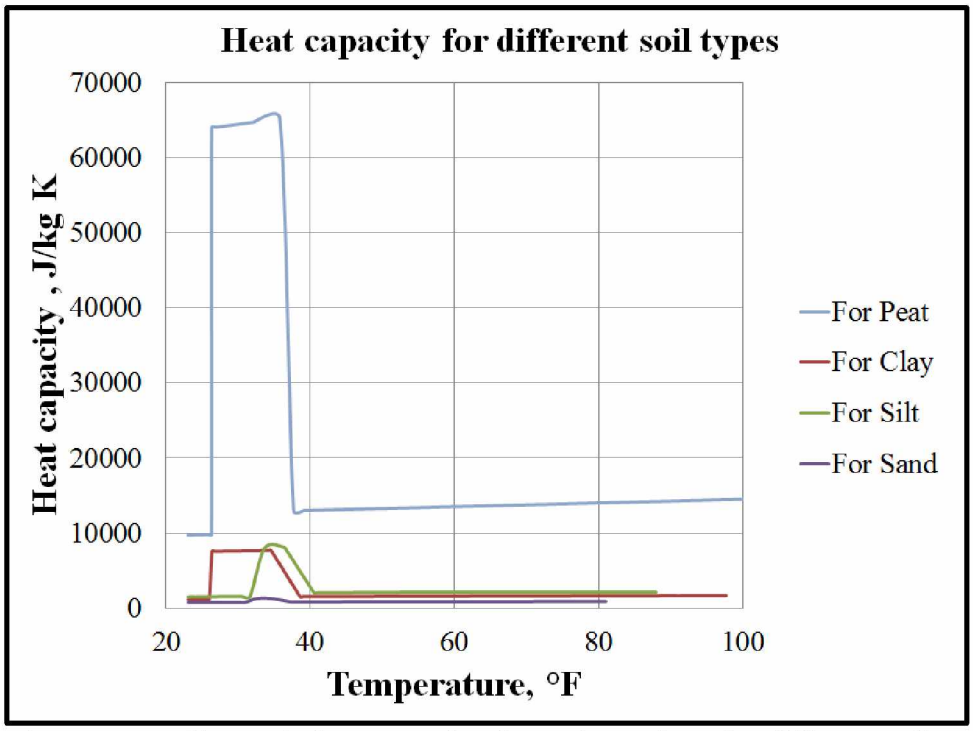

Figure 5.14: Change in heat capacity due to latent heat for different soil types with temperature and state.

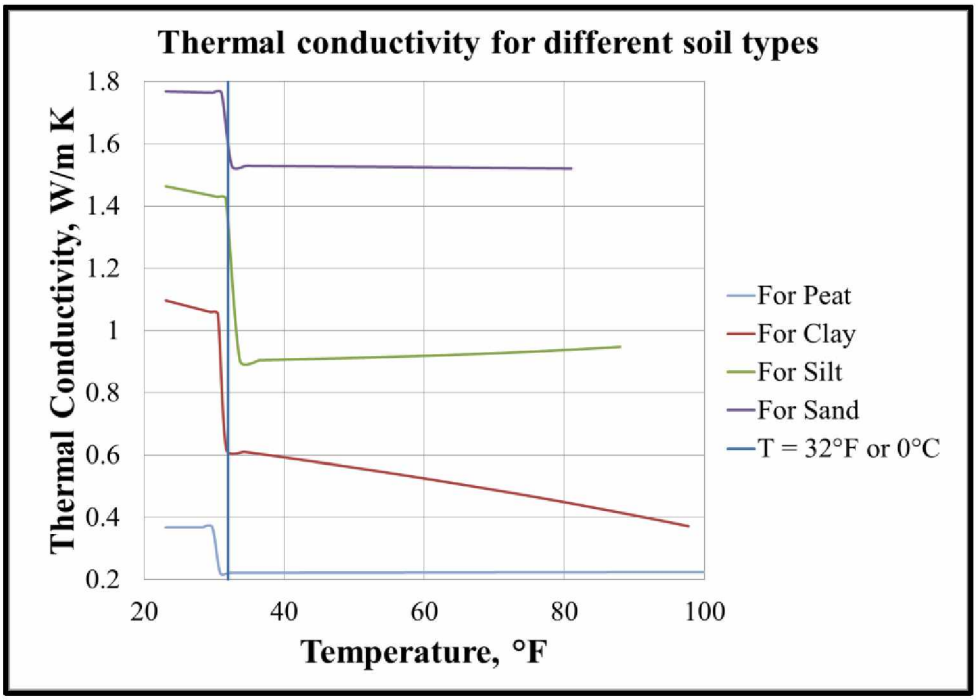

Figure 5.15: Change in thermal conductivity for different soil types with temperature and state.

Table 5.1: Thaw radii of different soil types for base model

Sr. No.	Time, years	Soil Type				
		Peat	Clay	Silt	Sand	
		Thaw radius, feet				
1	1	3.30	6.85	9.62	11.70	Thawing period
2	5	6.30	12.09	15.31	16.88	
3	10	8.80	15.13	17.80	19.60	
4	15	10.66	17.42	20.13	21.42	
5	20	12.29	18.99	21.37	23.17	
6	25	14.18	20.70	23.15	24.39	
7	30	15.37	21.83	24.30	25.79	
8	31	15.80	22.01	24.498	26.039	Refreezing period
9	33	16.38	21.12	21.206	20.821	
10	35	16.69	18.09	16.252	13.765	
11	37	16.77	15.71	10.931	2.657	
12	39	16.72	12.56	0.989	0.987	
13	41	16.56	9.04	0.987	0.985	
14	43	16.28	6.13	0.986	0.985	
15	45	15.93	0.99	0.985	0.984	

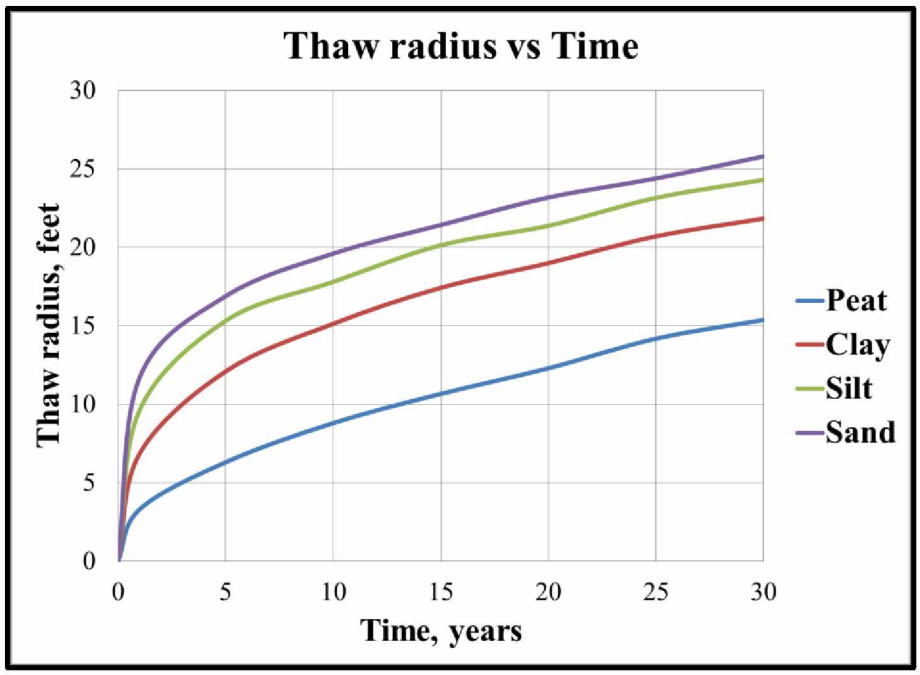

Figure 5.16: Thaw radius versus time for different soil types during thawing period for base model.

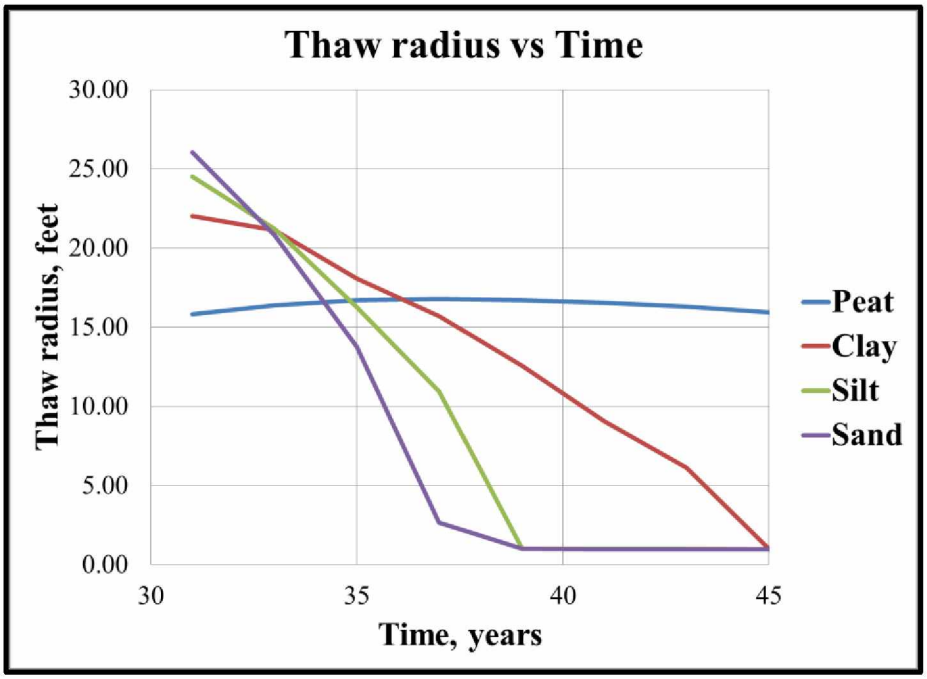

Figure 5.17: Thaw radius versus time for different soil types during refreezing period for base model.

Using the base model, the thaw radii at the end of a specific time period were validated with the actual data from the literature under similar conditions, as shown in Figures 5.18 and 5.19. Figure 5.18 shows the comparison between the post-simulation results obtained for sand to the thaw radius obtained through BP Alaska Inc. field experiment (Davies and Boorman, 1973) at the end of 12 months of thawing. Figure 5.19 shows the comparison between the post-simulation thaw radii for silt at different time periods with the finite element analysis performed by Smith and Clegg (1971) for similar soil type. For Figure 5.18, the input value for the oil flowing through the wellbore was changed according to the temperature value obtained from the literature. The same was done for the value of the initial temperature of the system. Thus inputs for each thermal property of frozen and thawed soils were validated.

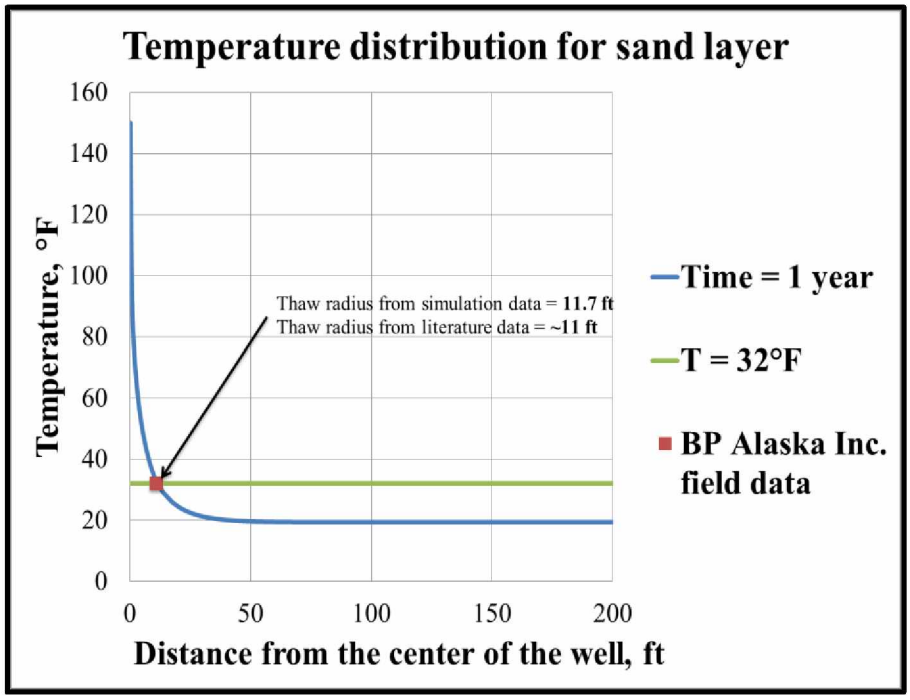

Figure 5.18: Comparison between simulation results and literature data for soil type sand.

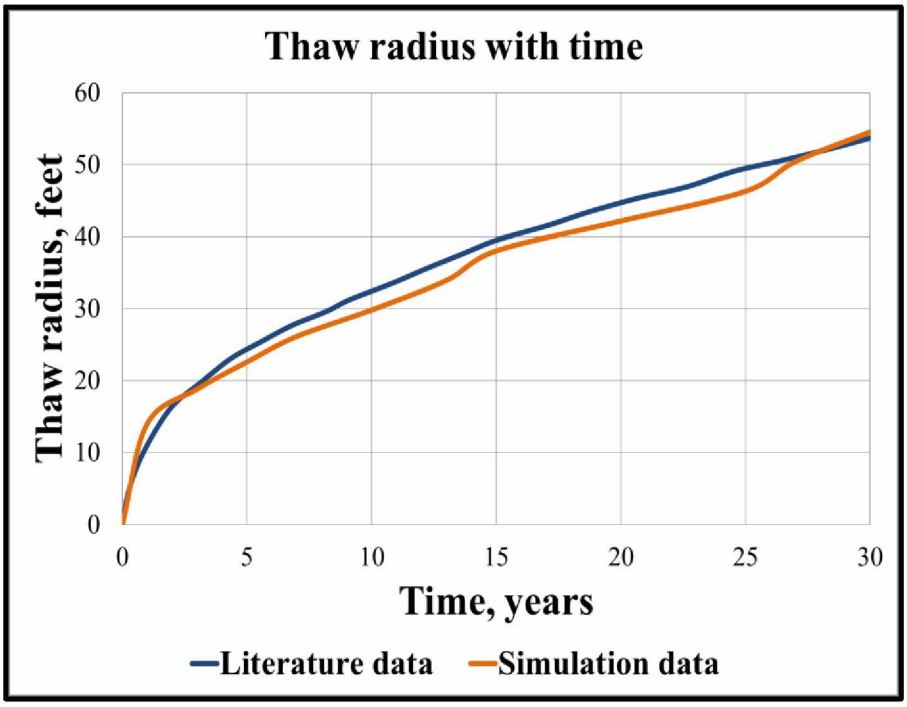

Figure 5.19: Comparison between simulation results and literature data for soil type silt. (Literature data from Smith and Clegg, 1971)

5.1.2 Main Model for Thermal Analysis

The main model involved modeling an entire oil well at Alaska's North Slope (Prudhoe Bay). The model had a total length of 2200 feet and was 200 feet wide. The 2000 feet thickness of the permafrost was taken into consideration. The last layer of soil of thickness 100 feet was assumed to contain no ice. The oil well completion data (Knepler, 1980) and lithology data (Matthews and Zhang, 2012) was obtained from the literature. Inputs for each thermal property of frozen and thawed soils were validated to a good extent for the base model. Similar inputs were used for the main model for different soils. The oil well in the main model was surrounded by different types of soils with varying water contents (Figure 5.19). The water content data was obtained from experimental results and from the literature (Smith and Clegg, 1971). Figure 5.20 shows the model layout for the main model.

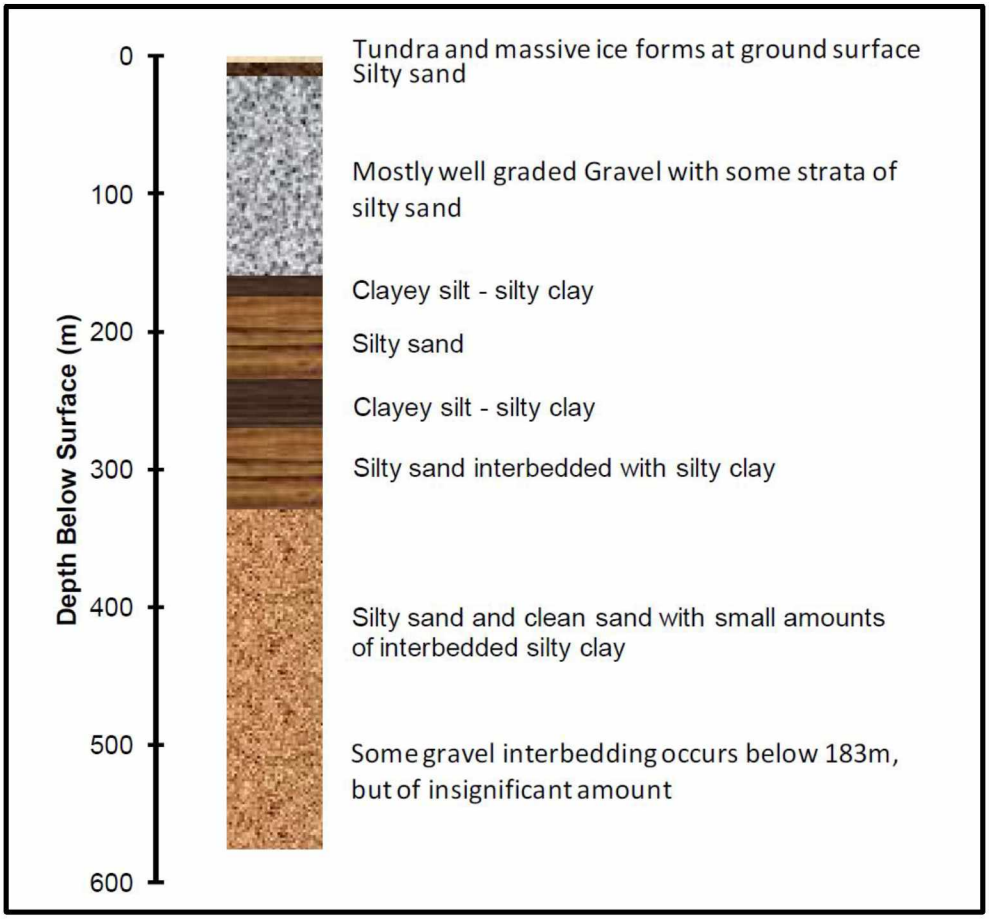

Figure 5.20: General soil profile for Prudhoe Bay based on core data. (From Matthews and Zhang, 2012)

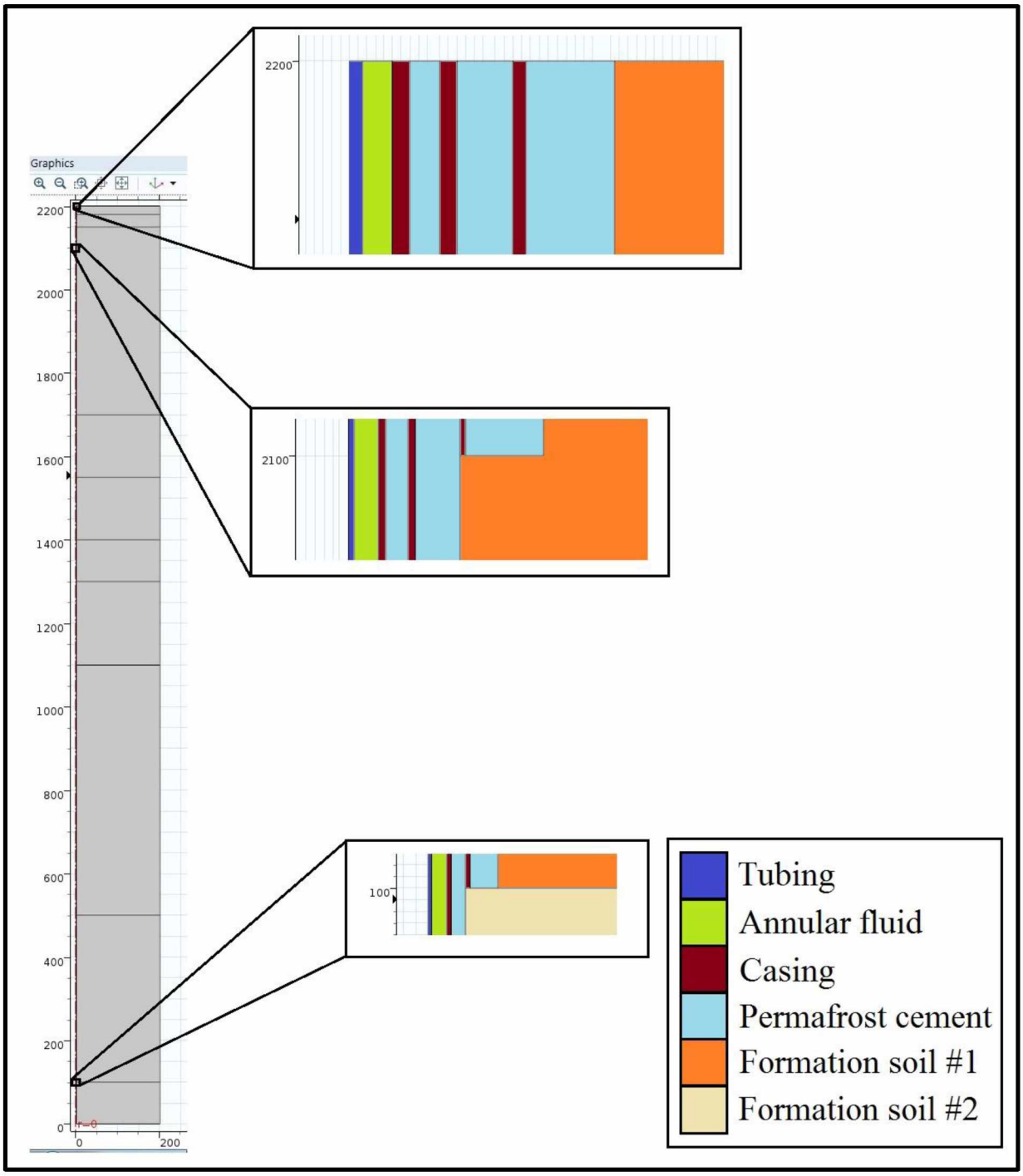

Figure 5.21: Model layout for main model.

5.1.2.1 Results for Main Model

The simulation was conducted by assuming an oil flowing temperature of 190°F and the whole geometry (i.e. permafrost) was assumed to be at 23°F initially. Figure 5.21 shows the model layout of the main model. Thaw radius was analyzed for each soil type with time, as summarized in Table 5.2. Figure 5.22 shows the thawing behavior for different soil types with time and Figure 5.24 shows the movement of the thaw front with time during the thawing period. Figure 5.23 shows the thaw radii during the refreezing period and Figure 5.25 shows the backward movement of the thaw front with time during the refreezing period. The zigzag pattern in Figures 5.24 and 5.25 is mainly due to the different lithology of the permafrost formation. For the 100 feet sand layer with no ice, the data points in Figure 5.24 and 5.25 only show the amount of heat penetration into the sand layer. Since its initial temperature assumed was 23°F. Figures 5.26 and 5.27, shows the post simulation main model images.

Table 5.2: Thaw radii of different soil types for main model

Sr. No.	Time, years	Soil type from top to bottom (thickness, feet)										
		Thaw radius, feet										
		Peat (20)	Silty sand (30)	Gravel (450)	Clayey silt (150)	Silty sand (150)	Clayey silt (100)	Silty sand (200)	Silty sand and/or silty clay (600)	Silty sand (400)	Sand (no ice) (100)	
1	0	0.00	0.00	0.00	0.00	0.00	0.00	0.00	0.00	0.00	0.00	Thawing period
2	1	11.94	13.16	15.72	8.99	13.23	9.10	8.24	11.73	13.24	24.61	
3	5	24.79	27.06	32.70	17.66	26.87	19.55	16.61	23.99	27.32	48.89	
4	10	34.89	37.66	45.40	23.99	36.02	24.12	22.78	32.44	37.16	65.05	
5	15	42.25	45.66	54.57	28.97	42.47	28.69	27.70	38.83	45.49	77.83	
6	20	51.09	52.71	62.99	33.65	47.39	32.35	31.42	44.40	51.72	89.32	
7	25	56.08	59.76	71.31	37.97	53.11	35.82	35.38	49.69	55.68	99.42	
8	30	62.75	66.11	78.89	40.17	57.72	38.55	39.21	53.47	61.76	111.58	
9	31	64.15	66.99	80.17	40.45	58.25	39.19	39.89	54.13	63.41	114.52	Refreezing period
10	33	66.40	68.66	82.07	40.99	59.25	40.34	41.01	56.29	66.46	119.59	
11	35	68.01	70.21	82.63	41.14	59.51	40.41	41.42	57.18	68.01	121.31	
12	37	69.01	70.85	81.80	40.92	59.04	39.96	41.28	57.49	68.67	120.89	
13	39	69.59	70.92	79.90	40.49	58.08	39.16	40.73	57.38	68.83	119.25	
14	41	70.03	70.69	76.87	39.92	56.76	38.09	39.88	57.16	68.82	116.68	
15	43	69.99	69.95	72.59	39.30	54.81	37.12	38.68	56.69	68.57	113.67	
16	45	69.75	68.96	66.86	38.53	52.14	35.82	37.14	55.98	68.23	109.95	

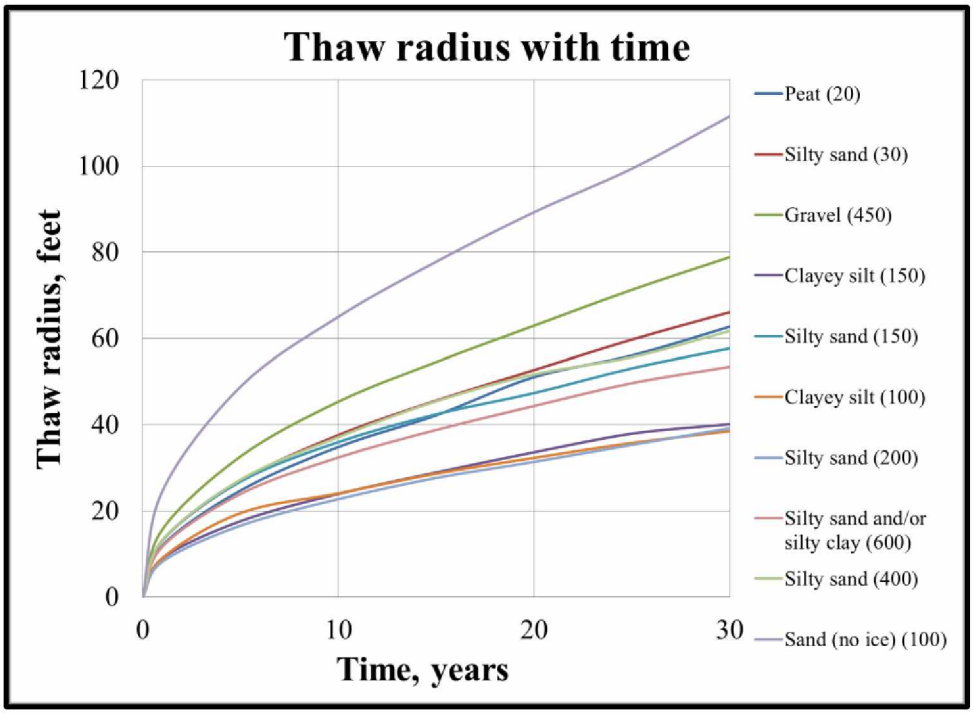

Figure 5.22: Thaw radius versus time for different soil types during thawing period for main model.

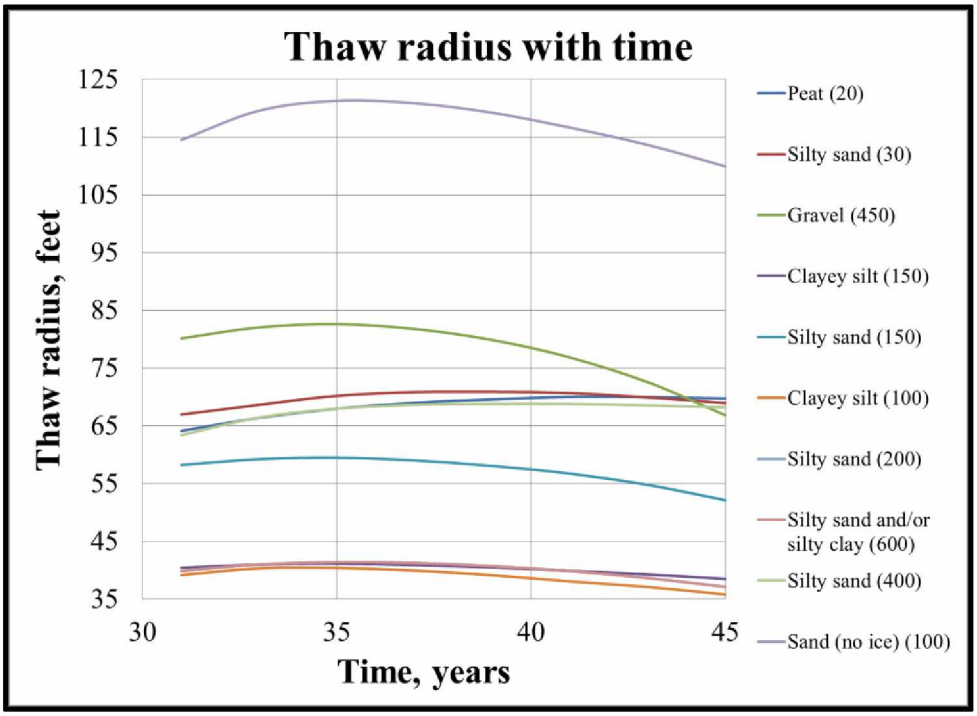

Figure 5.23: Thaw radius versus time for different soil types during refreezing period for main model.

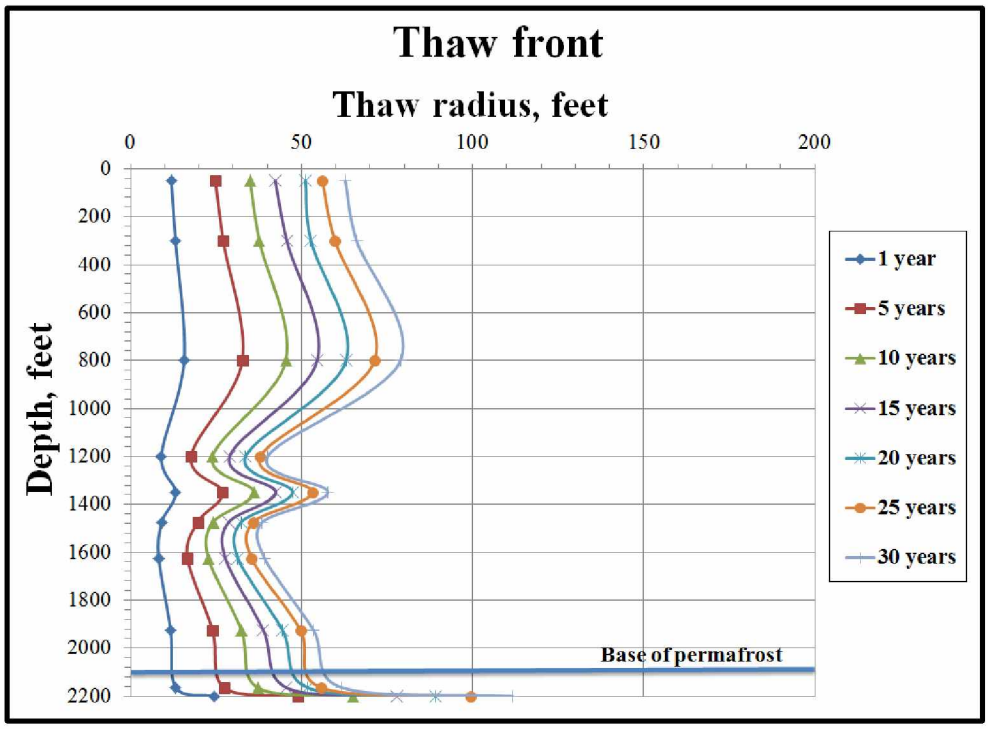

Figure 5.24: Movement of thaw front with time during thawing period.

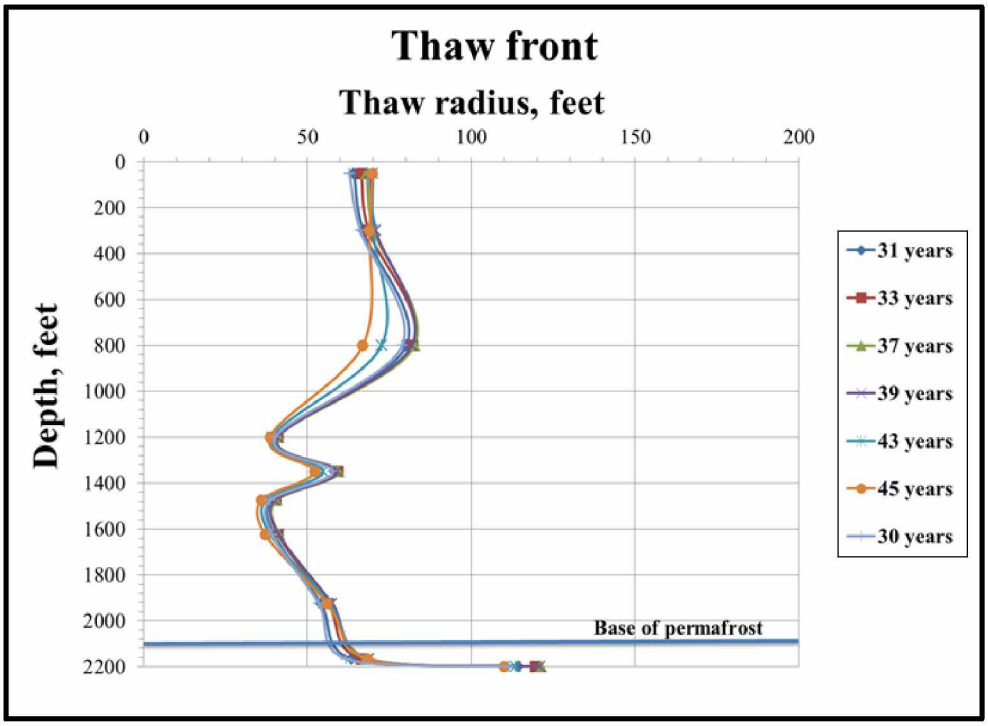

Figure 5.25: Movement of thaw front with time during refreezing period.

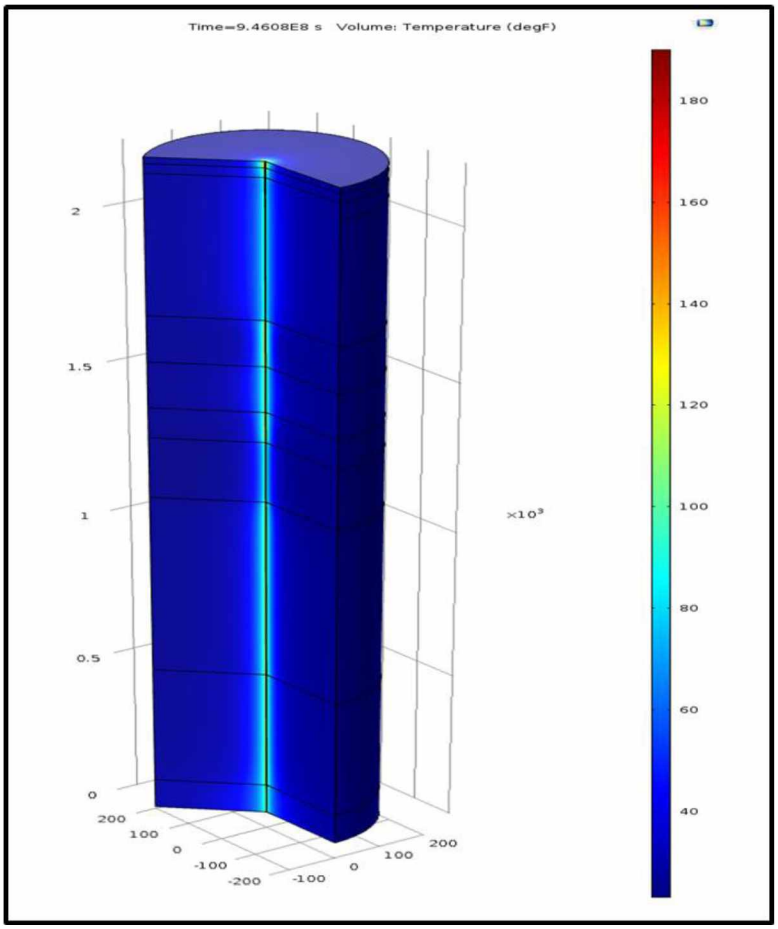

Figure 5.26: Post simulation model layout for main model.

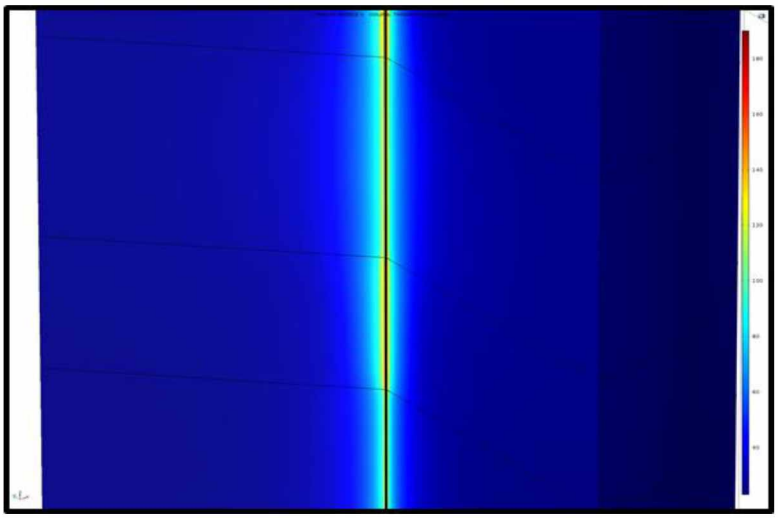

Figure 5.27: Zoomed in image of post simulation model layout for main model.

5.2 Mechanical Analysis

Mechanical analysis included studying and understanding the changes occurring in the loading conditions with time for post thaw soil conditions. The main objective of the analysis involved targeting and studying the resultant volumetric strain effects and the pressure changes along the length of the wellbore due to changes in the loading conditions in the surrounding weak thawed soils. Different soil types were taken into consideration and peat was considered for the active layer. Based on the literature review (section 2.7), this analysis studied the different post thaw tension and compressive effects along the wellbore due to change in lithology of the permafrost formation as a result of change in soil state.

5.2.1 Base Model for Mechanical Analysis

A two-dimensional model was designed in the solid mechanics module of the software where a 27-foot section of the well-soil system was modeled, as shown in Figure 5.28. The simulation work initially involved working on a base model. It consists of two components of a conventional oil and gas well, namely, casing and cement layer. Other than this, it had alternating 9-foot thick layers of two soil types, sand and clay, from top to bottom (Figure 5.28). The purpose behind building a base model was to look at the effect of change in the loading condition with time based on the change in the input parameters on the casing. This step of the analysis was necessary to ensure the software's capability to model the change in the loads due to changes in material properties (Young's modulus and density) during thawing with time. An extremely fine mesh was considered for the simulation purpose.

5.2.1.1 Input Parameters and Assumptions for Mechanical Analysis

The main aim behind the base model was to look at the effect of changing loading conditions with time due to continuous heat transfer between the well and the surrounding frozen soil. For the entire mechanical analysis, two loading effects were taken into consideration. First, the overburden loading caused by the weight of the overlying soil in the vertical direction, and second, the lateral loading as a result of overburden loading in the horizontal direction. For the mechanical properties of different types of soils considered, empirical correlations were used for Young's modulus of elasticity and density. The empirical correlations were obtained from "An Introduction to Frozen Ground Engineering" by Andersland and Ladanayi (2004) and from

Smith and Clegg (1971) for frozen and thawed soil states, respectively. The main reason behind using empirical correlations for Young's modulus was for modeling the changing loading effects along the wellbore due to changing material properties. The thermal properties used for the mechanical analysis are listed in Table A-41 of the appendix section.

The entire mechanical analysis followed four assumptions: (1) the initial temperature of the permafrost formation was 23°F; (2) there was no heat exchange at the boundary of the frozen soils; (3) soil freezing temperature was 32°F; and (4) the well-soil system was at equilibrium when the soil was in its frozen state. The initial step of the analysis included balancing the forces acting on the casing in all directions. This was done to take care of the initial equilibrium conditions of the frozen soil and the well.

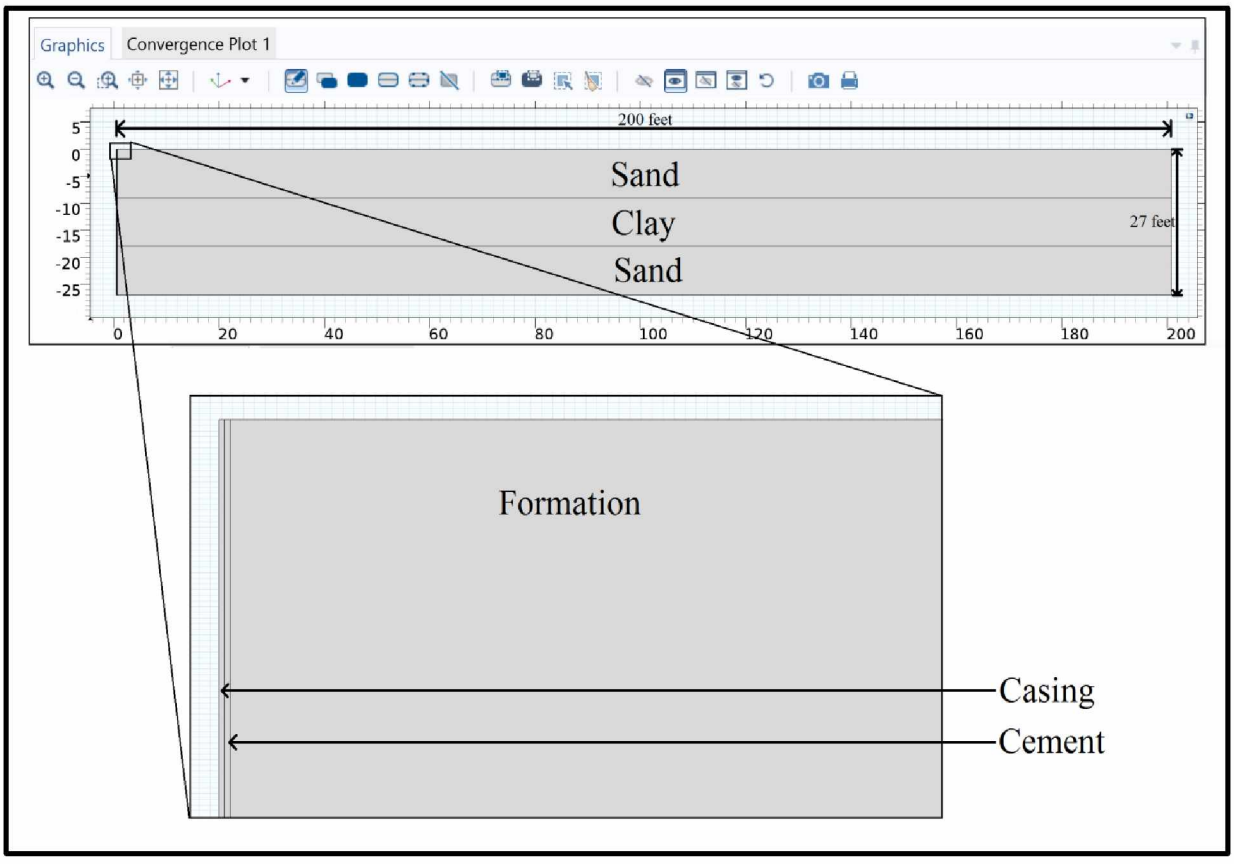

Figure 5.28: Model layout for base model for mechanical analysis.

5.2.1.2 Results for Base Model

Simulations were done for a period of 30 years. Since only casing and cement were considered for the well configuration, multiple simulation runs were conducted to achieve thaw radii for different time periods similar to those obtained in thermal analysis under similar conditions. A sample run was conducted on the base model to check the applicability of empirical correlations towards modeling changing loading conditions with changing soil properties. The simulation was conducted by assuming a casing (inner boundary) temperature of 39.2°F, while the whole geometry was assumed to be at 23°F initially.

Figures 5.29 and 5.30, shows changes in density of sand and clay due to thawing at different time periods. Figure 5.31 shows the change in modulus of elasticity with depth. These three plots show that COMSOL was able to model and conduct the simulation runs successfully by assuming change in the input property for a part of the same domain of the constructed geometry.

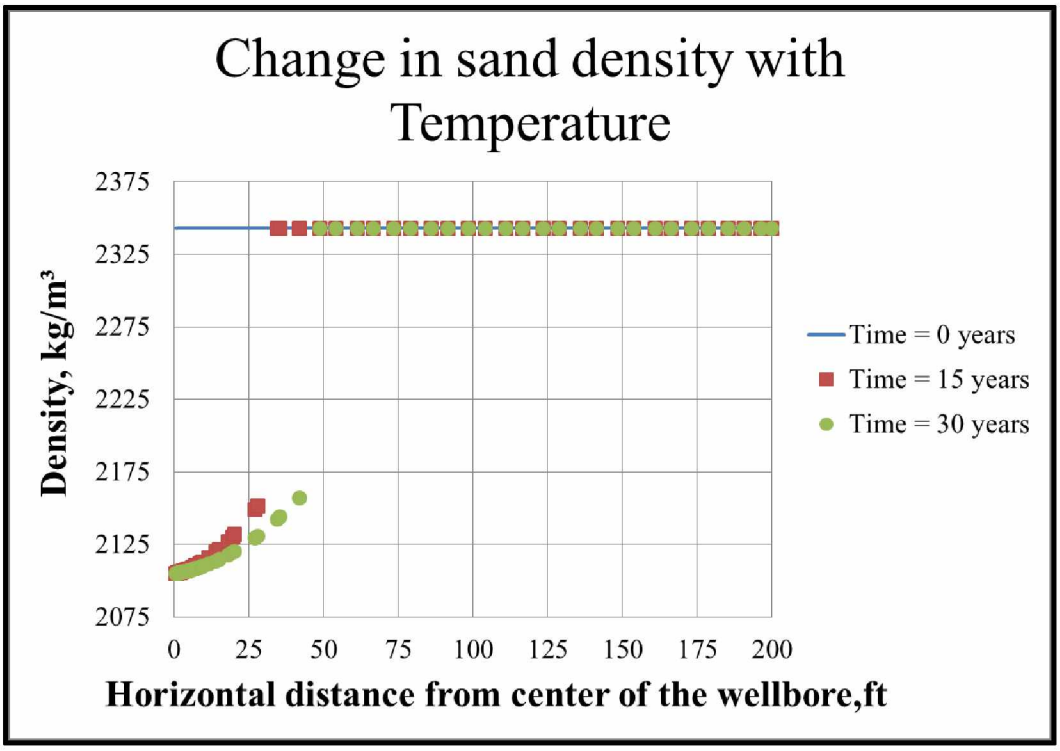

Figure 5.29: Change in density of sand due to thawing with time.

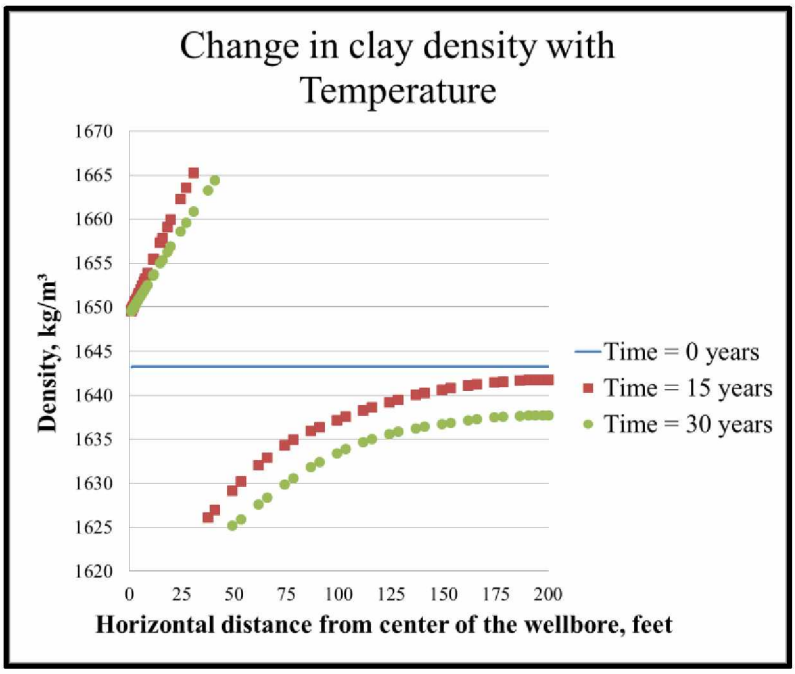

Figure 5.30: Change in density of clay due to thawing with time.

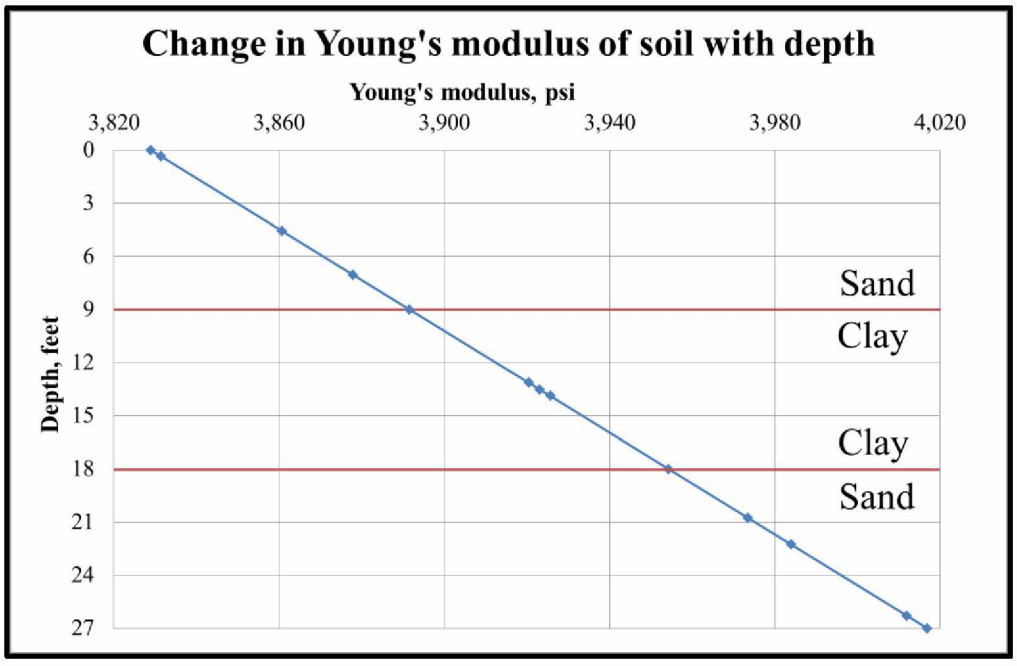

Figure 5.31: Change in modulus of elasticity with depth.

Figure 5.32 shows the change in overburden load and lateral load with depth. Changes in the material properties of the soil configuration caused change in the loads (forces) with soil type. Since overburden load depends on the density of the soil mass and the lateral load, which is because of the overburden, thus due to a change in density there was a change in the loading parameters. Figure 5.32 shows that according to assumption (4), the well-soil system is at equilibrium when the soil is in its frozen state, which implies no change in the loading condition for the frozen portion of the soil. Figure 5.33 show that as the soil changes its state from frozen to thawed as a result of heat transfer, the loading conditions change. The change in the loading conditions was not significant, according to Figure 5.33, because COMSOL could handle only a small change in the input properties for the same domain of the geometry. Thus, as the loads are derived from density and as a result of heat transfer the density changes, the loads tend to change too. The change in the loading condition was modeled successfully by COMSOL.

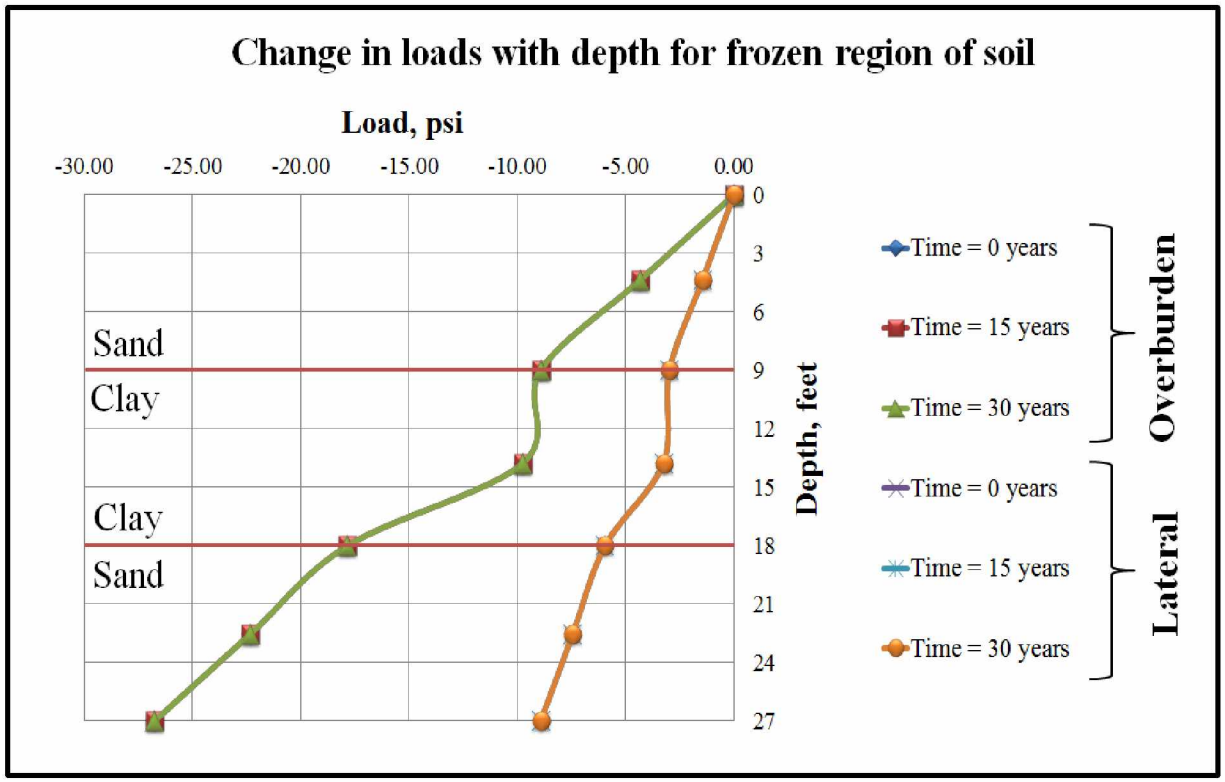

Figure 5.32: Change in overburden load and lateral load with depth for frozen state of the soil mass.

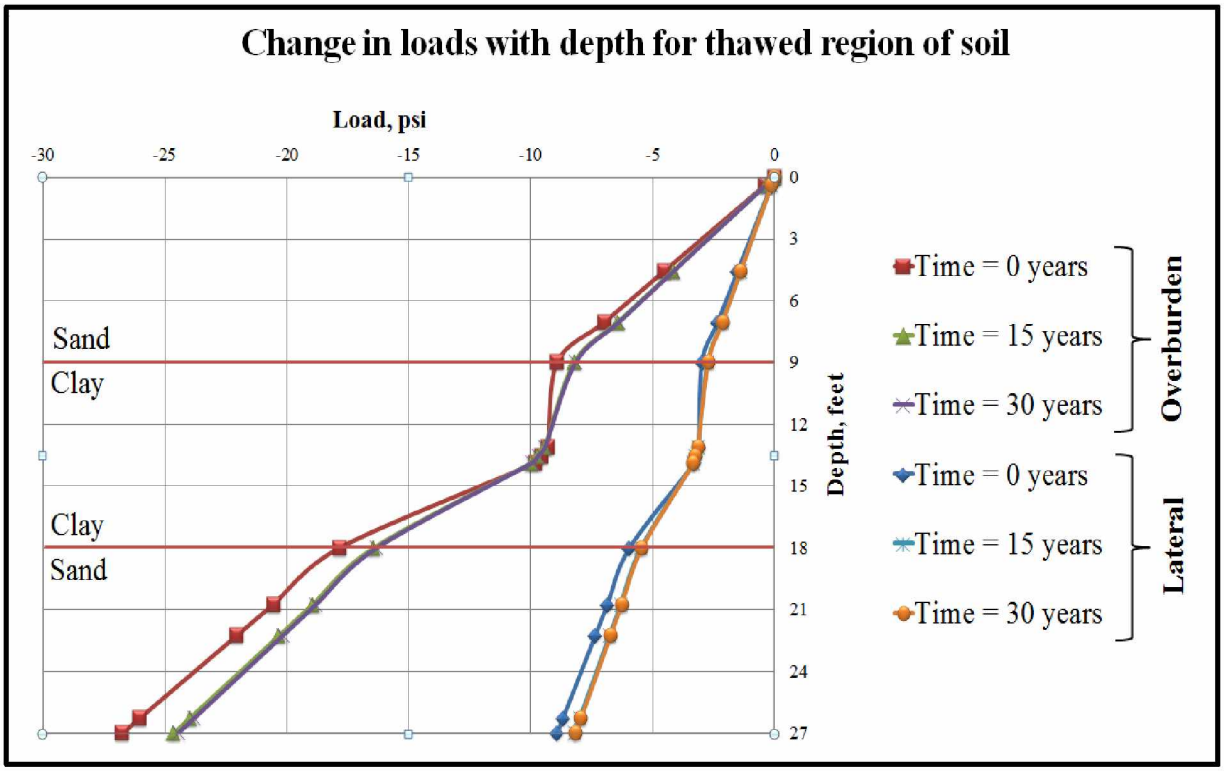

Figure 5.33: Change in overburden load and lateral load with depth for thawed state of the soil mass.

Figures 5.34 and 5.35, shows the change in the vertical and horizontal stresses due to loads acting on the frozen and thawed soil masses, respectively. Since the system is at equilibrium when the soil is frozen, there is no change in the vertical and horizontal stress, whereas when the soil changes its state due to thawing, the loads tend to change both vertically and horizontally, and thus the resultant stress also changes. The numbers in the plots (Figures 5.34 and 5.35) vary differently with respect to each soil type. Since the density change is greater in magnitude for clay compared to sand (Figures 5.29 and 5.30), the resultant vertical and horizontal stresses for the change in overburden and lateral loads vary with respect to each other. The initial loads are dependent on the density of the material; the magnitude of loads will also be higher in clay than in sand. Thus the change in reaction stresses is greater for clay than for sand. The sign convention in the plots only exhibits the direction in which the forces or loads are oriented.

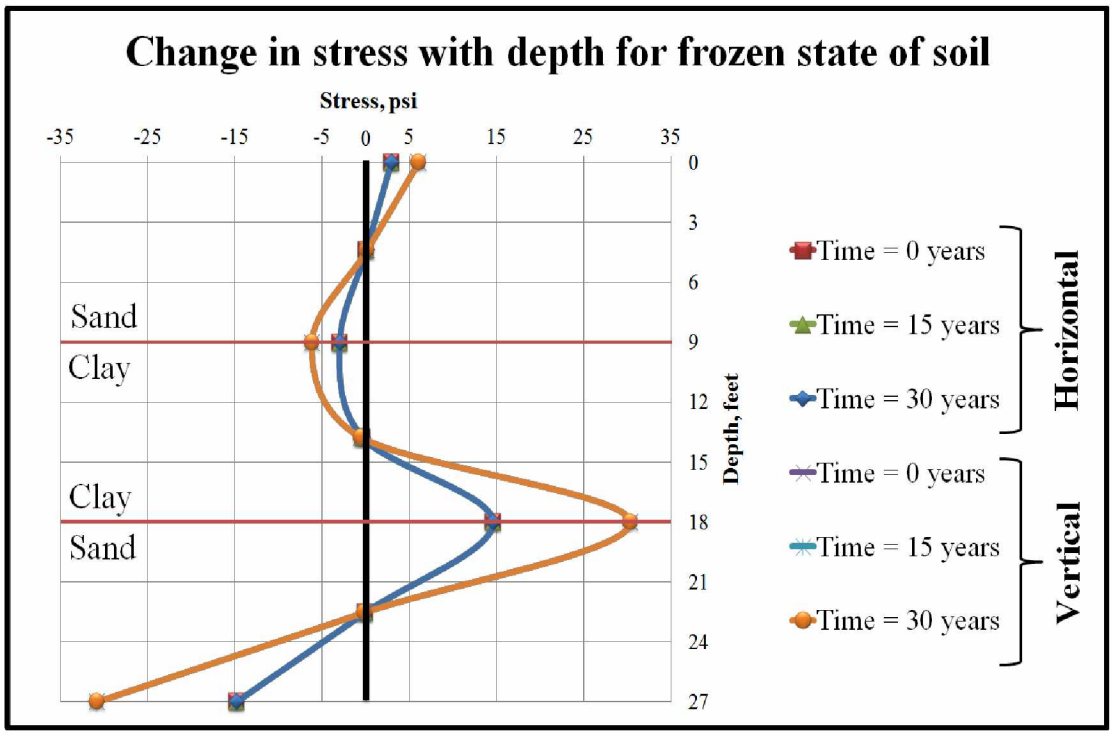

Figure 5.34: Change in the vertical and horizontal stresses in the soil mass for frozen state.

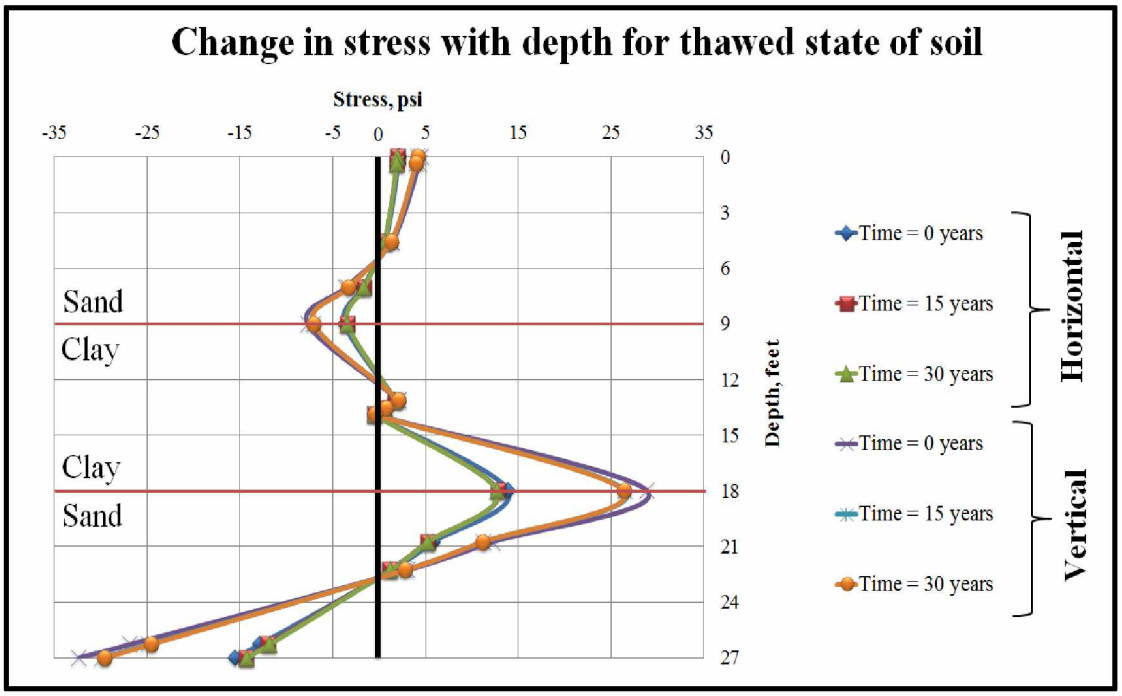

Figure 5.35: Change in the vertical and horizontal stresses in the soil mass for thawed state. (Note: Positive stress implies tension and negative stress implies compression)

Figure 5.36 shows the induced change in the volumetric strain of the soil due to the change in the loading conditions. Since the load magnitude was greater for clay, greater strain effects were observed for clay compared to strain effects for sand.

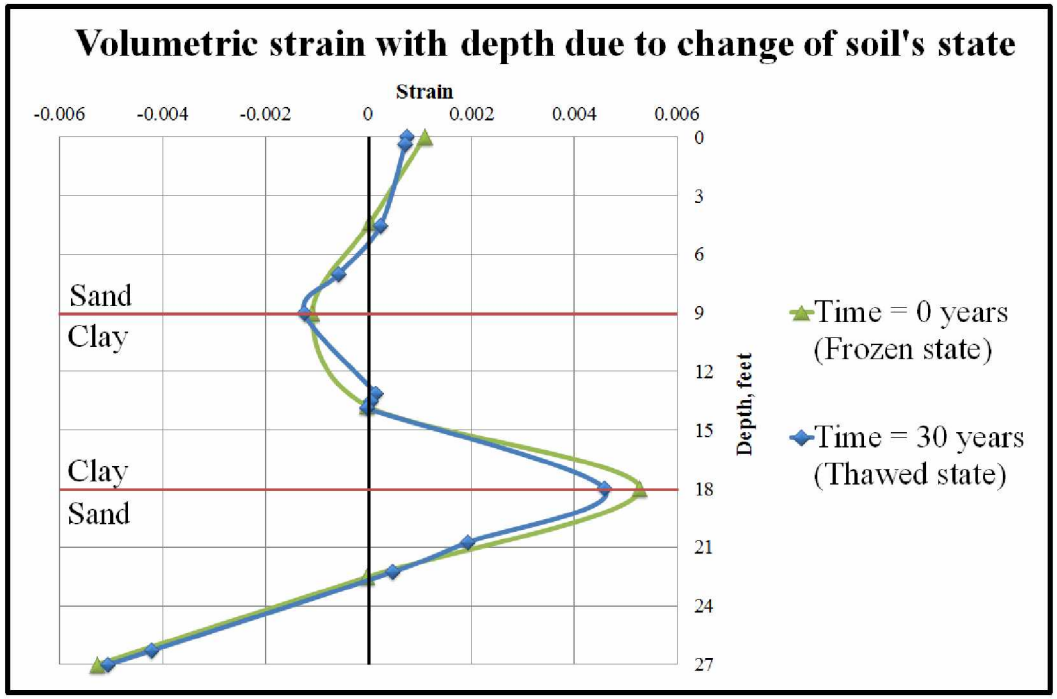

Figure 5.36: Change in volumetric soil strain due to change of state of soil mass.

Figure 5.37 shows the maximum change in pressure acting along the casing at the end of the thawing period (30 years) with respect to the initial pressure on the casing when the soil mass was frozen. The sign convention in Figure 5.37 shows the direction of the pressure acting on the casing due to the reaction stresses in the surrounding soil mass. The reaction stresses were the result of changing loading conditions from the soil mass. The change in pressure was calculated from data obtained from COMSOL and was the pressure at the end of 30 years of heat transfer minus the pressure at time = 0 years. Figures 5.38 and 5.39, shows the maximum change in the vertical and horizontal stresses along the casing at the end of 30 years of thawing. The sign convention in Figures 5.38 and 5.39 shows the increase (+) and decrease (-) of the stress values with respect to the stress values at time = 0 years. Figure 5.40 shows the strain effects along the casing at the end of 30 years of soil mass thawing. Due to higher loading in the clay, the strain effects are greater in the area surrounded by clay compared to those in the area surrounded by sand. The strain effects were not significant because the density changes for each soil type were

minimal. This was because of the software's limitation of not being able to handle significant changes in the material properties for the same domain of geometry.

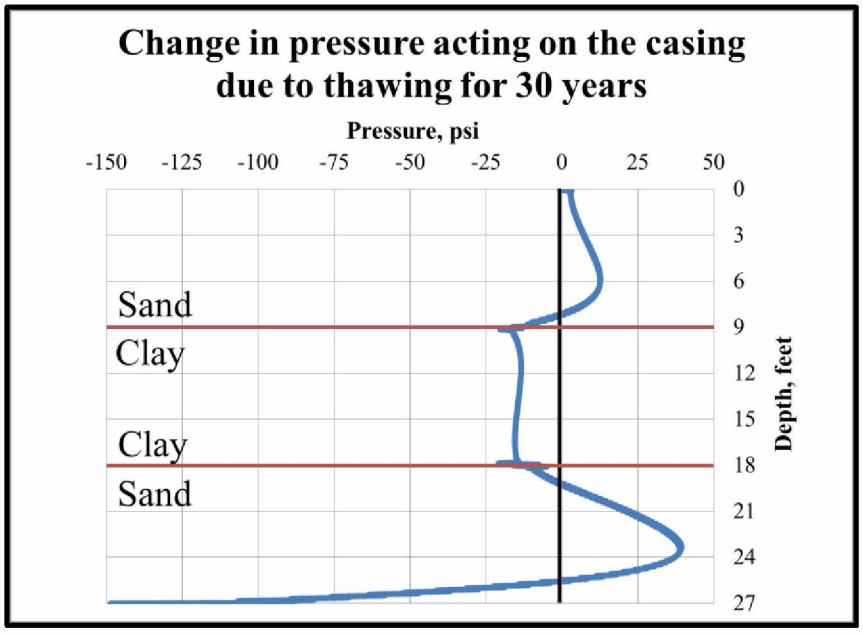

Figure 5.37: Change in pressure acting along the casing with depth due to change in soil type.

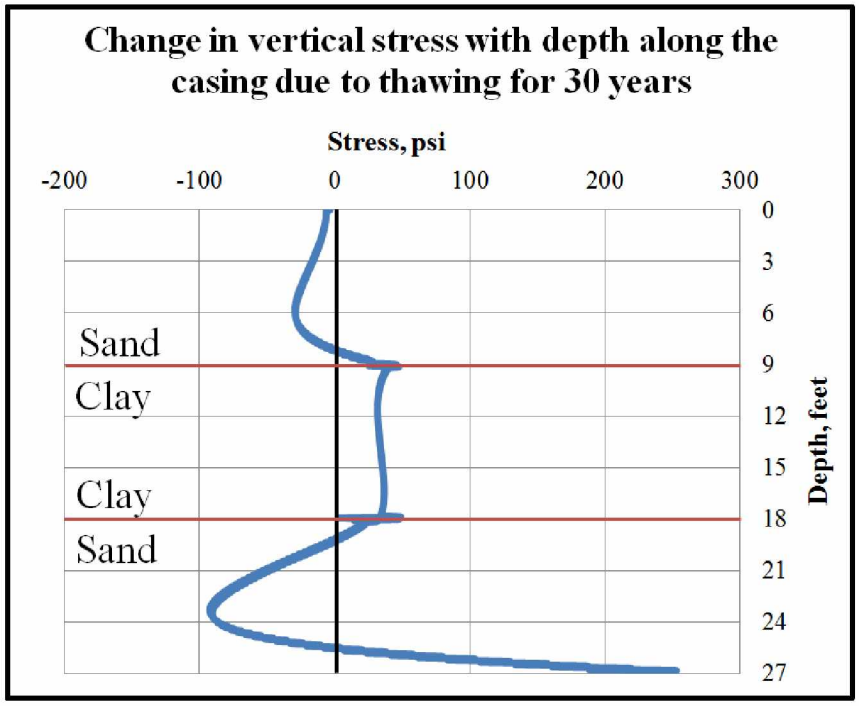

Figure 5.38: Change in the magnitude of the vertical stress at the end of 30 years with respect to stress values at time = 0 years.

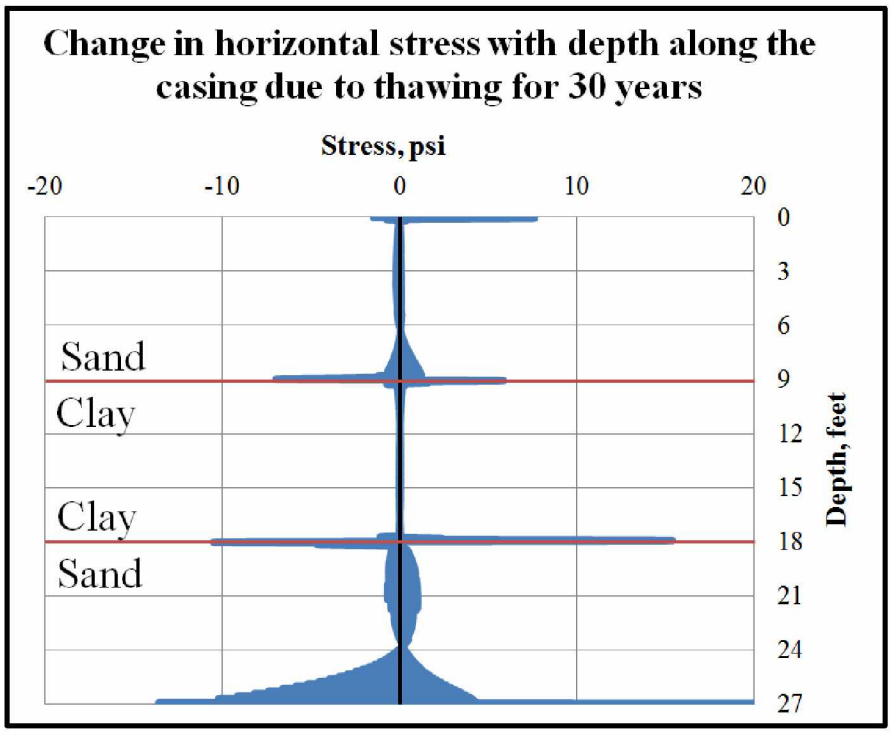

Figure 5.39: Change in the magnitude of the horizontal stress at the end of 30 years with respect to stress values at time = 0 years.

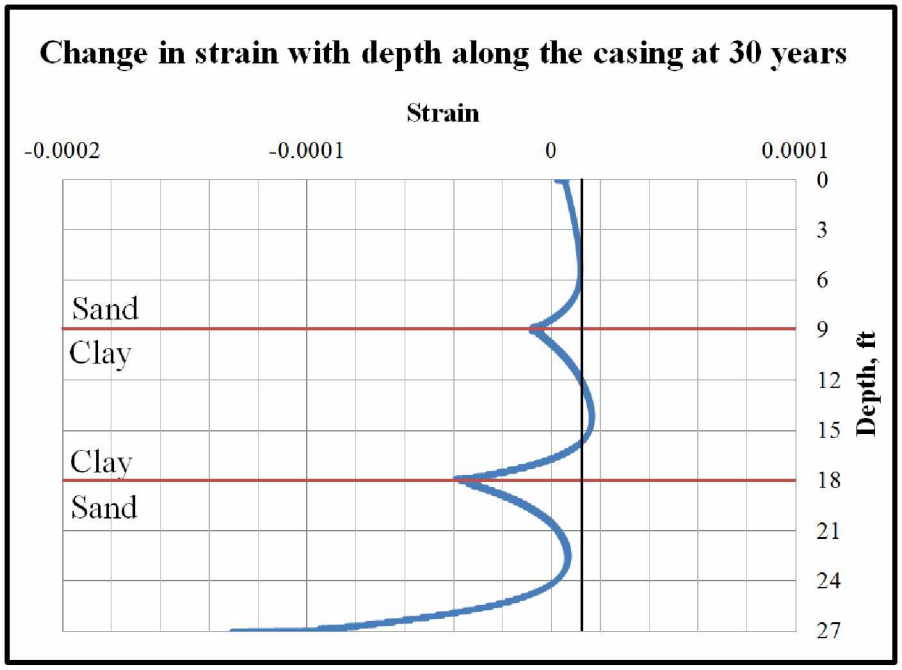

Figure 5.40: Strain along the casing at the end of 30 years of soil mass thawing.

Figures 5.41 and 5.42 show the horizontal temperature distribution for sand and clay, respectively. Figures 5.43 and 5.44 show post simulation results for the change in density of the soil mass and the overburden load at the end of 30 years of the thawing period, respectively.

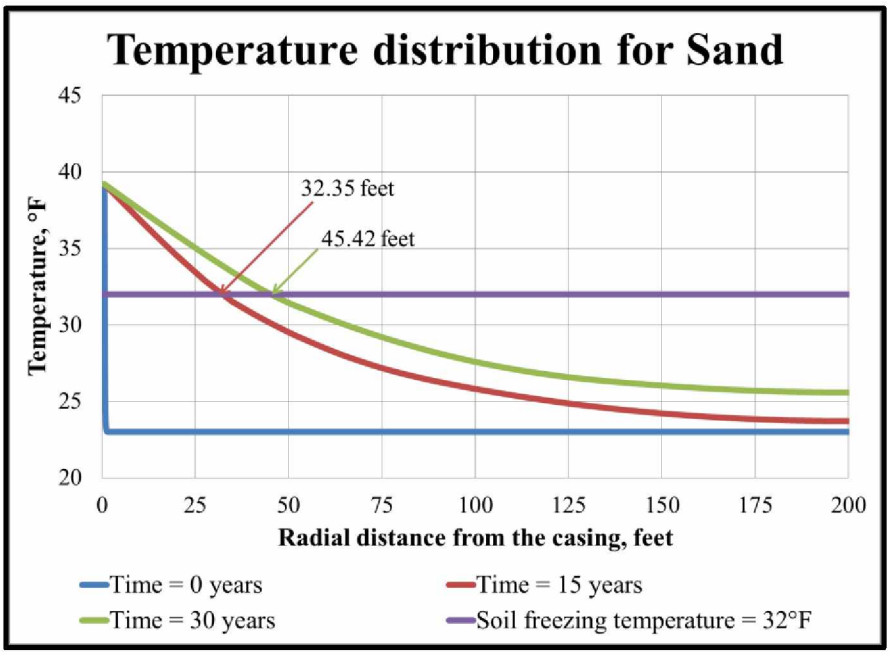

Figure 5.41: Radial temperature distribution with incremental time period for sand during thawing period for mechanical analysis.

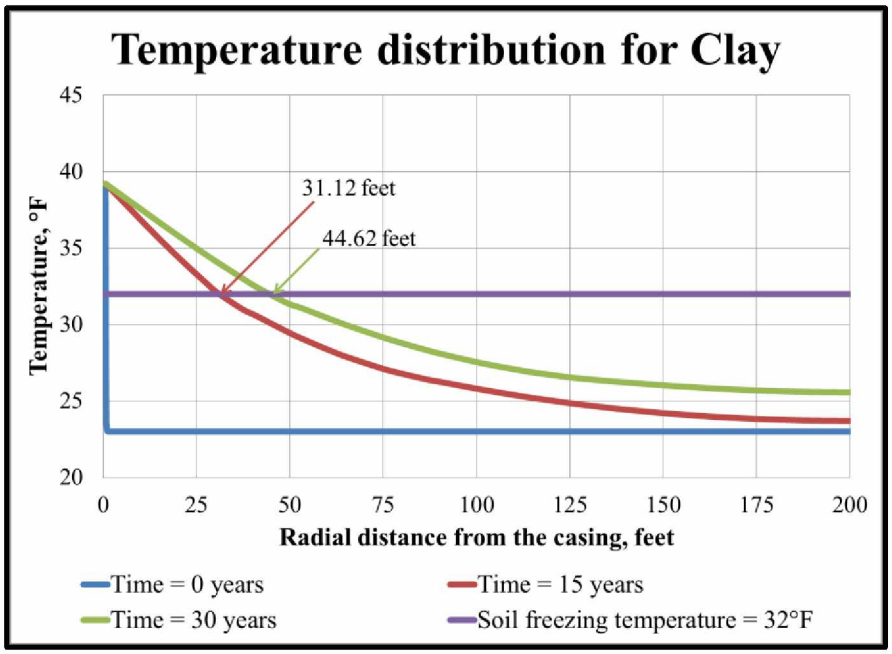

Figure 5.42: Radial temperature distribution with incremental time period for clay during thawing period for mechanical analysis.

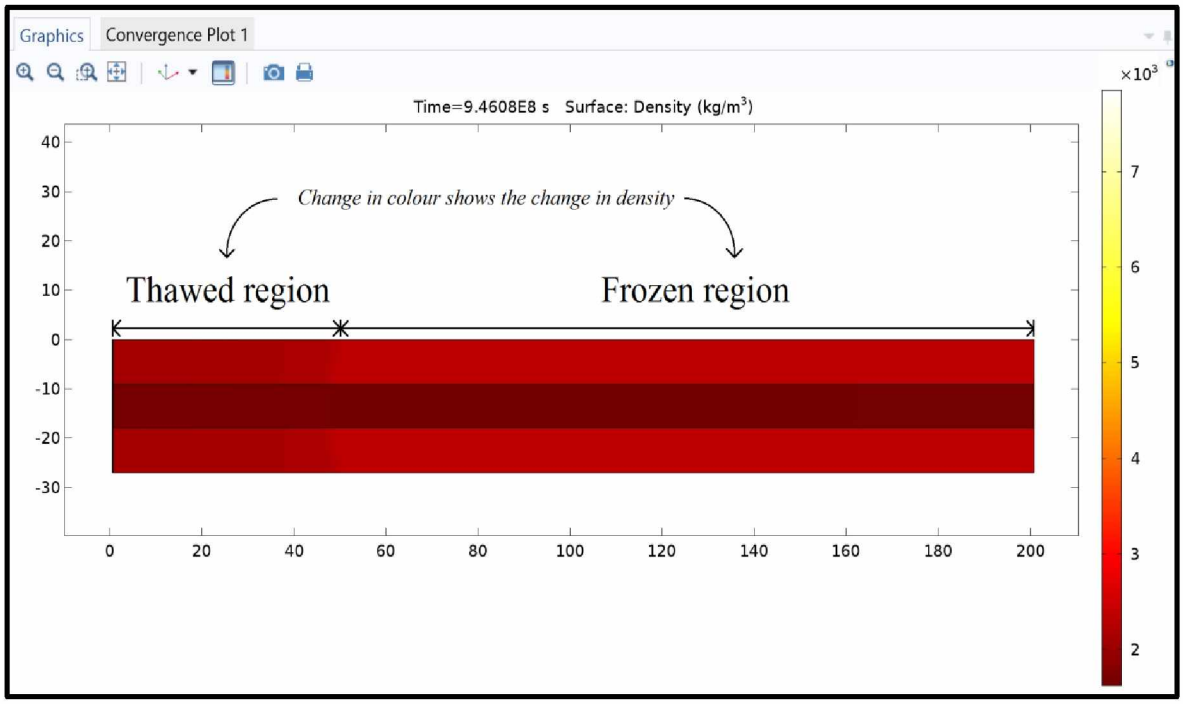

Figure 5.43: Post-simulation result showing change in density of the soil mass due to thawing for 30 years.

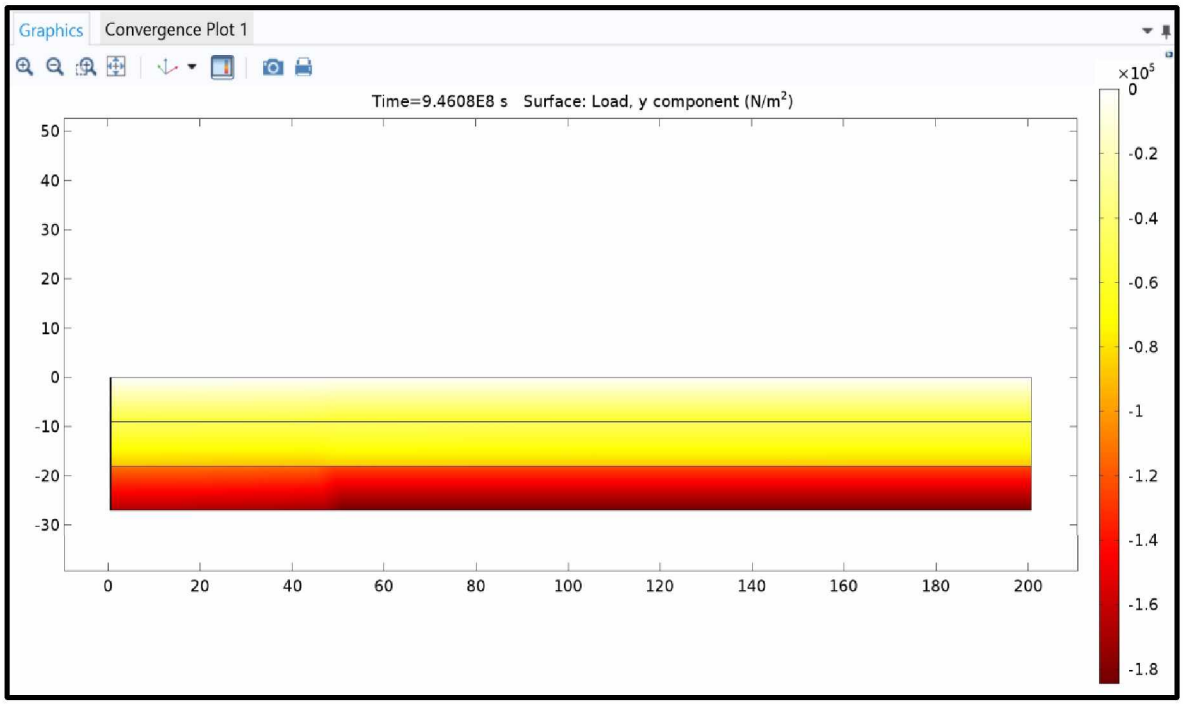

Figure 5.44: Post-simulation result showing the change in the overburden load at the end of 30 years.

According to the scientific literature, different soil types tend to behave differently along the length of the casing due to differences in compressibility. Thus, on the basis of Figures 5.37 and 5.38, the compression effects of fine-grained soils (clay) that are compressible in nature and the tension effect due to coarse-grained soils (sand) that are incompressible in nature were modeled successfully. Another important observation that matched the literature was that the compressive strain effects were greater than the tension strain effects, as shown in Figure 5.40.

5.2.2 Main Model for Mechanical Analysis

The main model involved modeling an entire oil well at Alaska's North Slope (Prudhoe Bay), similar to thermal analysis. The two-dimensional geometry model had a total length of 2100 feet and was 200 feet wide. The ~2000 foot thickness of the permafrost was taken into consideration. The oil well completion data (Knepler, 1980) and lithology data (Matthews and Zhang, 2012) was obtained from the literature. Inputs for each thermal property of frozen and thawed soils were the same as those in thermal analysis. Similar inputs were used for the mechanical properties in the main model for different soils as those used in the base model for mechanical analysis (Section 5.2.1). The oil well in the main model was surrounded by different types of soils with varying water contents. The water content data was obtained from experimental results and from the literature (Smith and Clegg, 1971). Figure 5.45 shows the main model layout.

5.2.2.1 Results for Main Model

Figures 5.46 and 5.47 show the change in overburden load and lateral load with depth for frozen and thawed soil masses, respectively. Due to change in the material property (density) of the soil configuration considered, which was changing with temperature, there were changes in the loads with soil type. Thus assumption (4) was taken into consideration by COMSOL for the main model. When the soil is frozen (Figure 5.46), the loads are not changing, whereas when the soil mass thaws, the loads tend to change. The change in the loading conditions is not significant according to Figure 5.47 because there was not much change in the density of the soil with depth. The curved arrows in Figure 5.47 show the area where there was a significant change compared to other soil layers considered.

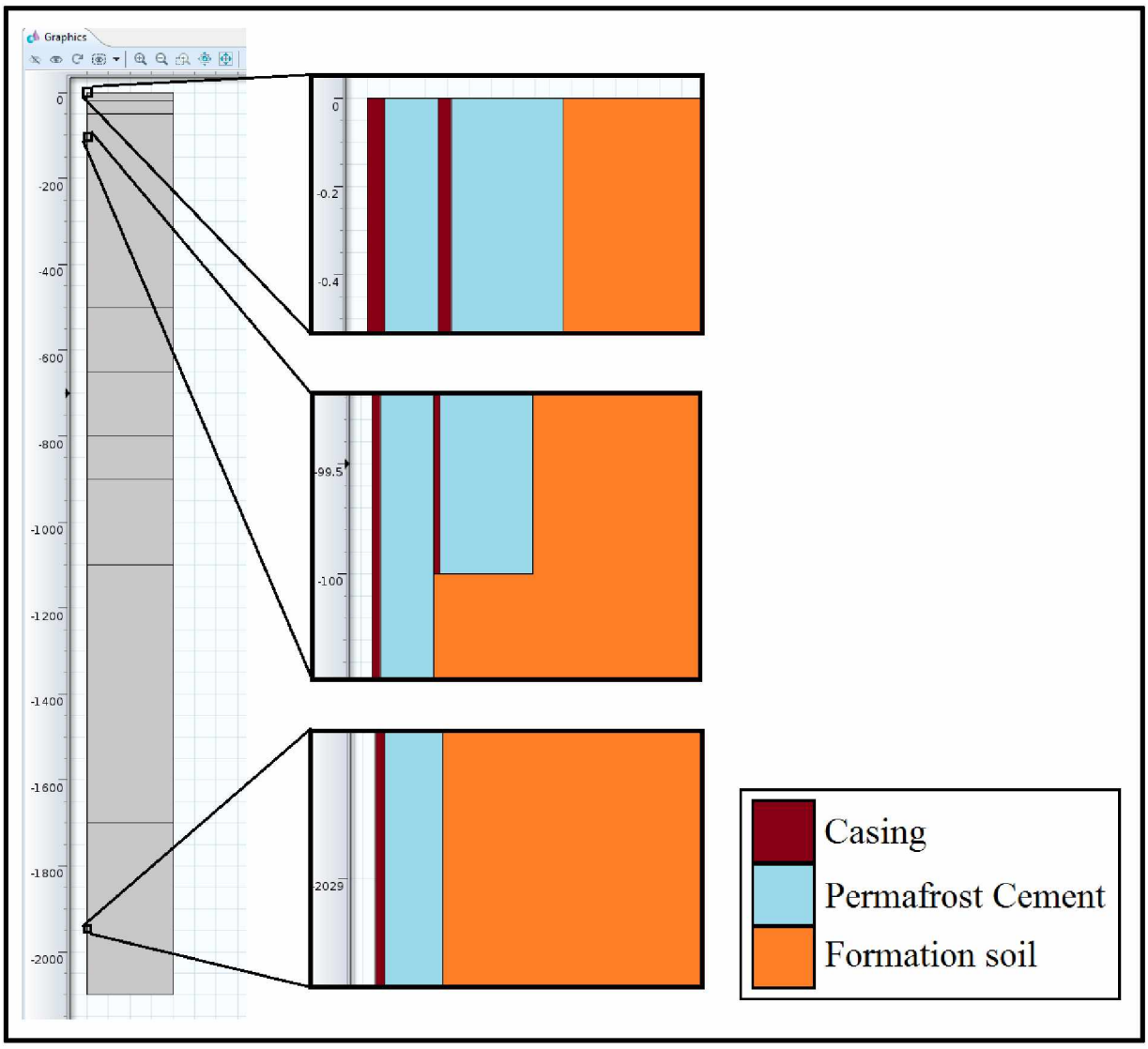

Figure 5.45: Model layout of main model for mechanical analysis.

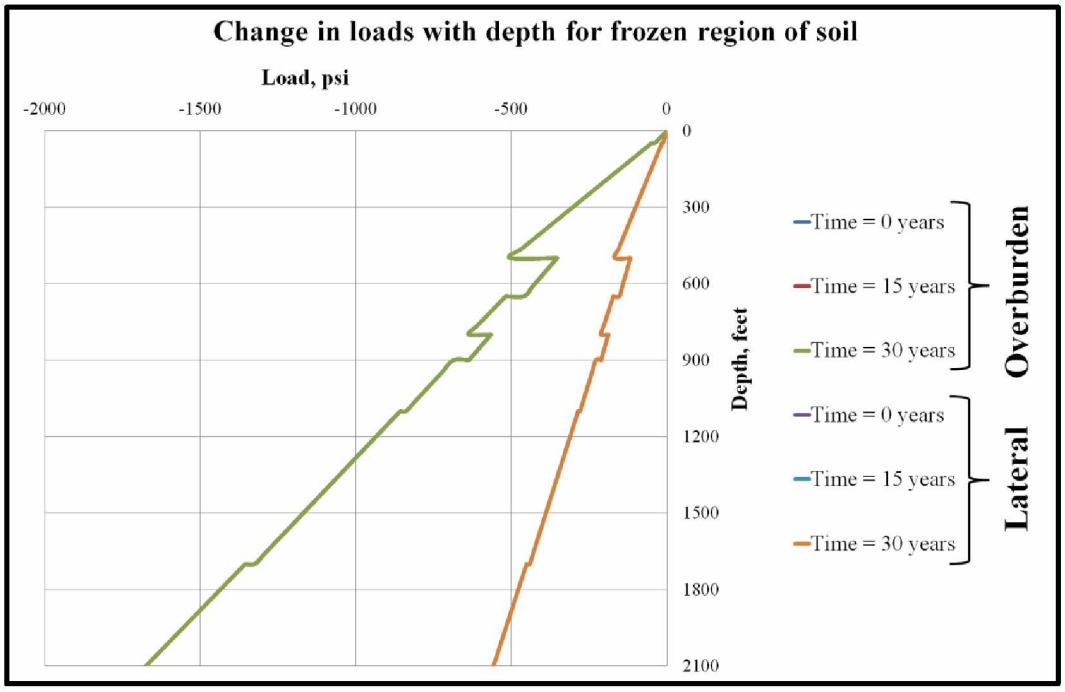

Figure 5.46: Change in overburden load and lateral load with depth for frozen state of the soil mass.

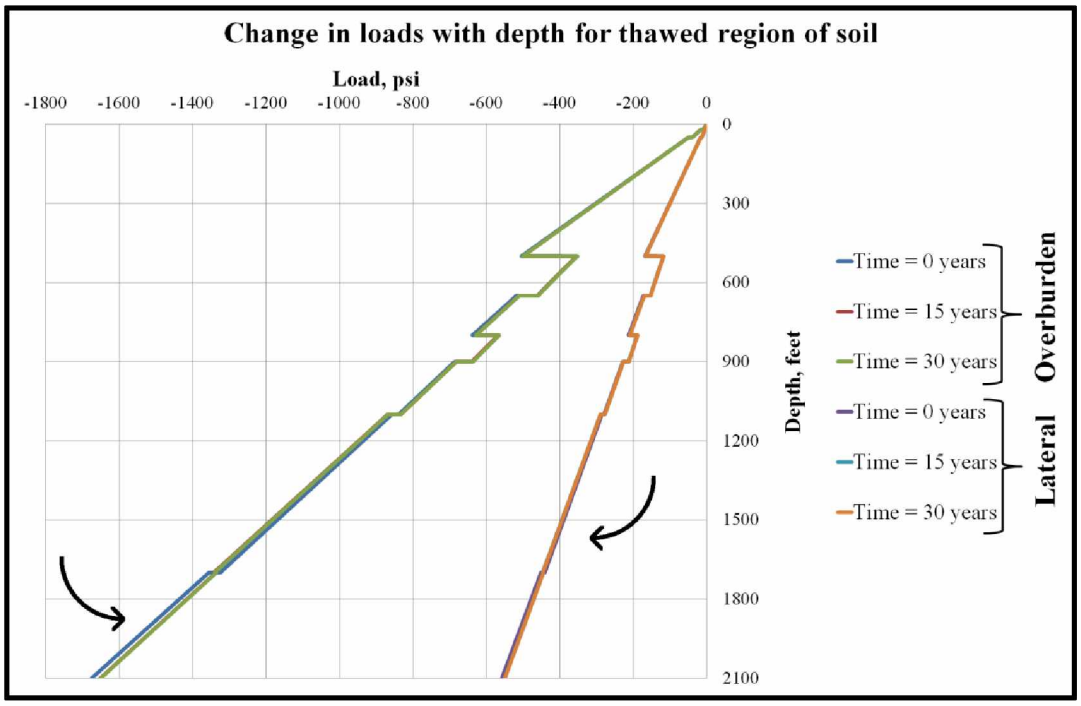

Figure 5.47: Change in overburden load and lateral load with depth for thawed state of the soil mass.

For the main model, two casings were taken into consideration: conductor casing and surface casing. The conductor casing and surface casing were up to a depth of 100 feet and 2100 feet respectively. Figures 5.48 and 5.49 shows the pressure along the length of the soil-wellbore interface for the conductor casing and surface casing, respectively. The sign convention in these two plots shows the direction in which the pressure changed as a result of changing vertical and horizontal stresses due to changes in vertical and horizontal loads. It also shows the direction in which the pressure was acting. On the basis of Figures 5.48 and 5.49, it can be said that the fine-grained soil was trying to push the casing inwards, whereas the coarse-grained soil was trying to pull the casing outwards. Most coarse-grained soils showed pressures acting outward, except for gravel, where it acted inward. The reason behind this was the Young's modulus of elasticity considered for gravel, which was less compared to the other underlying fine-grained soils considered. Young's modulus was not changing with temperature; rather, it was changing with depth, thus making the underlying soils have a greater Young's modulus than gravel.

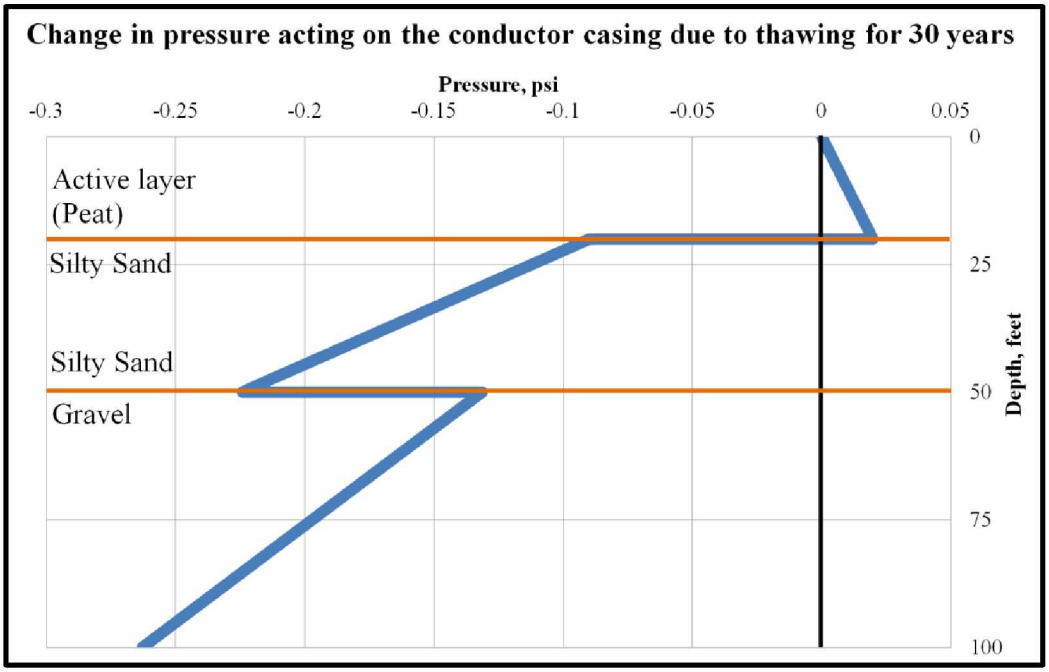

Figure 5.48: Change in pressure acting on the conductor casing at the end of 30 years of thawing.

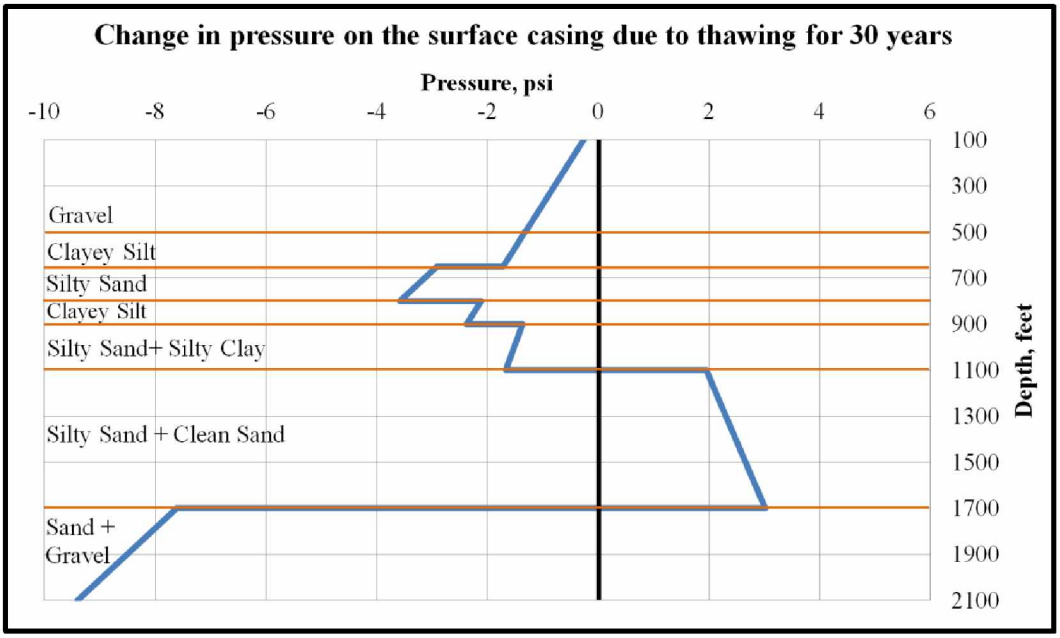

Figure 5.49: Change in pressure acting on the surface casing at the end of 30 years of thawing.

Figures 5.50 and 5.51 show the change in the horizontal and vertical stresses respectively with depth along the length of the interface of wellbore and soil formation for conductor casing (100 feet) respectively after 30 years of thawing period. Figures 5.52 and 5.53 shows the change in the horizontal and vertical stresses respectively with depth along the length of the interface of wellbore and soil formation for surface casing (2100 feet) after 30 years of thawing period. Stress calculations were done on the basis of post simulation data obtained from COMSOL. The sign convention in these four figures show the direction in which the change occurred, i.e., a positive sign implies an increase in the stress value, whereas a negative sign implies a decrease in the stress value. Thus comparing Figures 5.50 and 5.51 with Figure 5.48 shows that with an increase in stress value, pressure increased on the wellbore. For Figures 5.50 to 5.53, the abrupt change in the stress value with change in soil type was mainly because of the fixed constraint conditions considered in the model.

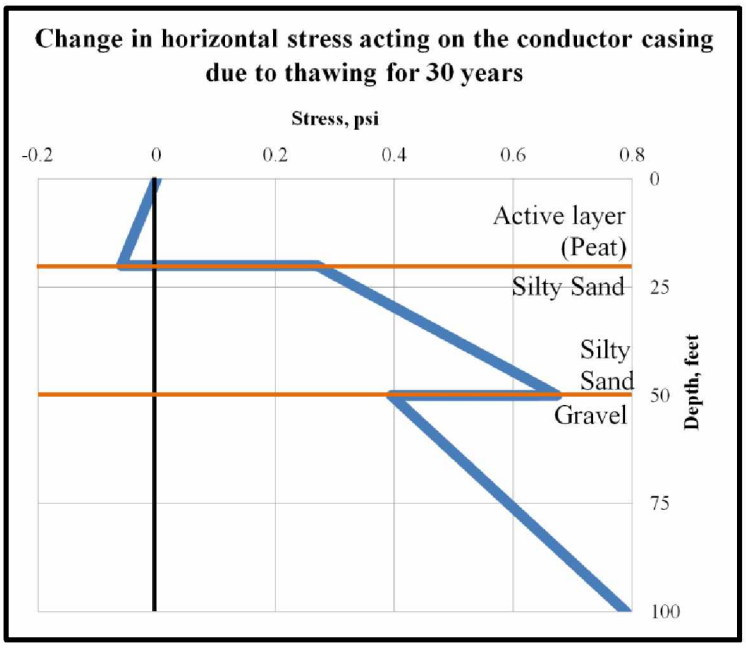

Figure 5.50: Change in horizontal stress acting along the well-soil interface for the first 100 ft of conductor casing after 30 years of thawing.

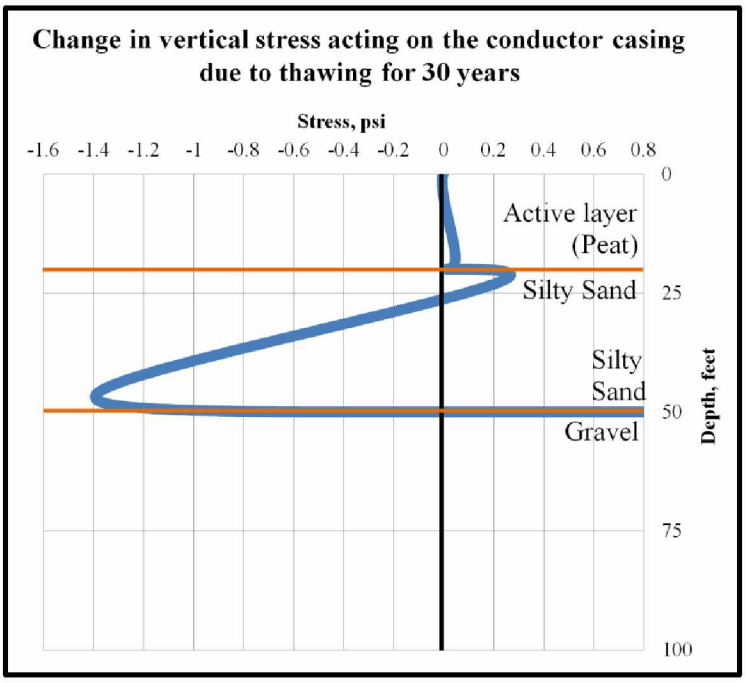

Figure 5.51: Change in vertical stress acting along the well-soil interface for the first 100 ft of conductor casing after 30 years of thawing.

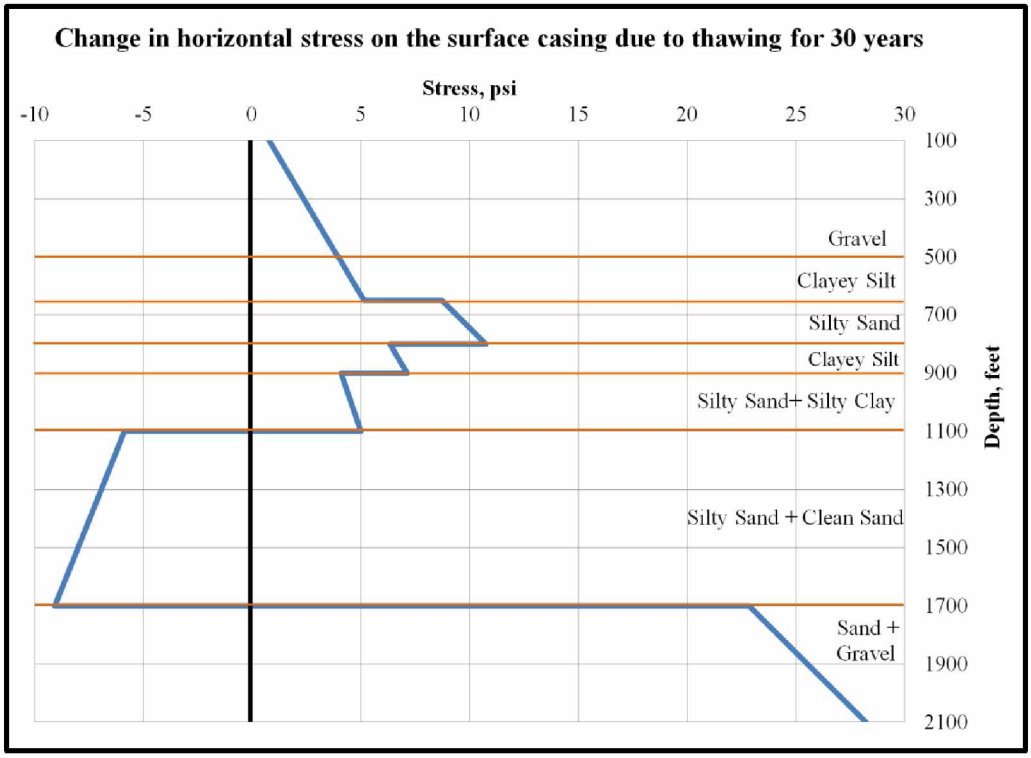

Figure 5.52: Change in horizontal stress acting along the well-soil interface for 2000 ft of surface casing after 30 years of thawing.

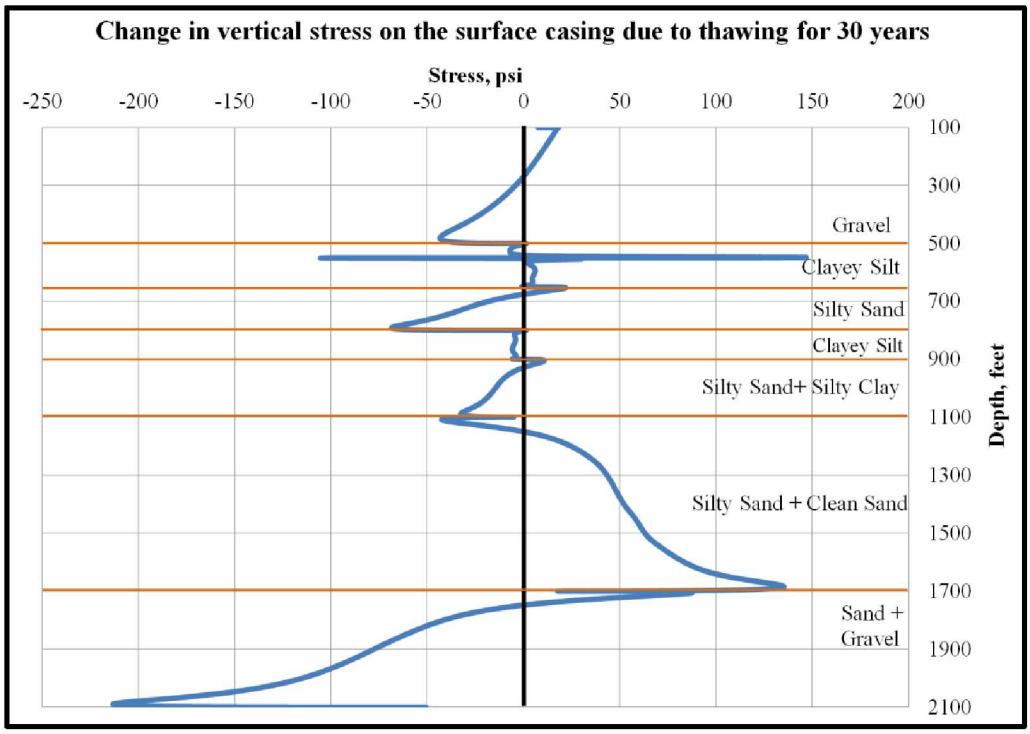

Figure 5.53: Change in vertical stress acting along the well-soil interface for 2000 ft of surface casing after 30 years of thawing.

Figure 5.54 shows changes in the vertical and horizontal stresses for the frozen section of the soil mass for three different time periods. The plots overlap each other, meaning no change in the stresses because of assumption (4), which states that the soil is in equilibrium when its temperature is less than 32°F. Figure 5.55 shows changes in the vertical and horizontal stresses for the thawed section of the soil mass at the end of 30 years of thawing. The changes in the stresses were not significant for the top few layers of the formation, thus the difference in the final stress values (at 30 years) and the initial stress values (at 0 years) was plotted with depth. This was done to understand the orientation of the changes occurring in the vertical and horizontal stresses with depth as the soil mass changes its state from frozen to thawed. The sign convention for Figures 5.54 and 5.55 shows the orientation of the forces in the soil mass. Figure 5.56 shows the resultant volumetric strain effects in the soil mass at the end of 30 years of thawing, as the soil tends to change its state from frozen to thawed due to continuous heat transfer between the casing and the frozen soil. The sign convention for Figure 5.56 is such that a positive sign implies tension strain effects whereas a negative sign implies compression strain effects.

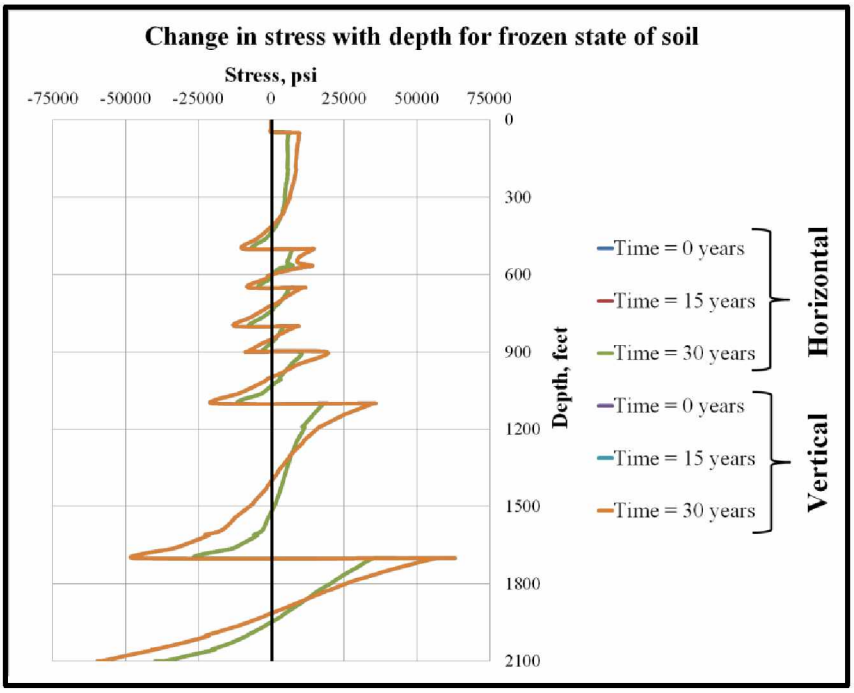

Figure 5.54: Change in the vertical and horizontal stresses with depth at three different time periods for frozen state of soil mass.

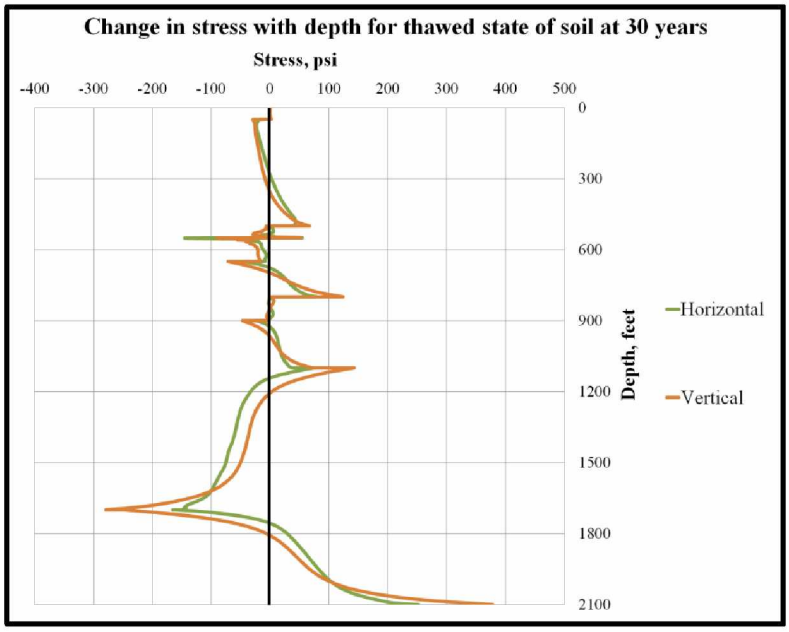

Figure 5.55: Change in the vertical and horizontal stresses with depth at the end of 30 years of thawing.

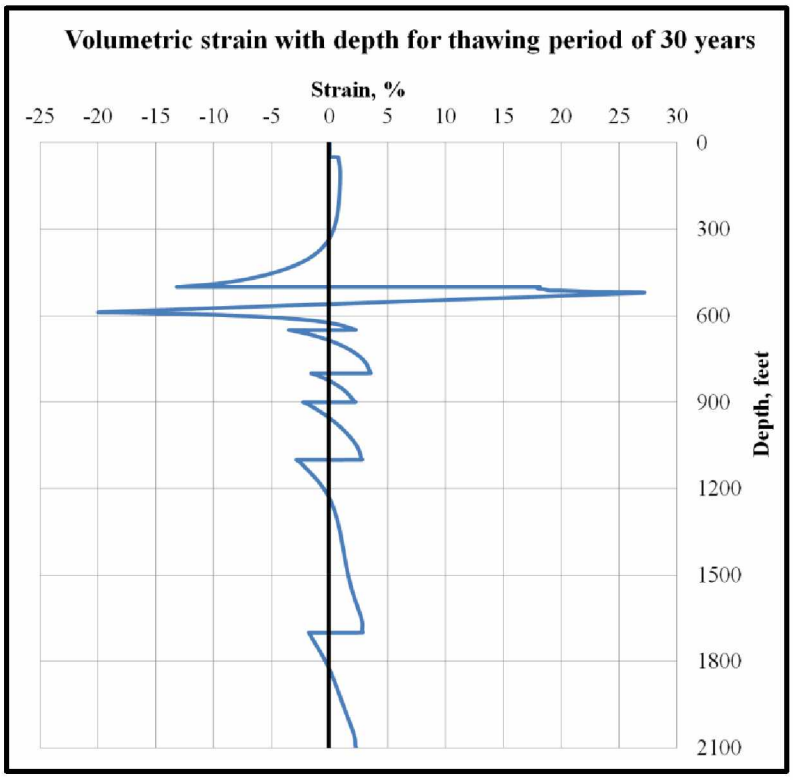

Figure 5.56: Resultant volumetric strain effects in the soil mass at the end of 30 years of thawing as the soil mass changes its state from frozen to thawed.

Figures 5.57 to 5.64 show the change in the density of the soil mass with temperature as a result of continuous heat transfer. The density of the active layer (peat) did not change with temperature and was assumed to be constant. Figures 5.59, 5.61, and 5.63 show higher density changes for the thawed region compared to others; this was mainly due to the variation of the water content in the soil mass. Fine-grained soils had greater water content compared to coarse-grained soils. Figure 5.65 shows the post simulation result for overburden load for the main model for mechanical analysis.

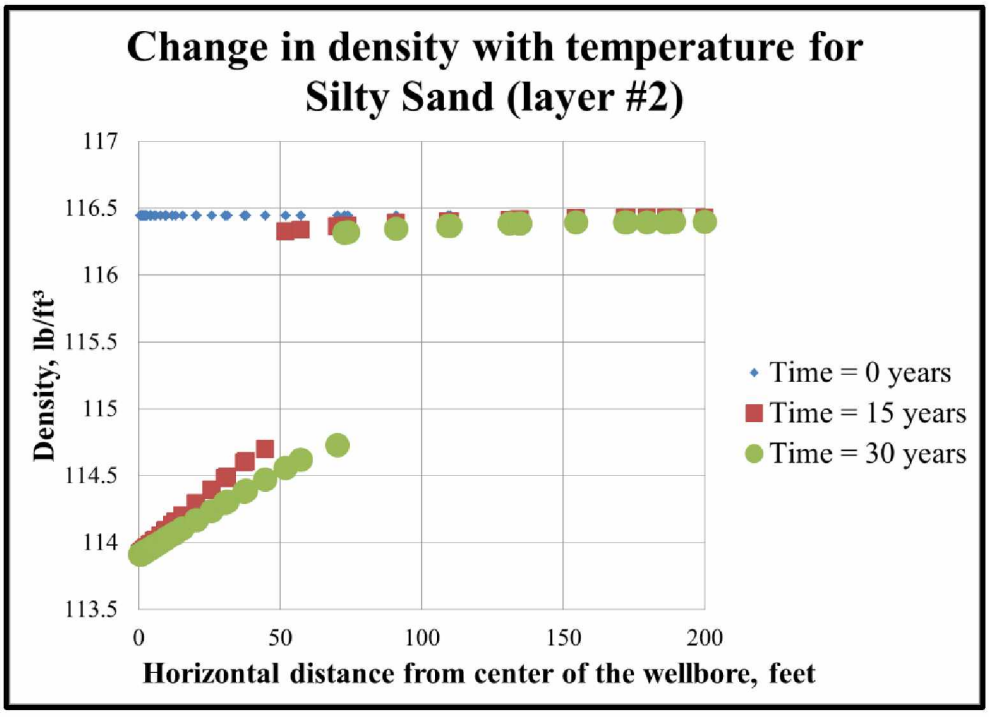

Figure 5.57: Change in density of Silty Sand (layer#2) with temperature at three different time periods.

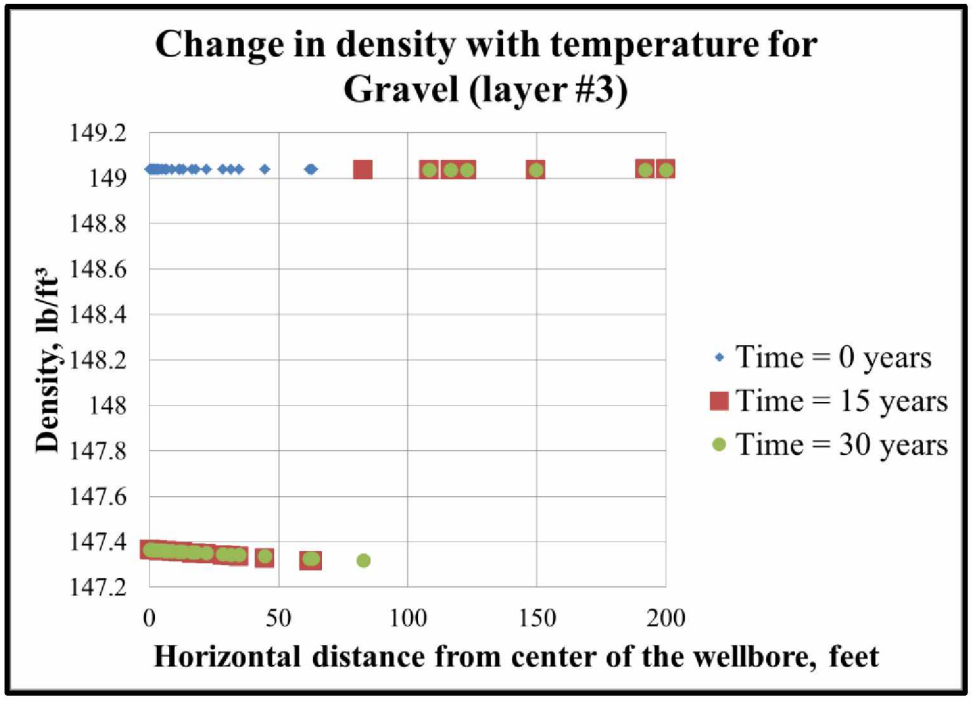

Figure 5.58: Change in density of Gravel (layer#3) with temperature at three different time periods.

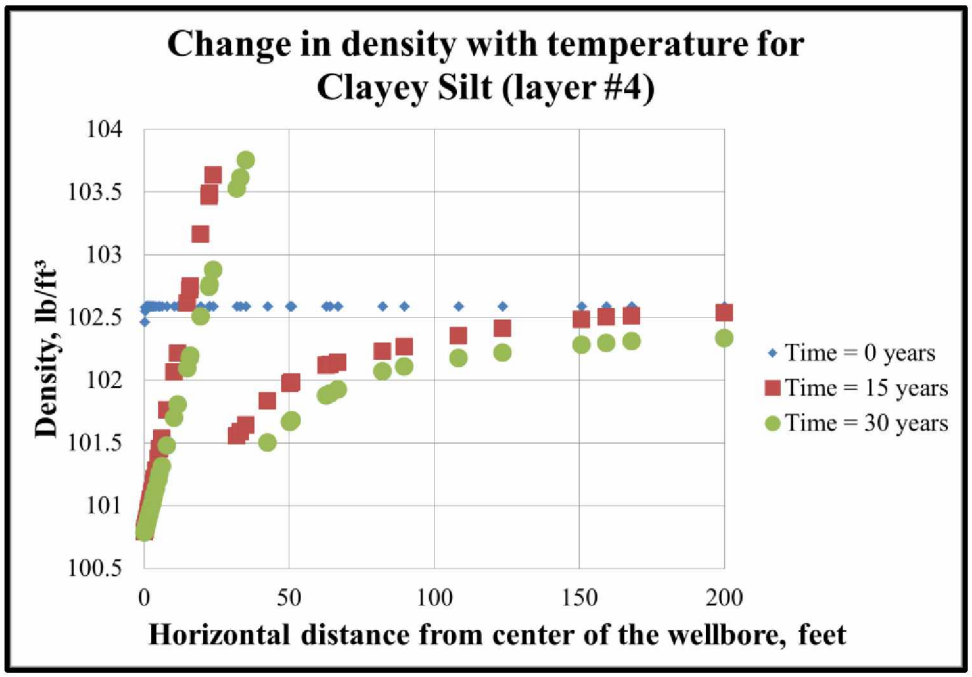

Figure 5.59: Change in density of Clayey Silt (layer#4) with temperature at three different time periods.

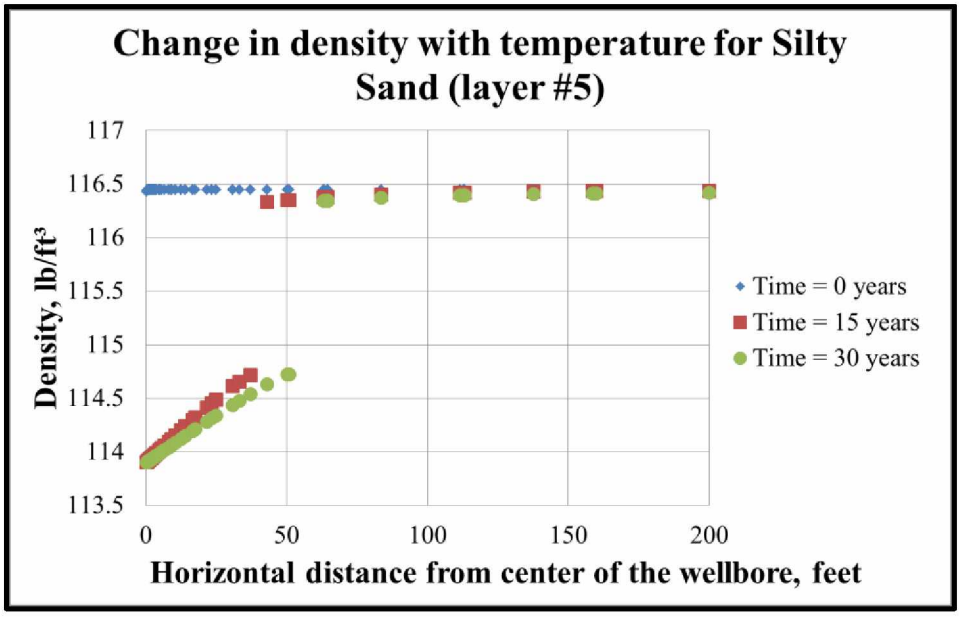

Figure 5.60: Change in density of Silty Sand (layer#5) with temperature at three different time periods.

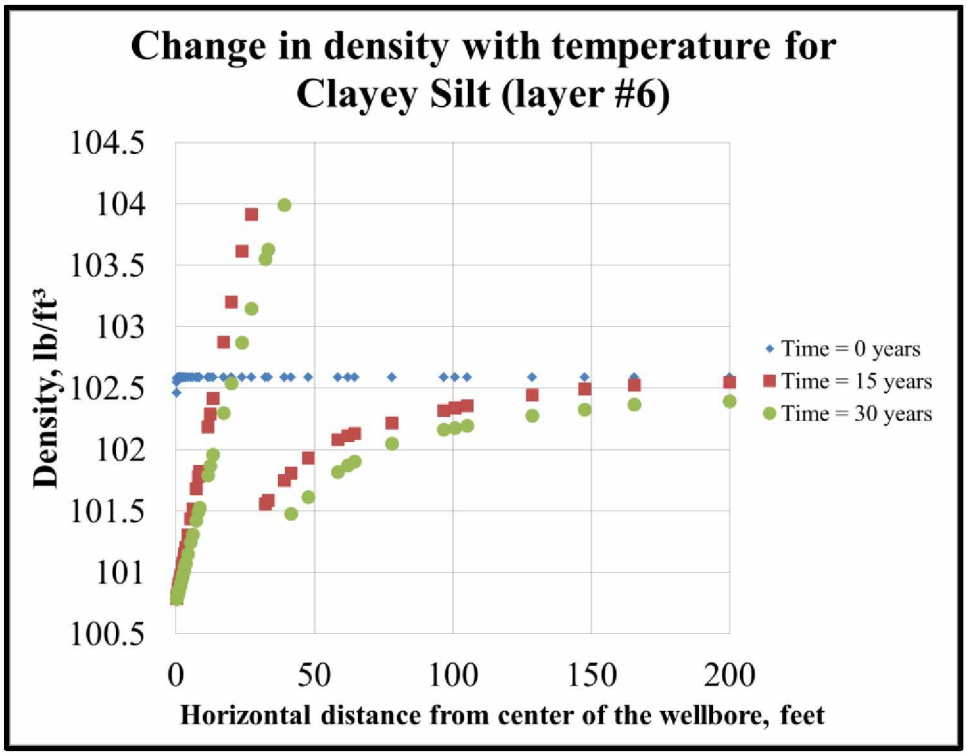

Figure 5.61: Change in density of Clayey Silt (layer#6) with temperature at three different time periods.

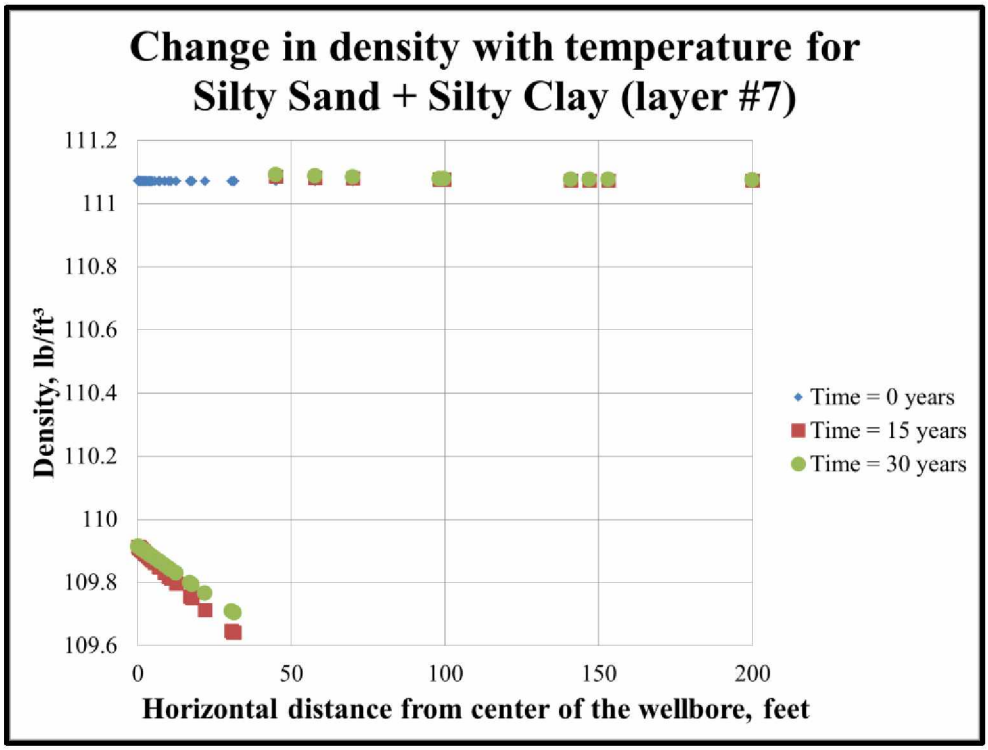

Figure 5.62: Change in density of Silty Sand + Silty Clay (layer#7) with temperature at three different time periods.

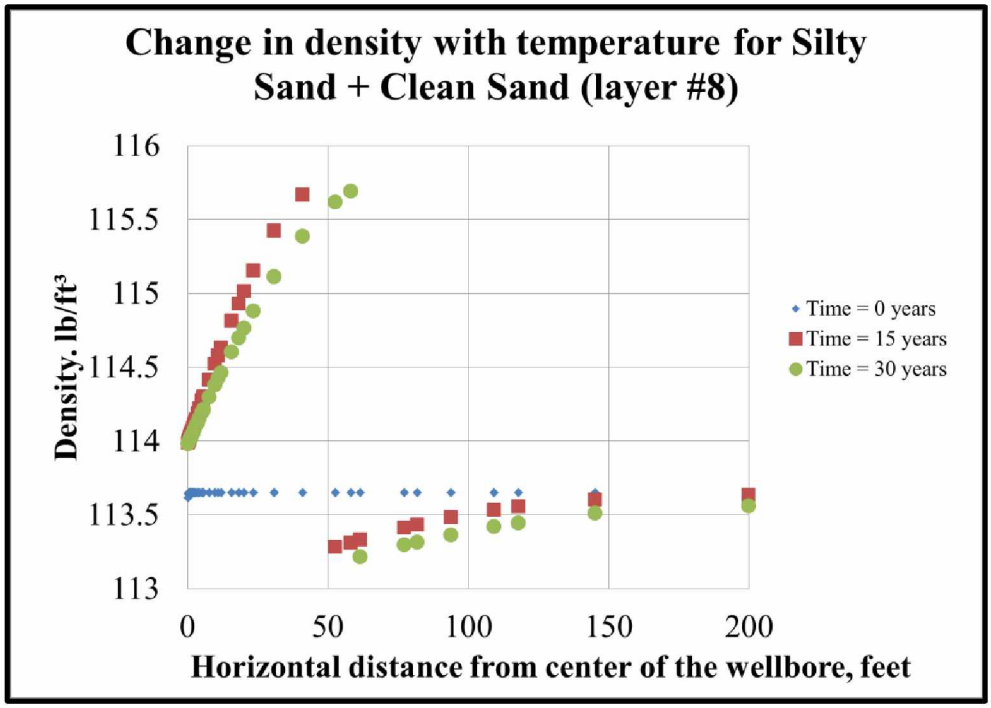

Figure 5.63: Change in density of Silty Sand + Clean Sand (layer#8) with temperature at three different time periods.

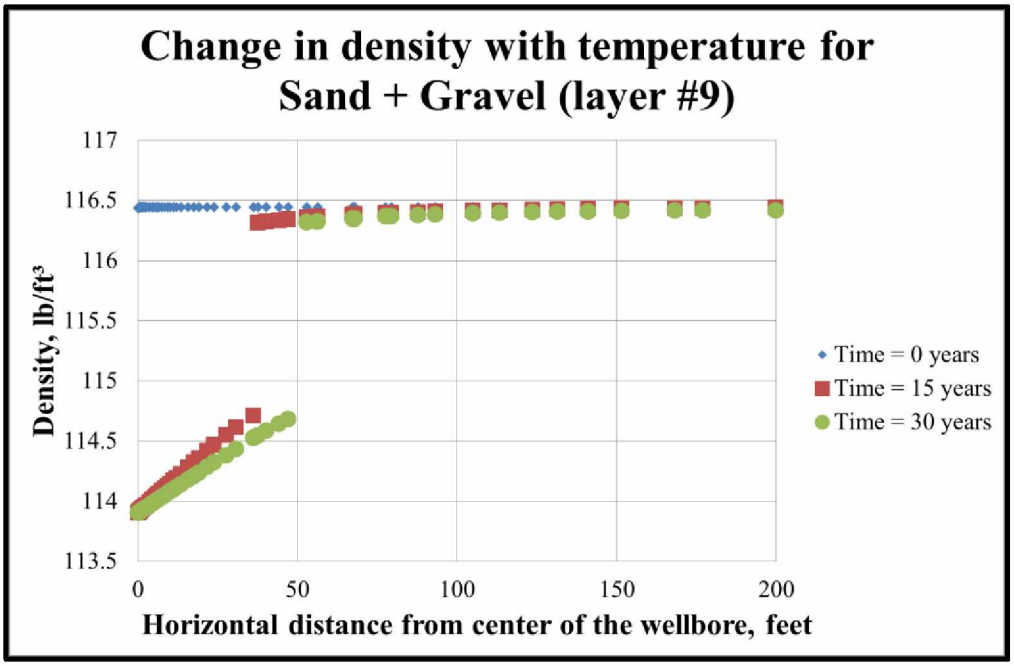

Figure 5.64: Change in density of Sand + Gravel (layer#9) with temperature at three different time periods.

Comparing thermal analysis and mechanical analysis on the basis of COMSOL's ability to conduct any of these analyses, then thermal analysis was conducted more successfully as compared to mechanical analysis. Due to limitations of the software version used for the analysis, certain important aspects required for mechanical analysis were not taken into consideration. The results obtained for mechanical analysis were not completely realistic and are somewhat qualitative and thus were not compared to the scientific literature data. For the purpose of getting an approximate understanding of the mechanical behavior of the soil mass along the length of the wellbore, the mechanical analysis was fairly helpful. It is recommended that the results shown in Section 5.2 should not be used for any experimental work, but they can be utilized to demonstrate the soil's qualitative behavior due to change of state.

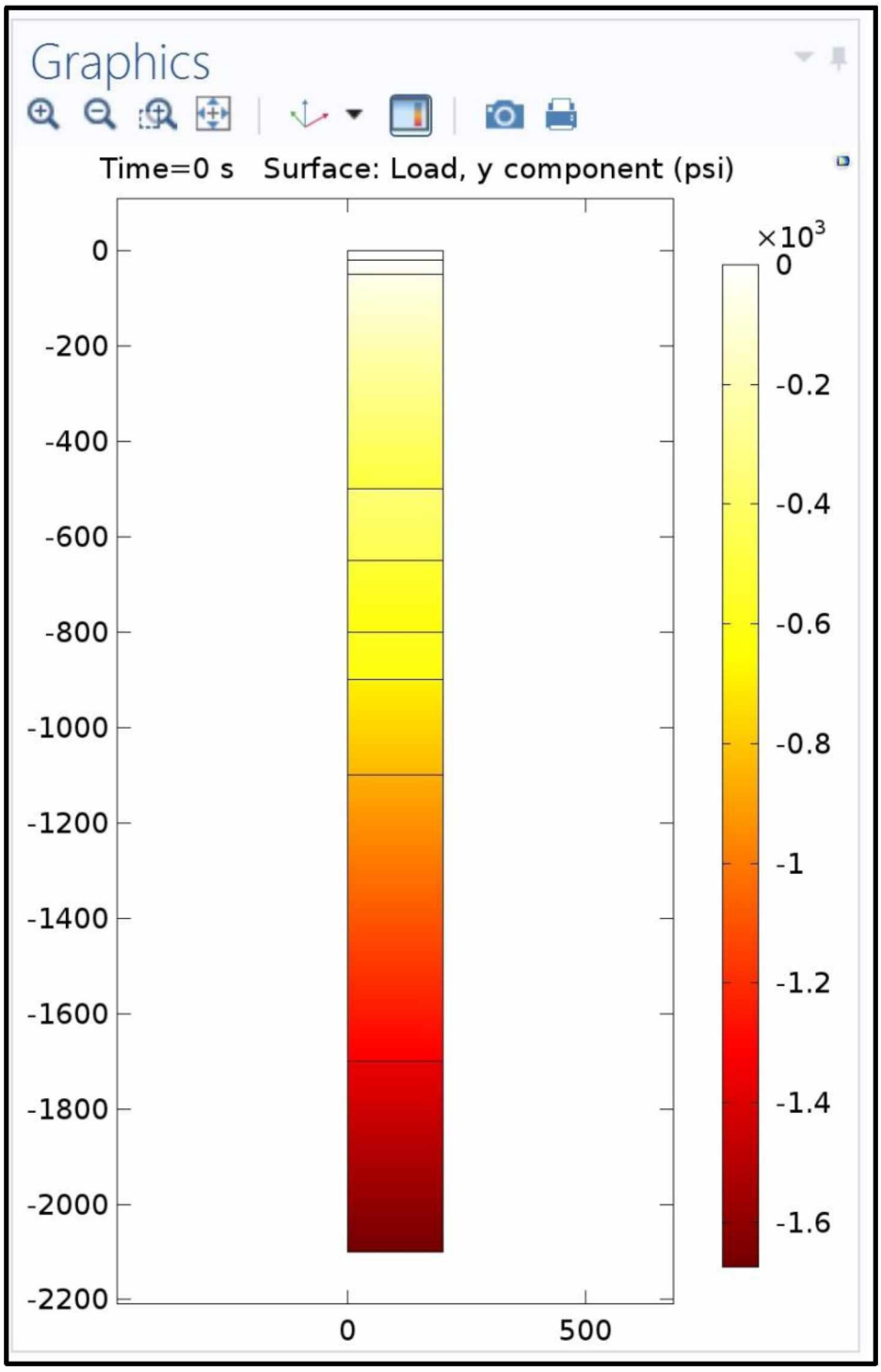

Figure 5.65: Post-simulation model layout for mechanical model.

CHAPTER 6 CONCLUSIONS AND RECOMMENDATIONS

6.1 Conclusions

The objective of the entire study was to understand permafrost thaw subsidence related issues by targeting different characteristics of soil's behavior when it changes its state with temperature and time. The study was focused mainly on gaining a better perspective of the complex interaction between wellbore and soil during progressive thaw. Data was obtained through two different approaches, experimental and numerical analysis. Following are the summarized conclusions for the entire study:

a. Detailed experimental study helped in the understanding of certain important characteristics of different soil types. Results obtained from soil gradation tests (section 4.1.1) and Atterberg limit tests (section 4.1.2) were very beneficial to understand the soil's ability to absorb water, since this is a very important consideration concerning frost heave behavior of soils. Frost heaving tests (section 4.1.4) showed that silt and clay, both fine-grained soils, had nearly conflicting frost heaving behavior. From Figures 4.27 and 4.29, it can be concluded that clay shows better heaving characteristics compared to silt, and thus the thaw settlement effects are more prominent in clayey soils.
b. The three-dimensional physical scale test (section 4.2) measured soil pressures successfully. This was a very important finding with respect to soil characteristics, which tend to change its stress state due to thawing and exert pressure in varying orientations depending on soil type.
c. Compression and tension effects induced by different soil types were observed successfully in the three-dimensional physical scale model test during the frost heaving test (Figures 4.41 to 4.43).
d. A two-dimensional axisymmetric thermal model was built in COMSOL Multiphysics™ (section 5.1). The phase change of ice to water when the soil mass changes its state from frozen to thawed was modeled successfully by taking latent heat (section 2.1.2) into consideration. Thaw radii for different thawing periods were analyzed and studied by varying the oil flowing temperature in the tubing.
e. A detailed thermal analysis (section 5.1.2) was conducted successfully for an entire oil well at Prudhoe Bay (on Alaska's North Slope). It was observed that for a thawing period

of 30 years, the surrounding frozen soil would thaw up to ~65 feet when the oil flowing temperature is 190°F, and during the shut-in period of the oil well, it would refreeze by ~8 feet for the next 15 years

f. A two-dimensional mechanical model was built in COMSOL Multiphysics™. This analysis involved studying the strain and pressure development along the length of the wellbore due to changes in stress state of the soil as a result of changes in the vertical and horizontal loading conditions. It was observed that for a thawing period of 30 years, a maximum compressive strain of ~20% and a maximum tension strain of ~25% developed.

g. Integrated thermal and mechanical analysis through COMSOL Multiphysics™ resulted in better understanding of futuristic scenarios for old oil wells that have been producing for more than 35 years.

h. The entire study can be concluded by stating that heat transfer between the wellbore and surrounding frozen soils cannot be eliminated completely, but if proper measures are taken at the oil well design and development stage, it can be minimized substantially in order to prevent any wellbore instability issues. For the future potential of thermal heavy oil recovery in Alaska's North Slope, permafrost thaw subsidence should be a major consideration in order to maximize oil production by preventing well instability.

6.2 Recommendations

The main objective of this study was to target soil behavior during changes in its state along the length of the wellbore. Even though two different approaches were planned to target different aspects during the progression of this study, not everything was achieved in a timely fashion. The work was still in progress at the time of writing this report. On the basis of all the data presented here, the following recommendations can increase the confidence level of this entire study:

a. The three-dimensional physical scale test considered only one layering scheme for the soil configuration. Although having alternate layers of fine-grained and coarse-grained soils is the optimum approach to look at the post thaw effects of different soil types, having layers of different fine-grained soils and mixtures with different coarse-grained soils will be a better match to the actual lithology of Alaska North Slope.

b. The one-dimensional consolidation test was not completed at the time of writing this report. The experimental setup was not completely ready to carry out any tests. However, running multiple tests on this setup can give an initial understanding of soil thawing characteristics and further data obtained from this test can be compared to the data obtained from the three-dimensional setup. This would aid in deriving correlations among the different variables targeted in this study initially.

c. The data used to perform computer simulation work for both analyses was based on the scientific literature. The soil type did not have an exact match to the soil type in the Alaska North Slope region. Actual data for different thermal and mechanical properties of soils can be obtained by performing experiments on soil samples from the Alaska North Slope region and can be used for numerical modeling purposes. This would further modify the post simulation results and would lead to better and more accurate results. Furthermore, simulation results can be compared to the data obtained from the two experimental approaches discussed in this report for deriving strong correlations for thaw settlement.

d. The mechanical analysis discussed in this study was based on numerous assumptions because of the software's limitations. Most of the input parameters were derived from the scientific literature. If more realistic input data is used with better software dedicated for modeling soil behavior, then the result would be better and more accurate, for understanding mechanical behavior of thawed soils compared to frozen soils.

REFERENCES

Andersland, Orlando B., & Branko, Ladanyi (2004). "Frozen Ground Engineering" Second Edition, John Wiley & Sons, Inc., Hoboken, New Jersey.

Brown. R. J. E. (1967). "Distribution of Permafrost in Canada". Ottawa: Geological Survey of Canada/National Research council of Canada

Couch, E. J., Keller, H. H. & Watts, J. W. (1970, April 1). "Permafrost Thawing Around Producing Oil Wells". Petroleum Society of Canada. doi:10.2118/70-02-06

Davies, B. E., & Boorman, R. D. (1973, January 1). "Field Investigation of Effect of Thawing Permafrost Around Wellbores at Prudhoe Bay". Society of Petroleum Engineers. doi:10.2118/4591-MS

Davies, B. E., Newby, N., & Smart, A. B. (1979, January 1). PD 6(1) "Deep Permafrost Oil Production: The First Two Years". World Petroleum Congress.

Darrow, M. M. (2007). "Experimental Study of Adsorbed Cation Effects on the Frost Susceptibility of Natural Soils". Department of Civil Engineering, College of Engineering and Mines, University of Alaska Fairbanks.

Dillon, M. R. (2012). "The Impact of a Fluctuating Freezing Front on Ice Formation in Freezing Soil". Department of Civil Engineering, College of Engineering and Mines, University of Alaska Fairbanks.

Farouki, Omar T. (1981). "Thermal Properties of Soil", United States Army Corps of Engineers, Cold Regions Research and Engineering Laboratory, Hanover, New Hampshire, U.S.A.

Goodman, M. A. November (1977). "Loading Mechanisms in Thawed Permafrost Around Arctic Wells", Journal of Pressure Vessel Technology. Pages 641-645

Goodman, Malcolm A. (1978). "World Oil's Handbook of Artic Well Completions", World Oil

Hansen, J., & S. L. Lebedev (1987). "Global Trends of Measured Surface Air Temperature" Journal of Geophysical Research

Knepler, J. R. (1980, January 1). "Completion Practices for Prudhoe Bay Wells. Society of Petroleum Engineers". doi:10.2118/8785-MS

Kanevskiy, M. Z., Stephani, E., Shur, Y. L., Jorgenson, M. T., Ping, C.-L., Fortier, D., & Dillon, M. (2011, January 1). "Permafrost of Northern Alaska". International Society of Offshore and Polar Engineers.

Lin, C. J., & Wheeler, J. D. (1978, March 1). "Simulation of Permafrost Thaw Behavior at Prudhoe Bay". Society of Petroleum Engineers. doi:10.2118/6063-PA

Merriam, R., Wechsler, A., Boorman, R., & Davies, B. (1975, March 1). "Insulated Hot Oil-Producing Wells In Permafrost". Society of Petroleum Engineers. doi:10.2118/4590-PA

Mitchell, R. F., & Goodman, M. A. (1978, March 1). "Permafrost Thaw-Subsidence Casing Design". Society of Petroleum Engineers. doi:10.2118/6060-PA

Matthews, C. M., & Zhang, G. (2012, December 3). "Importance of Deep Permafrost Soil Characterization for Accurate Assessment of Thaw Subsidence Impacts on the Design and Integrity of Arctic Wells". Offshore Technology Conference. doi:10.4043/23747-MS

Osterkamp, T. E., & Jorgenson, M. T. (2009). "Permafrost Conditions and Processes", Geological Monitoring: Boulder, Colorado, Geological Society of America, page 205-227.

Ruedrich, R. A., Perkins, T. K., Rochon, J. A., & Christman, S. A. (1978, March 1). "Casing Strain Resulting From Thawing of Prudhoe Bay Permafrost". Society of Petroleum Engineers. doi:10.2118/6062-PA

Smith, R. E., & Clegg, M. W. (1971, January 1). "Analysis and Design of Production Wells through Thick Permafrost". World Petroleum Congress.

Sengul, M. M., & Brigham, W. E. (1983, January 1). "Determination of Permafrost Thawing Around Oil Wells". Society of Petroleum Engineers. doi:10.2118/11734-MS

Shur, Y. L., & Ping, C. L. (1991). "Permafrost Dynamics and Soil Formation" in Kimble, J. M. and Ahres, R. J. USDA, Soil Conservation Service, National Soil Survey Center. Lincoln, N/F., page 112-118.

Shur, Y. L. (2014). "Introduction of Permafrost Engineering Courseware", College of Engineering and Mines, University of Alaska Fairbanks.

van Everdingen, R., Metz, M., & Hoekstra, P.(1985). "Unfrozen permafrost and other taliks". Workshop on permafrost geophysics, Vol. 85-5, pp. p.101-105.

van Everdingen, R. O. (1998). "Multi-language Glossary of Permafrost and Related Ground-Ice Terms". The Arctic Institute of North America, The University of Calgary, Calgary, Alberta, Canada. T2N 1N4

Xie, J. (2009). "Analysis of Thaw Subsidence Impacts on Production Wells". C-FER Technologies, Edmonton, Alberta, Canada. SIMULIA Customer Conference

Xie, J., & Matthews, C. M. (2011, January 1). "Methodology to Assess Thaw Subsidence Impacts on the Design and Integrity of Oil and Gas Wells in Arctic Regions". Society of Petroleum Engineers. doi:10.2118/149740-MS

APPENDIX A-1

Table A-1: Values for effective depth (L) on hydrometer and sedimentation cylinders of specific sizes (https://www.uic.edu/classes/cemm/cemmlab/Experiment%206-Grain%20Size%20Analysis.pdf)

Hydrometer 151H		Hydrometer 152H			
Actual Hydrometer Reading	Effective Depth, L (cm)	Actual Hydrometer Reading	Effective Depth, L (cm)	Actual Hydrometer Reading	Effective Depth, L (cm)
1.000	16.3	0	16.3	31	11.2
1.001	16.0	1	16.1	32	11.1
1.002	15.8	2	16.0	33	10.9
1.003	15.5	3	15.8	34	10.7
1.004	15.2	4	15.6	35	10.6
1.005	15.0	5	15.5	36	10.4
1.006	14.7	6	15.3	37	10.2
1.007	14.4	7	15.2	38	10.1
1.008	14.2	8	15.0	39	9.9
1.009	13.9	9	14.8	40	9.7
1.010	13.7	10	14.7	41	9.6
1.011	13.4	11	14.5	42	9.4
1.012	13.1	12	14.3	43	9.2
1.013	12.9	13	14.2	44	9.1
1.014	12.6	14	14.0	45	8.9
1.015	12.3	15	13.8	46	8.8
1.016	12.1	16	13.7	47	8.6
1.017	11.8	17	13.5	48	8.4
1.018	11.5	18	13.3	49	8.3
1.019	11.3	19	13.2	50	8.1
1.020	11.0	20	13.0	51	7.9
1.021	10.7	21	12.9	52	7.8
1.022	10.5	22	12.7	53	7.6
1.023	10.2	23	12.5	54	7.4
1.024	10.0	24	12.4	55	7.3
1.025	9.7	25	12.2	56	7.1
1.026	9.4	26	12.0	57	7.0
1.027	9.2	27	11.9	58	6.8
1.028	8.9	28	11.7	59	6.6
1.029	8.6	29	11.5	60	6.5
1.030	8.4	30	11.4		
1.031	8.1				
1.032	7.8				
1.033	7.6				
1.034	7.3				
1.035	7.0				
1.036	6.8				
1.037	6.5				
1.038	6.2				
1.039	5.9				

Table A-2: Values of K to be used for calculating particle diameter for hydrometer analysis (https://www.uic.edu/classes/cemm/cemmlab/Experiment%206-Grain%20Size%20Analysis.pdf)

Temperature °C	Specific Gravity of Soil Particles								
	2.45	2.50	2.55	2.60	2.65	2.70	2.75	2.80	2.85
16	0.01510	0.01505	0.01481	0.01457	0.01435	0.01414	0.0394	0.01374	0.01356
17	0.01511	0.01486	0.01462	0.01439	0.01417	0.01396	0.01376	0.01356	0.01338
18	0.01492	0.01467	0.01443	0.01421	0.01399	0.01378	0.01359	0.01339	0.01321
19	0.01474	0.01449	0.01425	0.01403	0.01382	0.01361	0.01342	0.01323	0.01305
20	0.01456	0.01431	0.01408	0.01386	0.01365	0.01344	0.01325	0.01307	0.01289
21	0.01438	0.01414	0.01391	0.01369	0.01348	0.01328	0.01309	0.01291	0.01273
22	0.01421	0.01397	0.01374	0.01353	0.01332	0.01312	0.01294	0.01276	0.01258
23	0.01404	0.01381	0.01358	0.01337	0.01317	0.01297	0.01279	0.01261	0.01243
24	0.01388	0.01365	0.01342	0.01321	0.01301	0.01282	0.01264	0.01246	0.01229
25	0.01372	0.01349	0.01327	0.01306	0.01286	0.01267	0.01249	0.01232	0.01215
26	0.01357	0.01334	0.01312	0.01291	0.01272	0.01253	0.01235	0.01218	0.01201
27	0.01342	0.01319	0.01297	0.01277	0.01258	0.01239	0.01221	0.01204	0.01188
28	0.01327	0.01304	0.01283	0.01264	0.01244	0.01255	0.01208	0.01191	0.01175
29	0.01312	0.01290	0.01269	0.01269	0.01230	0.01212	0.01195	0.01178	0.01162
30	0.01298	0.01276	0.01256	0.01236	0.01217	0.01199	0.01182	0.01165	0.01149

Table A-3: Values obtained from sieve analysis for silt sample #1 (Murie Building excavated soil)

Sr. No.	#Sieve Number	Size(mm)	Weight of Container (g)	Weight of (Container + Soil) (g)	Net weight of Soil (g)
1	30	0.600	378.20	423.00	44.80
2	40	0.425	337.00	353.60	16.60
3	50	0.300	349.40	391.80	42.40
4	100	0.147	342.80	417.70	74.90
5	140	0.106	336.50	382.10	45.60
6	170	0.090	350.20	391.40	41.20
7	200	0.075	339.90	425.90	86.00
8	Last pan	<0.053	379.90	1012.60	632.70

Table A-4: Values obtained from hydrometer analysis for silt sample #1 (Murie Building excavated soil)

Time (min)	Hydrometer reading	
2	1.019	
5	1.015	
15	1.01	
30	1.009	
60	1.01	
250	*1.008*	*(Not included in the calculation because the value was constant for the next time step)*
1440	1.008	

Table A-5: Calculated results for both the tests for silt sample #1 (Murie Building excavated soil)

Diameter, mm	Percent fine, %	Cumulative Mass, %
0.600	95.50	4.51
0.425	93.83	6.17
0.300	89.56	10.44
0.147	82.03	17.97
0.106	77.45	22.55
0.090	73.30	26.70
0.075	64.66	35.34
0.032	39.28	60.72
0.021	31.01	68.99
0.013	20.67	79.33
0.009	18.61	81.39
0.003	16.54	83.46
0.001	16.54	83.46

Table A-6: Values obtained from sieve analysis for silt sample #2 (Murie Building excavated soil)

Sr. No.	#Sieve Number	Size(mm)	Weight of Container (g)	Weight of (Container + Soil) (g)	Net weight of Soil (g)
1	30	0.600	378.10	415.40	37.30
2	40	0.425	337.10	361.50	24.40
3	50	0.300	349.60	376.10	26.50
4	100	0.147	342.70	396.60	53.90
5	140	0.106	336.50	370.90	34.40
6	170	0.090	350.20	374.70	24.50
7	200	0.075	339.70	387.70	48.00
8	Last pan	<0.053	379.90	1094.00	714.10

Table A-7: Values obtained from hydrometer analysis for silt sample #2 (Murie Building excavated soil)

Time (min)	Hydrometer reading	
2	1.025	
5	1.018	
15	1.013	
30	1.012	
60	1.007	
250	*1.009*	*(Not included in the calculation because the value was greater than the last time step)*
1440	1.006	

Table A-8: Calculated results for both the tests for silt sample #2 (Murie Building excavated soil)

Diameter, mm	Percent fine, %	Cumulative Mass, %
0.600	96.14	3.86
0.425	93.61	6.39
0.300	90.87	9.13
0.147	85.29	14.71
0.106	81.72	18.28
0.090	79.19	20.81
0.075	74.22	25.78
0.030	59.60	40.40
0.020	42.91	57.09
0.013	30.99	69.01
0.009	28.61	71.39
0.007	16.69	83.31
0.001	14.30	85.70

Table A-9: Values obtained from sieve analysis for clay from the Usibelli Coal Mine

Sr. No.	#Sieve Number	Size(mm)	Weight of Container (g)	Weight of (Container + Soil) (g)	Net weight of Soil (g)
1	30	0.600	87.70	90.30	2.60
2	40	0.425	87.80	88.90	1.10
3	50	0.300	87.40	89.00	1.60
4	100	0.147	88.50	141.80	53.30
5	140	0.106	86.70	137.50	50.80
6	170	0.090	86.90	125.10	38.20
7	200	0.075	87.30	100.70	13.40
8	Last pan	<0.053	439.60	784.98	345.38

Table A-10: Values obtained from hydrometer analysis for clay from the Usibelli Coal Mine

Time (min)	Hydrometer reading
2	1.024
5	1.021
15	1.0175
30	1.0165
60	1.016
250	1.008
1440	1.008

Table A-11: Calculated results for both the tests for clay from the Usibelli Coal Mine

Diameter, mm	Percent fine, %	Cumulative Mass, %
0.600	99.49	0.51
0.425	99.27	0.73
0.300	98.95	1.05
0.147	88.43	11.57
0.106	78.40	21.60
0.090	70.85	29.15
0.075	68.21	31.79
0.029	51.08	48.92
0.019	44.69	55.31
0.011	37.25	62.75
0.008	35.12	64.88
0.006	34.05	65.95
0.003	17.03	82.97
0.001	17.03	82.97

Table A-12: Values obtained from sieve analysis for sand

Sr. No.	#Sieve Number	Size(mm)	Weight of Container (g)	Weight of (Container + Soil) (g)	Net weight of Soil (g)
1	30	0.600	378.00	389.50	11.50
2	40	0.425	336.80	373.60	36.80
3	50	0.300	350.40	629.30	278.90
4	100	0.147	342.80	924.60	581.80
5	140	0.106	336.50	404.40	67.90
6	170	0.090	350.00	362.80	12.80
7	200	0.075	339.50	344.30	4.80
8	Last pan	<0.053	377.40	384.00	6.60

Table A-13: Calculated results for sand

Diameter, mm	Percent fine, %	Cumulative Mass, %
0.60	98.85	1.15
0.43	95.18	4.82
0.30	67.35	32.65
0.15	9.28	90.72
0.11	2.50	97.50
0.09	1.23	98.77
0.08	0.75	99.25
0.05	0.09	99.91

Table A-14: Values obtained from sieve analysis for gravel

Sr. No.	#Sieve Number	Size(mm)	Weight of Container (g)	Weight of (Container + Soil) (g)	Net weight of Soil (g)
1	30	0.600	378.10	893.00	514.90
2	40	0.425	337.00	369.70	32.70
3	50	0.300	349.40	481.10	131.70
4	100	0.147	342.80	614.60	271.80
5	140	0.106	336.60	368.20	31.60
6	170	0.090	350.20	355.50	5.30
7	200	0.075	339.60	342.00	2.40
8	Last pan	<0.053	379.80	384.70	4.90

Table A-15: Calculated results for gravel

Diameter, mm	Percent fine, %	Cumulative Mass, %
0.60	96.14	3.86
0.43	93.61	6.39
0.30	90.87	9.13
0.15	85.29	14.71
0.11	81.72	18.28
0.09	79.19	20.81
0.08	74.22	25.78
0.05	0.28	99.72

Table A-16: Final data obtained at the end of sieve analysis for each soil type

Sr. No	Soil sample	Weight of Dry Soil (g)	Weight of soil loss (g)
1	Silt sample A	994.50	10.30 (<2%)
2	Silt sample B	965.80	2.70 (<2%)
3	Usibelli clay	506.38	0.00 (<2%)
4	Sand	1002.00	0.90 (<2%)
5	Gravel	1000.00	4.20 (<2%)

Table A-17: Liquid limit data for Silt-Sample A, from the University of Alaska Fairbanks' (UAF) backyard (Murie Building excavated soil)

Sr. No	Empty Container Weights (g)	Number of blows	Wet weight of soil (g)	Dry weight of soil (g)	Water content (%)
1	15.37	28	21.21	19.45	43.14
2	15.09	17	22.31	20.03	46.15
3	15.15	19	21.62	19.61	45.07
4	15.12	24	22.39	20.15	44.53
5	15.02	25	20.91	19.12	43.66

Table A-18: Plastic limit data for Silt-Sample A, from UAF's backyard (Murie Building excavated soil)

Sr. No	Empty Container Weights (g)	Wet weight of soil (g)	Dry weight of soil (g)	Water content (%)
1	15.47	15.97	15.85	31.58
2	14.75	15.30	15.18	27.91
3	14.88	15.38	15.26	31.58

Table A-19: Liquid limit data for Silt-Sample B, from UAF's backyard (Murie Building excavated soil)

Sr. No	Empty Container Weights (g)	Number of blows	Wet weight of soil (g)	Dry weight of soil (g)	Water content (%)
1	25.82	12	36.51	34.20	27.57
2	25.64	28	43.96	40.18	26.00
3	25.93	20	36.65	34.39	26.71
4	25.94	24	36.17	34.01	26.77

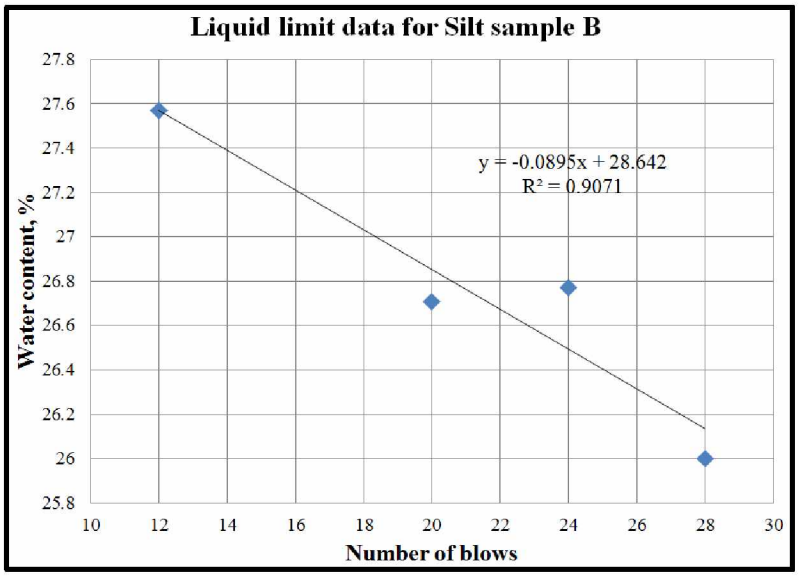

Figure A-1: Liquid limit data for silt-sample B.

Table A-20: Plastic limit data for Silt-Sample B from UAF's backyard (Murie Building excavated soil)

Sr. No	Empty Container Weights (g)	Wet weight of soil (g)	Dry weight of soil (g)	Water content (%)
1	25.65	26.62	26.43	24.36
2	25.75	26.65	26.48	23.29
3	25.82	26.51	26.37	25.45

Table A-21: Liquid limit data for clay from the Usibelli Coal Mine

Sr. No	Empty Container Weights (g)	Number of blows	Wet weight of soil (g)	Dry weight of soil (g)	Water content (%)
1	15.40	14	32.00	27.10	41.88
2	15.00	37	29.90	25.90	36.70
3	15.20	28	28.80	25.00	38.78
4	15.10	26	32.30	27.60	37.60
5	15.00	23	28.40	24.60	39.58

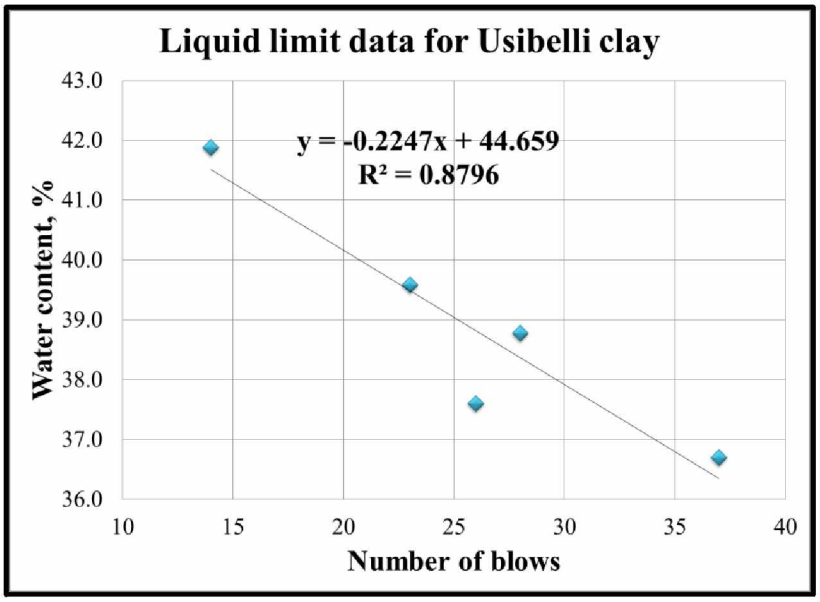

Figure A-2: Liquid limit data for clay from the Usibelli Coal Mine.

Table A-22: Plastic limit data for clay from the Usibelli Coal Mine

Sr. No	Empty Container Weights (g)	Wet weight of soil (g)	Dry weight of soil (g)	Water content (%)
1	15.30	16.50	16.20	33.33
2	14.80	15.80	15.70	11.11
3	15.00	15.40	15.30	33.33

Table A-23: Liquid limit data for clay from the Usibelli Coal Mine + 10% MI Gel

Sr. No	Empty Container Weights (g)	Number of blows	Wet weight of soil (g)	Dry weight of soil (g)	Water content (%)
1	25.39	22	39.33	35.22	41.81
2	25.63	20	41.38	36.68	42.53
3	25.81	25	40.15	35.98	41.00
4	25.55	18	43.05	37.77	43.21

Table A-24: Plastic limit data for clay from the Usibelli Coal Mine + 10% MI Gel

Sr. No	Empty Container Weights (g)	Wet weight of soil (g)	Dry weight of soil (g)	Water content (%)
1	25.78	26.47	26.32	27.78
2	25.93	26.49	26.37	27.27
3	25.92	26.56	26.43	25.49

Table A-25: Liquid limit data for clay from the Usibelli Coal Mine + 15% MI Gel

Sr. No	Empty Container Weights (g)	Number of blows	Wet weight of soil (g)	Dry weight of soil (g)	Water content (%)
1	25.75	32	38.88	33.74	64.33
2	25.64	28	38.07	33.00	68.89
3	25.54	25	37.83	32.60	74.08
4	25.63	15	45.50	36.93	75.84

Table A-26: Plastic limit data for clay from the Usibelli Coal Mine + 15% MI Gel

Sr. No	Empty Container Weights (g)	Wet weight of soil (g)	Dry weight of soil (g)	Water content (%)
1	25.38	25.64	25.57	36.84
2	25.80	26.27	26.15	34.29
3	25.48	25.84	25.72	50.00

Table A-27: Liquid limit data for clay from the Usibelli Coal Mine + 20% MI Gel

Sr. No	Empty Container Weights (g)	Number of blows	Wet weight of soil (g)	Dry weight of soil (g)	Water content (%)
1	19.34	24	33.08	27.76	63.18
2	19.47	29	30.72	26.40	62.34
3	15.21	19	33.48	25.73	73.67
4	19.42	30	37.84	30.36	68.37

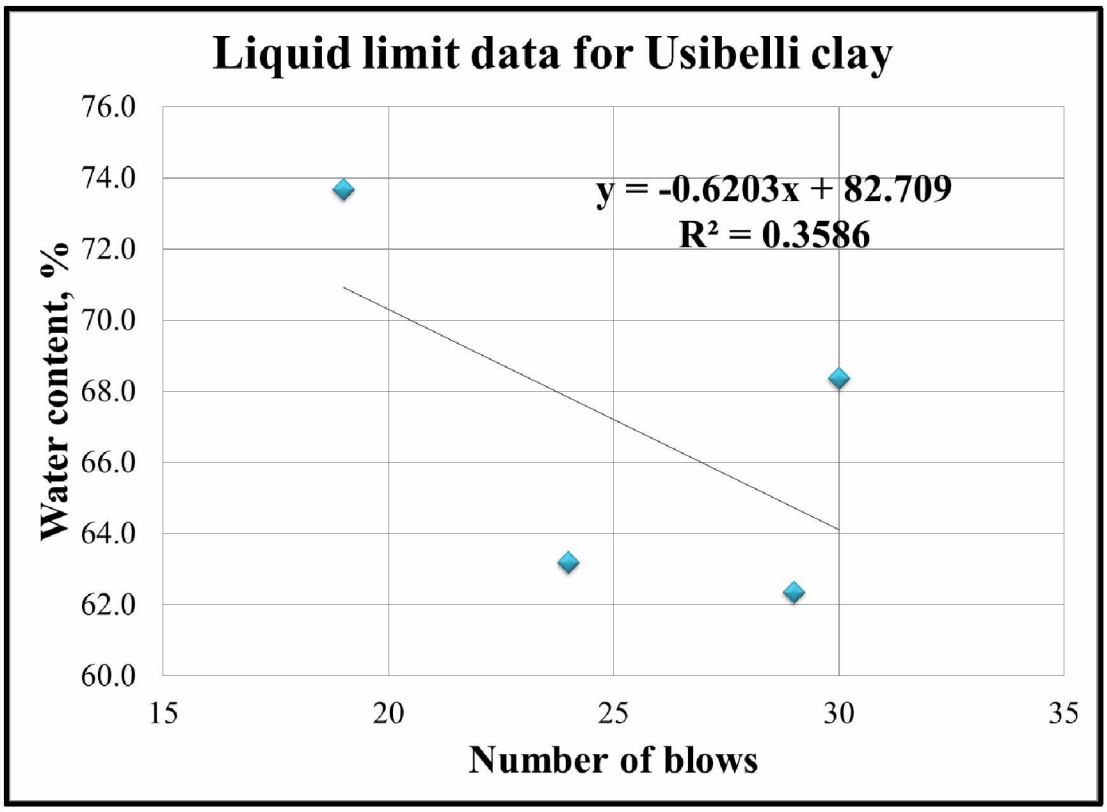

Figure A-3: Liquid limit data for clay from the Usibelli Coal Mine + 20% MI Gel.

Table A-28: Plastic limit data for clay from the Usibelli Coal Mine + 20% MI Gel

Sr. No	Empty Container Weights (g)	Wet weight of soil (g)	Dry weight of soil (g)	Water content (%)
1	19.37	20.18	19.98	32.79
2	19.77	20.18	20.08	32.26
3	19.24	19.66	19.57	27.27

Table A-29: Liquid limit data for silt sample A + 5% MI Gel

Sr. No	Empty Container Weights (g)	Number of blows	Wet weight of soil (g)	Dry weight of soil (g)	Water content (%)
1	19.25	27	33.51	29.94	33.40
2	19.76	32	30.91	28.26	31.18
3	19.42	19	29.62	27.09	32.99
4	19.32	25	30.79	28.00	32.14

Table A-30: Plastic limit data for silt sample A + 5% MI Gel

Sr. No	Empty Container Weights (g)	Wet weight of soil (g)	Dry weight of soil (g)	Water content (%)
1	19.78	20.64	20.44	30.30
2	15.21	16.07	15.90	24.64
3	19.34	19.79	19.70	25.00

Table A-31: Liquid limit data for silt sample A + 10% MI Gel

Sr. No	Empty Container Weights (g)	Number of blows	Wet weight of soil (g)	Dry weight of soil (g)	Water content (%)
1	15.19	34	25.38	22.73	35.15
2	19.33	26	31.06	27.84	37.84
3	19.36	25	36.00	31.31	39.25
4	19.26	23	33.99	29.76	40.29

Table A-32: Plastic limit data for silt sample A + 10% MI Gel

Sr. No	Empty Container Weights (g)	Wet weight of soil (g)	Dry weight of soil (g)	Water content (%)
1	19.49	20.07	19.93	31.82
2	25.55	26.40	26.10	54.55
3	19.36	19.87	19.74	34.21

Table A-33: Liquid limit data for silt sample A + 15% MI Gel

Sr. No	Empty Container Weights (g)	Number of blows	Wet weight of soil (g)	Dry weight of soil (g)	Water content (%)
1	25.55	32	33.19	30.77	46.36
2	25.63	27	33.20	30.71	49.02
3	25.54	20	38.87	34.22	53.57
4	25.80	25	39.20	34.41	55.63

Table A-34: Plastic limit data for silt sample A + 15% MI Gel

Sr. No	Empty Container Weights (g)	Wet weight of soil (g)	Dry weight of soil (g)	Water content (%)
1	25.40	25.94	25.83	25.58
2	25.39	26.05	25.92	24.53
3	25.44	25.90	25.81	24.32

Table A-35: Liquid limit data for silt sample A + 20% MI Gel

Sr. No	Empty Container Weights (g)	Number of blows	Wet weight of soil (g)	Dry weight of soil (g)	Water content (%)
1	19.35	15	29.88	25.44	72.91
2	19.46	22	28.97	25.41	59.83
3	19.42	27	27.60	24.61	57.61
4	15.22	35	24.45	21.04	58.59

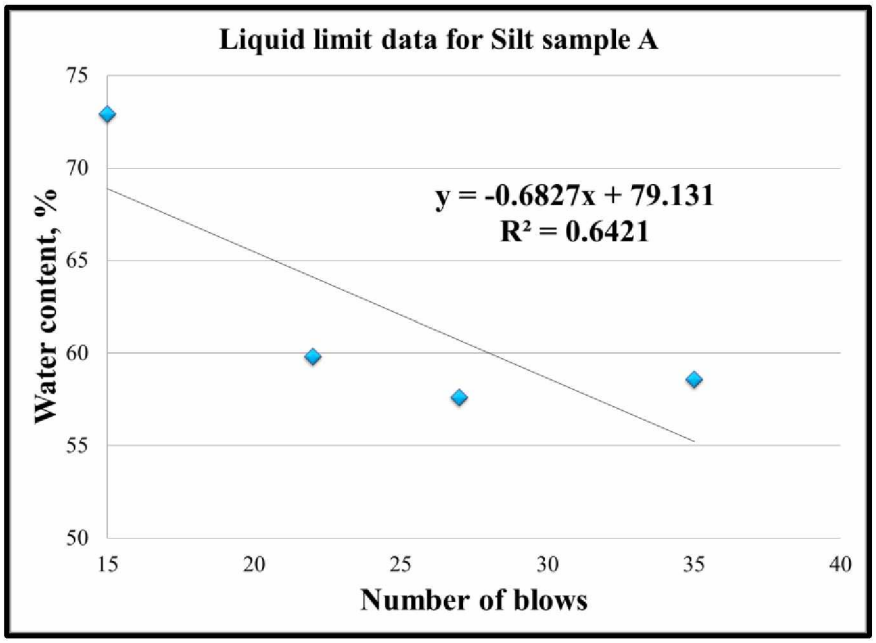

Figure A-4: Liquid limit data for silt sample A + 20% MI Gel

Table A-36: Plastic limit data for silt sample A + 20% MI Gel

Sr. No	Empty Container Weights (g)	Wet weight of soil (g)	Dry weight of soil (g)	Water content (%)
1	19.37	20.18	19.98	32.79
2	19.77	20.18	20.08	32.26
3	19.24	19.66	19.57	27.27

Table A-37: Initial data for soil layering test

Sr. No.	Vessel	Soil type	Layer sequence and Thickness, inches
1	Tub	Sand	3
2	Acrylic Cylinder #1	Sand	1.5
		Clay	4
		Silt	3.5
3	Acrylic Cylinder #2	Sand	2
		Clay	3.5
		Silt	4
4	Acrylic Cylinder #3	Sand	1.7
		Clay	3
		Sand	1.5
		Silt	4
		Sand	1.5
		Clay	2.5
		Silt	2.5
5	Acrylic Cylinder #4	Sand	2
		Silt	4
		Clay	4

Table A-38: Final data for soil layering test

Sr. No.	Vessel	Soil type	Layer sequence and Thickness, inches	
1	Tub	Sand	3	
2	Acrylic Cylinder #1	Sand	1.5	
		Clay	4	
		Silt	3.5	
3	Acrylic Cylinder #2	Sand	2	
		Clay	3.5	
		Silt	4	
4	Acrylic Cylinder #3	Sand	1.7	
		Clay	3	
		Sand	2.5	
		Silt	2.5	
		Sand	2.5	
		Clay	2.5	
		Silt	2	
5	Acrylic Cylinder #4	Sand	2	
		Silt	~	*(Silt and Clay got submerged into each other)*
		Clay	~	

Table A-39: Data collected from soil layering and consolidation tests for all the cylinders

Sr. No.	Vessel	Soil type	Bulk density, g/cm²	Dry density, g/cm²	Water content, %
1	Acrylic Cylinder #1	Sand	1.82	1.33	36.93
		Clay	1.91	1.37	40.02
		Silt	~	~	33.17
2	Acrylic Cylinder #2	Sand	~	~	8.42
		Clay	1.93	1.41	37.39
		Silt	1.91	1.43	33.09
3	Acrylic Cylinder #3	Sand	~	~	11.45
		Clay	1.98	1.39	35.77
		Sand	~	~	21.62
		Silt	1.88	1.43	31.09
		Sand	~	~	18.12
		Clay	~	~	~
		Silt	~	~	~
4	Acrylic Cylinder #4	Sand	~	~	9.99
		Silt	1.84	1.39	32.98
		Clay	1.81	1.30	38.86

Table A-40: Data for different soil types at the end of the frost heave test in the three-dimensional physical scale test

Sr. No	Soil type from bottom to top	Bulk density, g/cm²	Dry density, g/cm²	Water content, %
1	Sand	1.52	1.46	4.47
2	Clay	1.89	1.49	27.35
3	Sand	~	~	13.55
4	Clay	1.94	1.55	25.16
5	Silt	1.91	1.55	23.35

Table A-41: Thermal properties for different components of an oil well (Merriam et. al., 1975)

Sr. No	Material	Thermal conductivity, W/m K	Heat capacity at constant pressure, J/kg K	Density, kg/m³
1	Tubing	64.00	8025.25	460.55
2	Annular fluid	0.58	998.00	4176.00
3	Casing	64.00	8025.25	460.55
4	Cement	0.73	1465.38	1842.12

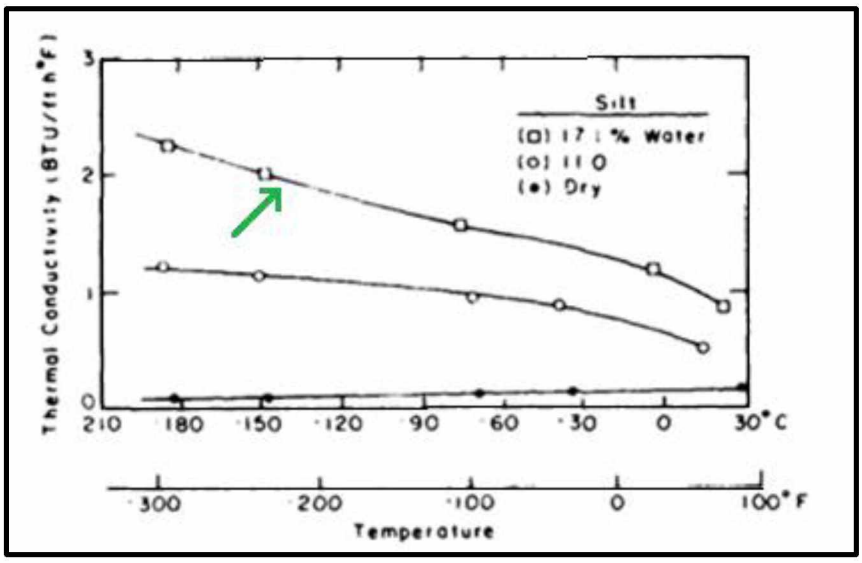

Figure A-5: Plot used to obtain empirical correlation for thermal conductivity of silt. (From Farouki, 1981)

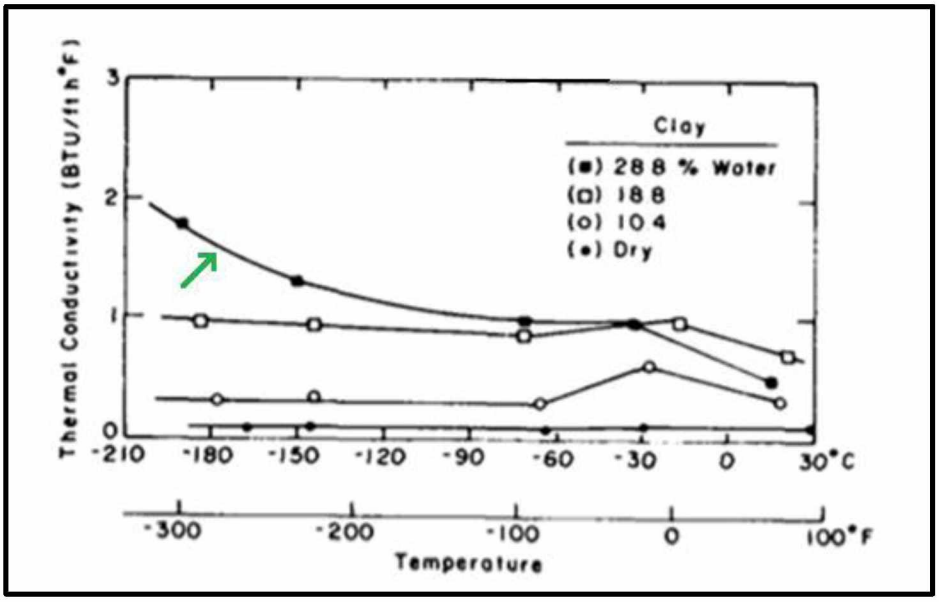

Figure A-6: Plot used to obtain empirical correlation for thermal conductivity of clay. (From Farouki, 1981)

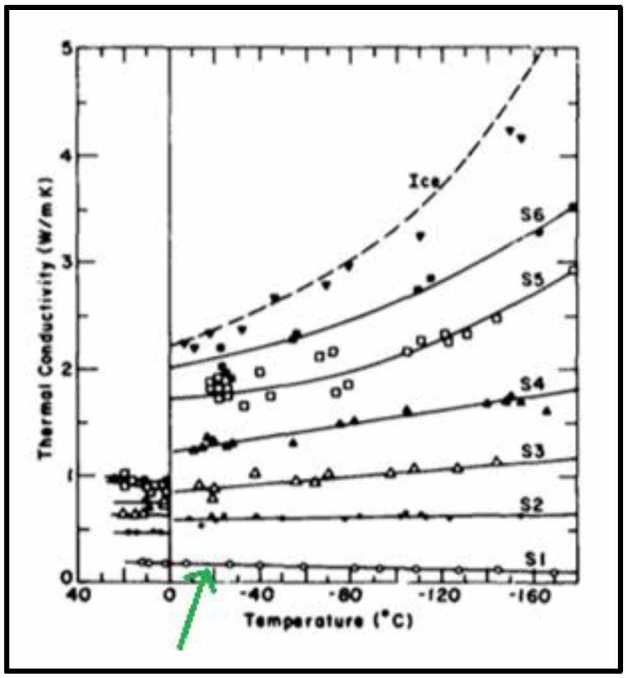

Figure A-7: Plot used to obtain empirical correlation for thermal conductivity of sand. (From Farouki, 1981)

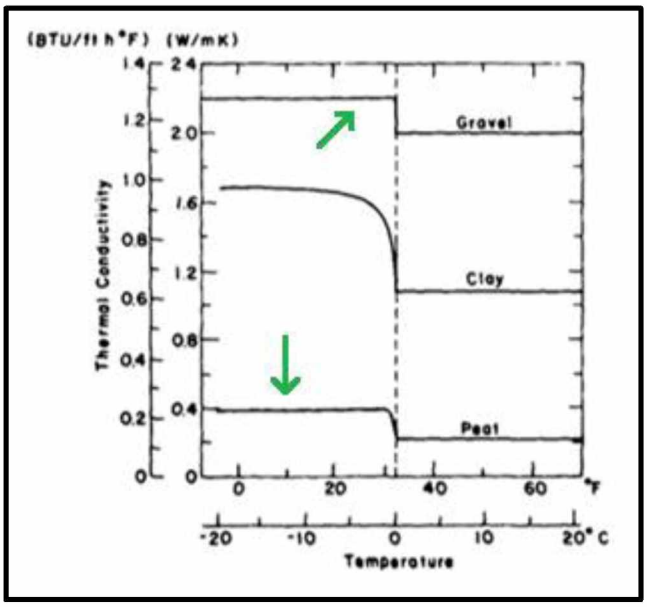

Figure A-8: Plot used to obtain empirical correlation for thermal conductivity of peat and gravel. (From Farouki, 1981)

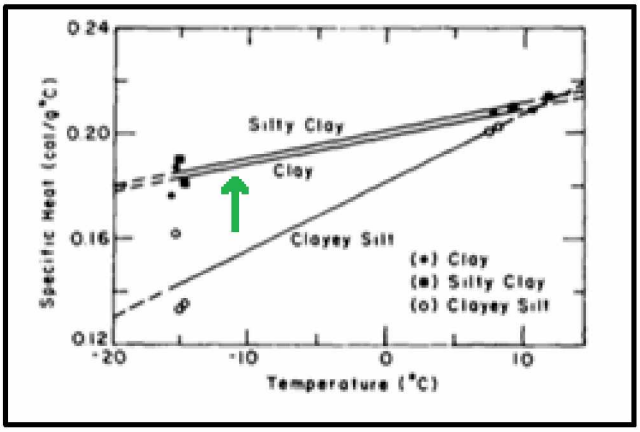

Figure A-9: Plot used to obtain empirical correlation for specific heat of clay. (From Farouki, 1981)

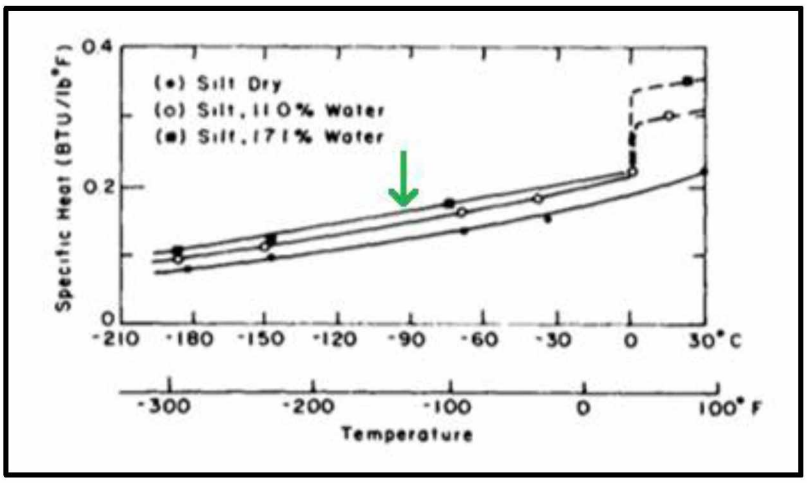

Figure A-10: Plot used to obtain empirical correlation for specific heat of silt (From Farouki, 1981)

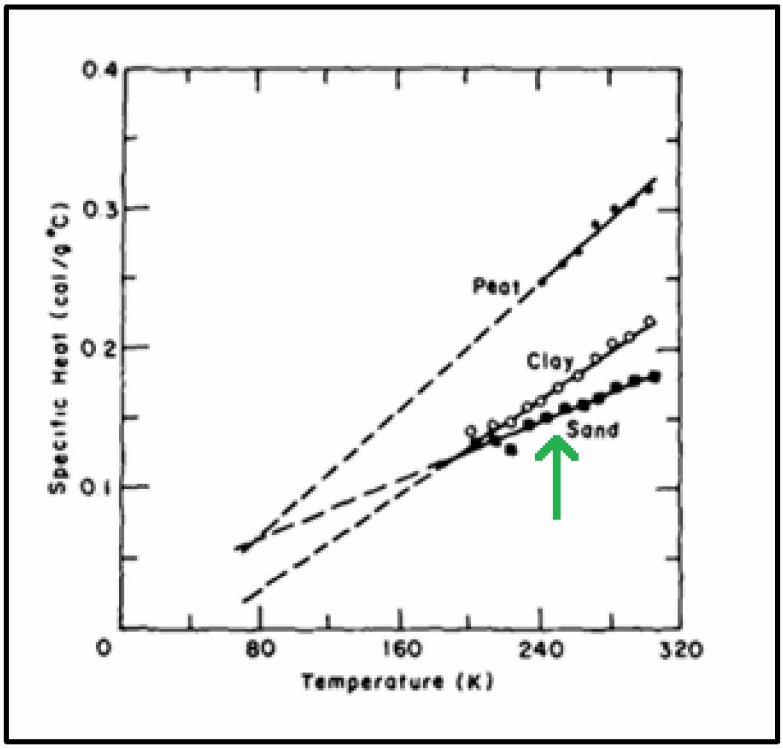

Figure A-11: Plot used to obtain empirical correlation for specific heat of sand and peat (From Farouki, 1981)

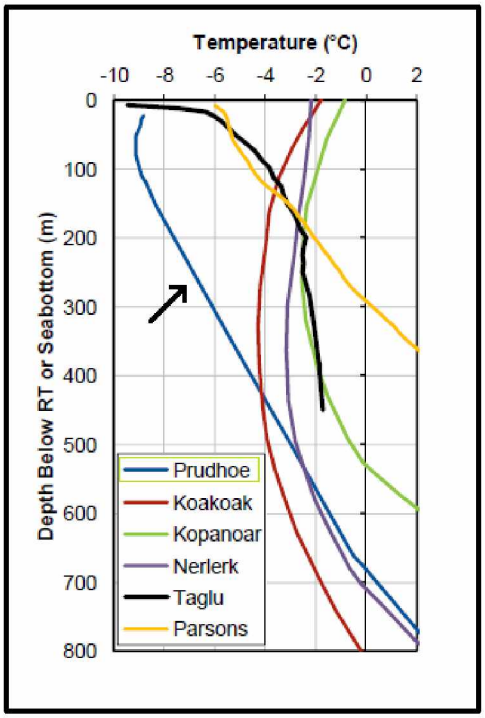

Figure A-12: Subsurface temperature profiles for well locations in Alaska, the Mackenzie Delta and Canadian Beaufort Sea (Matthews and Zhang, 2012)